VIBRATIONAL, ROTATIONAL AND LASER-INDUCED FLUORESCENCE STUDIES OF Br_2

By

DINAKAR KANJILAL

DEPARTMENT OF PHYSICS
INDIAN INSTITUTE OF TECHNOLOGY KANPUR
DECEMBER, 1983

VIBRATIONAL, ROTATIONAL AND LASER-INDUCED FLUORESCENCE STUDIES OF Br_2

A Thesis Submitted
In Partial Fulfilment of the Requirements
for the Degree of
DOCTOR OF PHILOSOPHY

By

DINAKAR KANJILAL

to the

DEPARTMENT OF PHYSICS
INDIAN INSTITUTE OF TECHNOLOGY KANPUR
DECEMBER, 1983

DEDICATED

TO

MY PARENTS

Certificate

This is to certify that the work presented in this thesis titled 'VIBRATIONAL, ROTATIONAL AND LASER-INDUCED FLUORESCENCE STUDIES OF Br_2' is the original work of Mr. Dinakar Kanjilal done under our joint supervision, and it has not been submitted elsewhere for a degree.

G.N. Rao
Professor of Physics

Putcha Venkateswarlu
Professor of Physics

ACKNOWLEDGEMENTS

I express my deep sense of gratitude to Professor Putcha Venkateswarlu for introducing me to this field and his stimulating guidance throughout the course of this work. I am extremely grateful to Professor G N Rao for his able guidance and encouragement during this work. It is a great pleasure for me to record my indebtedness and thanks to them.

I wish to express my sincere gratitude to all of my teachers, past and present, for their help in shaping my ideas and knowledge acquired to date.

I am grateful to Dr Y V Rao for his valuable help in this work. I am thankful to Dr S K Basu, Dr M S Ansari, Dr G Chakrapani, Dr R K Thareja, Dr B Rai, Dr Bansilal and Dr M K Dheer for their help at various stages of this work. I record my hearty thanks to Mrs Pramila and Mr Raghuram for their help, cooperation and companionship. I extend my thanks to Prof H D Bist for letting me use the argon ion laser and Spex double monochromator. I thank Dr M B Patel for his help during the recording of the fluorescence spectra.

I am thankful to Mr A K Ganguli for excellent tracing, Mr S L Yadav for neat typing, and Mr L S Rathaur and Mr H K Panda for cyclostyling the thesis. I thank Mr N V G Swamy and Mr T Sadagopan of our Electronics workshop, Mr M J Baskaran of Central Glass Blowing Shop and Mr K S Ubhey of Mechanical workshop for their help during this work. I thank Messrs

Raghava Verma, Mahendra Pal, A Banerjee and M M Sharma in preparation of this thesis. I am thankful to all my friends and colleagues whose names could not be mentioned here.

Financial help provided by the authorities of IIT Kanpur is gratefully acknowledged. Thanks are due to Department of Science and Technology, Government of India, and National Bureau of Standards, Washington for their financial assistance through research projects to IIT Kanpur. Thanks are also due to Herzberg Institute of Astrophysics, National Research Council Ottawa, Canada where Professor Venkateswarlu carried out high resolution work and made some of the data available to me.

I record my thanks to Head, Computer Centre, IIT Kanpur for providing extensive computational facilities on DEC 1090 computer. Hearty thanks are offered to Mr Nirmal Roberts of the Computer Centre for his help while working on some of the computer programs which are available from me on request.

I express my profound regards to my parents for their constant inspiration. I extend my sincere thanks to my brothers, sister and all other members of our family for their encouragement.

Dinakar Kanjilal

Dinakar Kanjilal

TABLE OF CONTENTS

LIST OF TABLES

LIST OF FIGURES

SYNOPSIS

VIBRATIONAL, ROTATIONAL AND LASER-INDUCED FLUORESCENCE STUDIES OF Br_2

DINAKAR KANJILAL

Ph D

DEPARTMENT OF PHYSICS
INDIAN INSTITUTE OF TECHNOLOGY KANPUR
December, 1983

The spectra of halogen molecules have the distinction of receiving the attention of a great many investigators over the past several decades. The knowledge gained from these studies, besides being of interest for halogen molecules in particular, has made significant contributions to our understanding of the spectra and structure of diatomic molecules in general. This understanding in turn helps us to predict many of the physical and chemical properties of the molecules.

Owing to the importance of bromine molecule (Br_2) in the field of lasers and that of spectroscopy an effort has been made in this thesis to study some of the aspects of this molecule. The 2900 Å system of bromine has recently come into prominence after the observation of strong ultra-violet laser oscillations in this system. The laser-induced fluorescence (LIF) has started receiving a lot of interest with the advent of various kind of lasers.

In the first chapter a general introduction to the salient features of diatomic molecular spectroscopy which are relevant to the present workhave been mentioned.

Experimental set-ups used at this Institute (IIT Kanpur) have been described in brief in Chapter 2. Experimental details of recording and analysing the spectra have been mentioned in respective chapters.

The vibrational analysis of the 2900 Å system of bromine in presence of argon has been reported in Chapter 3. The emission spectra of $^{81}Br_2$ and natural bromine in presence of argon and the transient absorption spectrum of bromine in presence of nitrogen obtained by flash photolysis method were used in the vibrational analysis. The emission spectra and the transient absorption spectrum have been found to correspond to the same system (D' - A') having the lower state as A' $^3\Pi_{2u}$ arising out of the configuration($\sigma_g)^2(\pi_u)^4(\pi_g)^3(\sigma_u)^1$. The variation of intensity of the band system, and the observed isotope-shifts of the band heads were used to do the vibrational analysis. The final vibrational constants for the lower and the upper states were computed by simultaneously fitting all the positions of the band heads of the three isotopic species ($^{81}Br_2$, $^{79}Br^{81}Br$, $^{79}Br_2$) of bromine, obtained from emission and absorption spectra, to the following polynomial in $\rho(v'+\frac{1}{2})$ and $\rho(v''+\frac{1}{2})$:

$$\nu = \Delta T_e + \sum_{i=1}^{m} C'_{vi}[\rho(v'+\tfrac{1}{2})]^i - \sum_{j=1}^{n} C''_{vj}[\rho(v''+\tfrac{1}{2})]^j$$

where v' and v'' are the vibrational constants of the upper

state and lower state respectively and $\rho = (\mu/\mu')^{\frac{1}{2}}$, μ and μ' being the reduce masses of an isotopic species and another isotope respectively.

Chapter 4 of the thesis deals with the rotational analysis of 0-8, 0-9, 0-10, 0-11, 1-8, 1-12, 3-5 and 4-5 bands of the high resolution emission spectrum of 2900 Å system of $^{81}Br_2$, in presence of argon, excited by a mild radio frequency oscillator. The rotational bands were photographed in the 20th and 21st order with reciprocal dispersion of the order of 0.1 Å/mm. The rotational analysis of the 0-10, 0-11, 1-12, 3-5 and 4-5 bands of $^{81}Br_2$ has been reported for the first time. The rotational constants B_v'', B_v', D_v'' and D_v' of each of the bands were obtained by band-by-band least-squares fit of the rotational lines of the corresponding band. The results of the bands having either upper or lower vibrational level as common were merged to obtain the most precise, single value for each of the rotational constants of the band system. The values of B_v and D_v for the upper and lower electronic states can be expressed as

$$B_v' = 0.041395 - (1.722 \times 10^{-4})\ (v' + \tfrac{1}{2}),$$

$$D_v' = 1.210 \times 10^{-8} - (3.93 \times 10^{-9})\ (v' + \tfrac{1}{2}) + (1.73 \times 10^{-9})\ (v' + \tfrac{1}{2})^2,$$

$$B_v'' = 0.057612 - (4.256 \times 10^{-4})\ (v'' + \tfrac{1}{2}) - (1.86 \times 10^{-5})\ (v'' + \tfrac{1}{2})^2,$$

$$D'' = 8.329 \times 10^{-8} - (1.11 \times 10^{-8})\ (v'' + \tfrac{1}{2}) + (8.18 \times 10^{-10})(v'' + \tfrac{1}{2})^2.$$

The plates used for the analyses of the emission spectra of $^{81}Br_2$ and the transient absorption spectrum of Br_2 were recorded by Professor Putcha Venkateswarlu at Herzberg Institute of Astrophysics, National Research Council, Ottawa, Canada.

In Chapter 5 Rydberg-Klein-Rees (RKR) potentials of the states involved in 2900 Å system of $^{81}Br_2$ have been calculated using the vibrational and rotational constants of bromine obtained in this work. The potentials thus obtained are used to calculate the R-centroids and Franck-Condon factors (FCF's) for the band system. The Franck-Condon factors obtained were found to be in consistence with the vibrational analysis.

Chapter 6 describes the recording and analysis of the $B\ ^3\Pi_{0_u^+} \rightarrow X\ ^1\Sigma_g^+$ resonance fluorescence doublets of bromine excited by 5145 Å radiation of cw argon-ion laser. The vibrational-rotational level of the upper state excited by the laser beam has been found to be $v' = 40$, $J' = 14$ using the latest constants available. The intensity of the resonance doublets obtained has been compared with those expected from known Franck-Condon factors. The variation of electronic transition moment with R-centroid ($\bar{R}$) has been reported for the region of $\bar{R}$ concerned.

The self-quenching cross-section (σ_s) of the vibrational-rotational level of bromine excited by the 5145 Å radiation of the argon-ion laser has been determined in Chapter 7. A Stern-Volmer plot of the reciprocal of the bromine fluorescence intensity against the reciprocal of the corresponding bromine vapor pressure has been used to calculate σ_s.

Summary and conclusions of the work have been given in

CHAPTER 1

INTRODUCTION

The study of molecular spectra is one of the most important means for understanding molecular structure. During the last several decades the field of Molecular Spectroscopy has developed vigorously and a lot of progress has been made in the investigation and theoretical interpretation of the molecular spectra so that a wealth of detailed information about the motion of the electrons and the vibration and rotation of the nuclei in the molecule can be obtained for the understanding and prediction of various physical and chemical properties of the molecule under consideration. The advent of lasers, coupled with the development of associated techniques, has generated a renewed interest in the field. The theory of the spectra of diatomic molecules has been discussed in considerable detail in many relevant papers[1-3] and textbooks.[4-8] Systematic reviews on the subject were presented, for the first time, by Mulliken.[1-3] A detailed discussion about the various aspects of diatomic molecular spectra has been given by Herzberg in his authoritative book[5] on the subject. Salient features of the theory which are relevant to this thesis are presented in this chapter.

1.1 Classification of Energy Levels

In diatomic molecules the ratio of the nuclear mass to the electronic mass is quite large. This implies, as will be shown below, that the energy associated with the motion of the nuclei is much smaller than that associated with the motion of the electrons about the nuclei. Now, the period of a motion is of the order of $\hbar$ divided by its energy. So the nuclear periods are much longer than the electronic periods. Therefore, the nuclear motion can be calculated under the adiabatic approximation that the electrons have their steady motion for each instantaneous arrangement of the nuclei. Then the nuclear motions can be classified into translations and rotations of the quasi-rigid equilibrium arrangement and internal vibrations of the nuclei about equilibrium. The translational motion is the same as that of a free particle, and gives rise to no non-classical features. So, the molecular energy levels may be classified into electronic, vibrational and rotational types.

Let the molecule have linear dimensions of the order of a_o. Then the momentum uncertainty of the electron is at least of the order of $\hbar/a_o$. So, the energy associated with the motion of a valence electron can be written as[7]

$$E_e \sim \frac{\hbar^2}{m a_o^2}, \qquad (1.1)$$

where m is the mass of the electron and $\hbar = h/2\pi$, h being Planck's constant.

The energy associated with a fairly low mode of vibration is

$$E_v \sim \hbar \left(\frac{K_o}{M}\right)^{1/2} \qquad (1.2)$$

where M is the molecular mass which is of the order of a typical nuclear mass. K_o is the stiffness constant. Since a displacement along the normal mode by the order of the molecular size a_o must produce an energy change of the order of E_e, one can put $K_o \sim (E_e/a_o^2)$, so that

$$E_v \sim \left(\frac{m}{M}\right)^{\frac{1}{2}} E_e. \qquad (1.3)$$

The moment of inertia of the molecule is of the order of Ma_o^2. Now, the angular momentum of a fairly low mode of rotation turns out to be of the order of $\hbar$, so one may write

$$E_r \sim \frac{\hbar^2}{Ma_o^2} \sim \left(\frac{m}{M}\right) E_e. \qquad (1.4)$$

For values of a_o of the order of an Angstrom unit, E_e corresponds to transition frequencies in the visible and ultraviolet regions of the spectrum. E_v is roughly a hundred times smaller than E_e and corresponds to the transitions in the near infrared. E_r is about a hundred times smaller than E_v and corresponds to the transitions in the far infrared. In this work transitions between various rotational-vibrational levels of different electronic states of bromine molecule (Br_2) have been studied.

1.2 Schrödinger Equation

The time independent Schrödinger equation for a diatomic molecule, having n electrons, is[7]

$$\left[-\frac{\hbar^2}{2m}\sum_{i=1}^{n}\nabla_i^2 - \sum_{j=1}^{2}\frac{\hbar^2}{2M_j}\nabla_j^2 + V \right]\psi = E\psi, \qquad (1.5)$$

where M_j is the mass of the jth nucleus, ∇_j^2 is the Laplace operator in terms of the coordinates of the jth nucleus, ∇_i^2 is the Laplace operator for the ith electron, and V is the sum of the electrostatic interactions between all pairs of electrons and nuclei.

According to the discussion in section 1.1, the total wave function ψ involves the nuclear coordinates $\underline{R}_j$ only parametrically, and Eq. (1.5) can be regarded as a wave equation in the $\underline{r}_i$ for the motion of the electrons with respect to the nuclei which are fixed in space. In this case, electronic wave function is approximately $\psi_e(\underline{r}_i)$ and corresponds to the energy eigenvalue $U(\underline{R}_j)$. Then the nuclear motion can be found by regarding $U(\underline{R}_j)$ as a potential function and using it to obtain a nuclear wave-function $\psi_n(\underline{R}_j)$. ψ, therefore, can be written as

$$\psi(\underline{r}_i, \underline{R}_j) = \psi_e(\underline{r}_i)\psi_n(\underline{R}_j), \qquad (1.6)$$

where ψ_e satisfies the equation

$$\left[-\frac{\hbar^2}{2m}\sum_{i=1}^{n}\nabla_i^2 + V \right]\psi_e(\underline{r}_i) = U(\underline{R}_j)\psi_e(\underline{r}_i). \qquad (1.7)$$

For each arrangement of the nuclei, $U(\underline{R}_j)$ is obtained as an eigenvalue of Eq.(1.7). There will, in general, be several solutions corresponding to different electronic states of the molecule.

Substitution of Eq.(1.6) into Eq.(1.5) gives, with the help of Eq.(1.7),

$$[-\sum_{j=1}^{2}\frac{\hbar^2}{2M_j}\nabla_j^2 + U(\underline{R}_j)]\psi = E\psi. \qquad (1.8)$$

Now, in the Born-Oppenheimer[9] approximation that the electronic part of the wave function does not change much as the nuclei move, an approximate Schrondinger equation for the nuclear motion can be obtained as

$$[-\sum_{j=1}^{2}\frac{\hbar^2}{2M_j}\nabla_j^2 + U(\underline{R}_j)]\psi_n(\underline{R}_j) = E\psi_n(\underline{R}_j). \qquad (1.9)$$

The eigenfunction ψ_n corresponds to that of a vibrating rotator. In a first approximation ψ_n can be written[4,5] as the product $(1/R)\psi_v\psi_r$ where ψ_v is the vibrational eigenfunction of a linear oscillator, depending on the change of internuclear distance, and ψ_r is the rotational eigenfunction, depending only on the orientation of the molecule in space. Thus, in a first approximation, the total eigenfunction can be expressed as

$$\psi = \psi_e \frac{1}{R}\psi_v\psi_r. \qquad (1.10)$$

This resolution holds, to a good approximation, also when the electron spin and magnetic interaction of angular momenta are included.

For a given electronic state characterized by a certain electronic eigenfunction and several electronic quantum numbers, a variety of functions for ψ_v and ψ_r may be obtained depending on the values of the vibrational and rotational quantum numbers (v and J).

1.3 Resolution of the Total Energy

The total energy E of a molecule, to a very good approximation, can be written as

$$E = E_e + E_v + E_r \,, \tag{1.11}$$

where E_e, E_v and E_r correspond to the energies due to the electronic motion, vibration and rotation of the molecule. The electronic energy E_e of a state is considered to be the minimum value of the potential energy function U of the stable electronic state. In terms of term values (cm^{-1}) the above equation can be written as

$$T = T_e + G + F \,. \tag{1.12}$$

For a molecule with zero average electronic angular momentum, G and F can be expressed, in the vibrating rotator model, as

$$G = \omega_e(v+\tfrac{1}{2}) - \omega_e x_e(v+\tfrac{1}{2})^2 + \omega_e y_e(v+\tfrac{1}{2})^3 + \omega_e z_e(v+\tfrac{1}{2})^4 + \ldots$$
$$= \sum_{i=1}^{n} C_{vi}(v+\tfrac{1}{2})^i, \tag{1.13}$$

$$F = B_v J(J+1) + D_v J^2(J+1)^2 + \ldots \tag{1.14}$$

The rotational constants B_v and D_v can be expressed as

$$B_v = B_e - \alpha_e(v+\tfrac{1}{2}) + \gamma_e(v+\tfrac{1}{2})^2 + \delta_e(v+\tfrac{1}{2})^3 + \varphi_e(v+\tfrac{1}{2})^4 + \ldots$$
$$= \sum_{j=1}^{m} C_{rj}\,(v+\tfrac{1}{2})^{j-1}, \tag{1.15}$$

$$D_v = D_e + \beta_e(v+\tfrac{1}{2}) + \ldots$$
$$= \sum_{k=1}^{p} C_{dk}(v+\tfrac{1}{2})^{k-1}. \qquad (1.16)$$

1.4 Spectrum

The wave number of any spectral line (in emission or in absorption) can be obtained by taking the difference of two terms, one of higher energy (T') and the other one of lower energy (T''):

$$\nu = T' - T''$$
$$= (T_e' - T_e'') + (G' - G'') + (F' - F'')$$
$$= \nu_e + \nu_v + \nu_r . \qquad (1.17)$$

All the spectral lines associated with a definite pair of electronic states, hence with a definite set of T_e', T_e'' and ν_e values, collectively form a 'band system'. This is then divided into limited groups of lines called 'bands', each band being associated with a definite pair of vibrational states (v',v'') and so with definite G', G'' and ν_v values. The lines whose arrangement contributes to the fine structure of a band correspond to a variety of values of ν_r resulting from various possible pairs of values J', J'' of the rotational quantum numbers. The various lines are distributed over a limited frequency region on both sides of the 'band origin' ν_0, given by $\nu_0 = \nu_e + \nu_v$.

When $\Lambda = 0$ in both electronic states between which the transition takes place, the selection rule for J is

$$\Delta J = J' - J'' = \pm 1, \qquad (1.18)$$

but when $\Lambda \neq 0$ for either or both the electronic states the selection rule becomes

$$\Delta J = 0, \pm 1 \qquad (1.19)$$

Thus, in the case of a $^1\Sigma - ^1\Sigma$ transition only P and R branches appear corresponding to $\Delta J = -1$ and $+1$, respectively. However, in a $^1\Pi - ^1\Sigma$ transition, since $\Lambda = 1$ for a $^1\Pi$ state, in addition to the P and R branches a Q branch will also be expected corresponding to $\Delta J = 0$. The wave numbers of the P, Q and R branches are given by

$$\nu_P(J) = \nu_o + F'(J-1) - F''(J), \qquad (1.20)$$

$$\nu_Q(J) = \nu_o + F'(J) - F''(J), \qquad (1.21)$$

$$\nu_R(J) = \nu_o + F'(J+1) - F''(J) \qquad (1.22)$$

Now, using Eq. (1.14) for F and neglecting the small correction term D_v, P and R branches can be represented by a single formula

$$\nu = \nu_o + (B_v' + B_v'')m + (B_v' - B_v'')\, m^2 \qquad (1.23)$$

where $m = -J$ for the P branch and $m = J + 1$ for the R branch.

When $B_v' < B_v''$, that is when the internuclear distance of the upper state is greater than that of the lower state, $(B_v' - B_v'')$ is negative. It then follows from Eq. (1.23) and the fact that $m = J+1$ for an R branch that initially the $(B_v' + B_v'')m$ term may overweigh $(B_v' - B_v'')\, m^2$ term and the wave number will increase. However, as J increases the squared term will eventually outweigh the single power term and the wave number will decrease. In this case the band

head will be formed in the R branch and the band will be red-degraded. Conversely, for $B'_v > B''_v$ the band head will lie in the P branch and the band will be violet-degraded.

1.5 Effect of Nuclear Identity

If the two nuclei of a diatomic molecule are identical, the wave function must be symmetric with respect to an interchange of their space and spin coordinates if the nuclei have zero or integral spin, or antisymmetric if they have half integral spin. The parity of the nuclear wave function is even or odd according as J is even or odd. An interchange of the space coordinates of the two nuclei is equivalent to a change in sign of their relative position vector $\underline{R}$, so that the parity determines the space symmetry of the wave function. So, for nuclei with zero or integral spin, the spin function must be symmetric for even J and antisymmetric for odd J. For nuclei of half integral spin the spin function must be antisymmetric for even J and symmetric for odd J.

Now, for two nuclei of spin Ih each, the total of $(2I+1)^2$ spin states can be divided into $(I+1)(2I+1)$ symmetric states and $I(2I+1)$ antisymmetric states. So in a gas which is in statistical equilibrium, the ratio of the number of molecules with even J to the number of molecules with odd J will be $(I+1)/I$ if I is zero or an integer, and $I/(I+1)$ if I is a half integer. This effect

gives rise to alternating intensities in the rotational band spectra of homonuclear diatomic molecules. For larger I values this effect is not very prominent since the ratio tends to 1.

The above ratio should be modified by the Boltzmann factor if the spacing between rotational levels is not small compared to the thermal energy kT.

1.6 Electronic States

In diatomic molecules the electric field due to the two nuclei is axially symmetric about the internuclear axis. So, the component of the total electronic orbital angular momentum $\underline{L}$ of the electrons about the internuclear axis is a constant of motion. The precession of $\underline{L}$ about the internuclear axis gives rise to the constant component $M_L\hbar$ where

$$M_L = L,\ L-1,\ L-2,\ \ldots\ldots,\ -L. \qquad (1.24)$$

The electronic states are classified according to the value of Λ where

$$\Lambda = |M_L| \ . \qquad (1.25)$$

For $\Lambda = 0, 1, 2, 3, \ldots$, the corresponding molecular state is designated as $\Sigma, \Pi, \Delta, \Phi, \ldots$ state.

The spins of the electrons form a resultant $\underline{S}$, the corresponding quantum number S being integral or half integral as the total number of electrons in the molecule is even or odd. The internal magnetic field in the direction

of the nuclear axis resulting from the orbital motion of the electrons causes a precission of $\underline{S}$ about the field direction with a component $\hbar\Sigma$. The allowed values of Σ are

$$\Sigma = S,\ S-1,\ S-2,\ldots\ldots,-S. \qquad (1.26)$$

The total electronic angular momentum $\underline{\Omega}$ is obtained by adding and $\underline{\Lambda}$ and $\underline{\Sigma}$. The quantum number of the resultant electronic angular momentum about the internuclear axis is obtained from the relation

$$\Omega = |\Lambda + \Sigma|. \qquad (1.27)$$

Different values of $\Lambda+\Sigma$ correspond to somewhat different energies of the resulting molecular states. The value of $\Lambda+\Sigma$ is added as a right subscript. $(2S+1)$ is called the multiplicity of the state and it is added to the term symbol as a left superscript.

In diatomic molecules any plane passing through the internuclear axis is a plane of symmetry. The Hamiltonian of the molecule remains invariant under a reflection through such a plane. Since the sign of the angular momentum about the axis is changed under such a reflection, the state obtained from the reflection is not completely identical with the initial state. So all electronic terms with non-zero values of Λ are doubly degenerate corresponding to two directions of $\underline{\Lambda}$ along the nuclear axis. When $\Lambda = 0$, the state of the molecule is not changed at all on reflection so that Σ terms are not degenerate. After such a reflection the wave function

of a Σ term can only be multiplied by a constant. Since double reflection in the same plane is an identity transformation, this constant must be ± 1. Accordingly, there will be two states Σ^- and Σ^+ depending upon whether the wave function changes its sign and does not change its sign respectively on reflection through such a plane of symmetry.

For a state with $\Omega = 0$, $\Lambda \neq 0$ a slight splitting exists even for the fixed centre system. Again the wave function of one of the components remain unchanged, and that of the other changes its sign upon reflection at any plane through the two nuclei. In the case of a $^3\Pi_0$ state they are distinguished as $^3\Pi_{0+}$ and $^3\Pi_{0-}$. Where Λ is not defined one distinguishes 0^+ and 0^- states corresponding to Σ^+ and Σ^- states.

If the two nuclei in the molecule have the same charge, the field in which the electrons move has a centre of symmetry at the point bisecting the line joining the nuclei. Hence the Hamiltonian is invariant with respect to a simultaneous change of sign of the coordinates of all the electrons in the molecule. Since the operator of this transformation also commutes with the orbital angular momentum operator, we have the possibility of classifying the terms with a given value of Λ according to their parity: when the coordinates of the electrons change sign, the wave functions of even (g) states are unchanged while those of odd (u) states change sign. Thus for molecules with like nuclei one gets Σ_u, Σ_g, Π_u, Π_g, ... states.

1.7 Coupling of Angular Momenta

The influence of rotational and electronic motion on each other can be classified grossly as four types of Hund's[10] cases as discussed below.

1.7.1 Case (a)

In this case the interaction of nuclear rotation with electronic motion (spin as well as orbital) is assumed to be very weak whereas the electronic motion itself is coupled very strongly to the line joining the nuclei. Here the total electronic angular momentum $\underline{\Omega}$ directed along the axis of the molecule combine with nuclear angular momentum $\underline{N}$ to give the resultant vector $\underline{J}$ which characterizes the total angular momentum of the molecule.

In this case, neglecting centrifugal stretching terms, the variable part of the rotational energy is given by

$$F_v = B_v \left[J(J+1) - \Omega^2 \right], \qquad (1.28)$$

where for a given value of Ω, J can have the values

$$J = \Omega, \Omega+1, \Omega+2, \ldots. \qquad (1.29)$$

Levels corresponding to $J < \Omega$ do not occur.

1.7.2 Case (b)

This case is characterized by a weak (or zero) coupling of $\underline{S}$ to the internuclear axis. Here $\underline{\Lambda}$ and $\underline{N}$ form the resultant vector $\underline{K}$, the total angular momentum apart from spin. The corresponding quantum number K can have integral values

$$K = \Lambda, \ \Lambda+1, \ \Lambda+2, \ldots. \qquad (1.30)$$

$\underline{K}$ and $\underline{S}$ form a resultant $\underline{J}$, the total angular momentum of the molecule. For a given K, the possible values of J are

$$J = (K+S),\ (K+S-1),\ (K+S-2),\ldots. \qquad (1.31)$$

The rotational energy in this case is given approximately by

$$F_v(K) = B_v[K(K+1) - \Lambda^2]. \qquad (1.32)$$

A transition is possible from case (a) to case (b) when nuclear rotation is increased.

1.7.3 Case (c)

In some molecules, particularly for heavy molecules, the interaction between $\underline{L}$ and $\underline{S}$ may be stronger than the interaction with the internuclear axis. So, Λ and Σ are not defined in those cases. Here $\underline{L}$ and $\underline{S}$ form a resultant vector $\underline{J}_a$ which is then coupled to the internuclear axis with a component Ω. Ω and $\underline{N}$ then form the resultant angular momentum $\underline{J}$ as in case (a). The rotational energy and their J values are given by the same formulae as for case (a).

1.7.4 Case (d)

In this case the coupling between $\underline{L}$ and the internuclear axis is very weak but that between $\underline{L}$ and the axis of rotation is strong. Here the angular momentum of nuclear rotation which is called $\underline{R}$ is quantized. The quantum number R can have the values $0, 1, 2, \ldots$. $\underline{R}$ and $\underline{L}$ are added to give the total angular momentum $\underline{K}$. For a given R, the corresponding quantum number K can have the values

$$K = (R+L),\ (R+L-1),\ (R+L-2),\ldots,|R-L|\ . \qquad (1.33)$$

$\underline{K}$ and $\underline{S}$ add together to give the total angular momentum $\underline{J}$ as in case (b). But this coupling is usually very weak in this case so that $\underline{S}$ and hence $\underline{J}$ can be neglected and only $\underline{K}$ can be used. Here the rotational energy is given, to a first approximation, by

$$F_v(R) = B_v R(R+1). \qquad (1.34)$$

In an electronic transition, from a detailed analysis of the rotational structure of the bands, the values of Ω, Λ and the multiplicity are allotted, and the two electronic states involved are identified.

1.8 Electron Orbitals

The term manifold for the electronic states of a diatomic molecule may be determined from the electronic configuration, that is, from the knowledge of the quantum numbers and symmetries of the different one electron orbitals. The electron orbitals are described in terms of the orbits to which they would go in the limits of united atom where the internuclear distance is diminished to zero and the separated atoms where the internuclear distance is increased to infinity.

The possible states, in the united atom, are characterized by the quantum numbers n and l. If the united atom is split in such a way that the distance between the two nuclei is still small then the quantum numbers n and l are still approximately defined. The orbital angular momentum $\underline{l}$

of the electron is space quantized so that its component along the internuclear axis is $\lambda\hbar$ where λ can take the values

$$\lambda = l, l-1, l-2, \ldots, 0. \qquad (1.35)$$

For $\lambda = 0,1,2,3,\ldots$, the corresponding electron state is designated as $\sigma, \pi, \delta, \varphi, \ldots$ state. For n =1, there is one state given by $1s\sigma$. For n = 2, one gets three states as $2s\sigma$, $2p\sigma$ and $2p\pi$. n=3 corresponds to six states: $3s\sigma$, $3p\sigma$, $3p\pi$, $3d\sigma$, $3d\pi$ and $3d\delta$. As the separation of the two nuclei increases the splitting between the states with different λ for the same n and the same l increases, and n and l lose more and more their meaning as quantum numbers.

When the two separated atoms that correspond to the diatomic molecule approach each other, an electronic field is produced, in which $\underline{l}$ is space quantized so that its component along the internuclear axis is $m_l\hbar$. So, the electronic orbitals are again designated by $\lambda (= m_l)$ values. In designating an electron the n and l values that it has in separated atom (1s, 2s, 2p,....) are usually added after the symbol that indicates the λ value . Thus one gets $\sigma 1s$, $\sigma 2p$, $\pi 2p$ and so on.

If the two nuclei have equal charges, the electron orbitals are called even (g) or odd (u) according as the eigenfunction remains unaltered or changes sign by reflection at the origin. Thus one writes $\sigma_g 1s$, $\sigma_u 1s$, $\sigma_g 2s$, $\sigma_u 2s$ $\sigma_g 2p$, $\sigma_u 2p$ and so on. In the united atom approach the parity of the electron orbitals is determined by $(-1)^l$. So, one gets $1s\sigma_g$, $2s\sigma_g$, $2p\sigma_u$, $2p\pi_u$, $3s\sigma_g$, $3p\sigma_u$, $3p\pi_u$, etc.

Finally, the electronic orbitals for the two limits of $R \rightarrow 0$ and of $R \rightarrow \infty$ must be correlated to give the desired molecular orbitals appropriate to the intermediate distances between the nuclei.

To a certain approximation each individual electron in a molecule can be characterized by the quantum number introduced above. A certain electron configuration of the molecule is defined by stating the quantum numbers of all the electrons in the molecule. States with different electron configurations have different, frequently widely different, energies. Since all the electrons are not independent of one another, a given electron configuration may give rise to several electronic states of the molecule.

On the basis of Pauli principle each σ shell can contain only two electrons and each of $\pi, \delta, \ldots$ shells can contain only four electrons.

1.9 Electronic Configuration of Halogen Molecules

The ground state configuration of all the halogen molecules can be represented by the 10 outer electrons of the 'np' shell as

$$(\sigma_g\, np)^2\ (\pi_u\, np)^4\ (\pi_g\, np)^4$$

where n = 2, 3, 4, and 5 for F_2, Cl_2, Br_2 and I_2 respectively. This configuration gives the term $^1\Sigma_g^+$ which is to be correlated with 0_g^+ of case (c) type and which represents the ground state of all the halogen molecules.

Leaving off 'np' which is common, the ground state of the halogen molecules can also be generally represented as $(\sigma_g)^2\ (\pi_u)^4\ (\pi_g)^4\ (\sigma_u)^0\ 0_g^+\ (^1\Sigma_g^+)$. The various excited states are then obtained by suitable excitation of the inner electrons. Thus by exciting one π_g electron to the next state σ_u of the same shell we get two ungerade terms $^1\Pi$ and $^3\Pi$ which under case (c) type of coupling resolve into one (1_u) and four $(0_u^+,\ 0_u^-, 1_u, 2_u)$ terms respectively. Similarly by the excitation of an electron in π_u and σ_g states various other terms are obtained. Systematic theoretical development of the spectroscopy of halogens has been reported by Mulliken in a series of papers[11-15]. A simplified potential energy level diagram[15,16] of the iodine molecule, emphasizing the states involved in the visible and ultraviolet transitions, have been shown in Fig 1.1. Similar types of potential energy curves may be expected for bromine.

The valence shell electronic states of Br_2 have the molecular orbital (MO) electron configurations of the type $\sigma_g^2\ \sigma_u 2/\sigma_g^m\ \pi_u^p\ \pi_g^q\ \sigma_u^n$ with m+p+q+n = 10 and with MO's σ_g, σ_u of the form 4s$\pm$ 4s and 4pσ $\pm$ 4pσ and π_u, π_g of the form 4p$\pi\pm$ 4pπ in the simplest LCAO approximation. According to Mulliken's notation 'm p q n' denotes the different electronic configurations. As for example, the ground state of Br_2 corresponds to 2440 configuration. The lowest excited states belong to 2431 configuration which is obtained by exciting one π_g electron to the vacant σ_u orbital. Similarly

other electronic states are obtained by exciting other electrons to the vacant orbitals. The lower energy valence-shell states of Br_2 dissociates to $^2P_{3/2}$ + $^2P_{3/2}$, $^2P_{3/2}$ + $^2P_{1/2}$ and $^2P_{1/2}$ + $^2P_{1/2}$. The higher energy valence-shell states have ion-pair structure and tend to dissociate into $Br^-(^1S)$ and $Br^+(^3P_2, ^3P_1, ^3P_0, ^1D$ or $^1S)$. These ion-pair states are characterized by low vibrational frequencies and large internuclear distances.

potential for rotation!

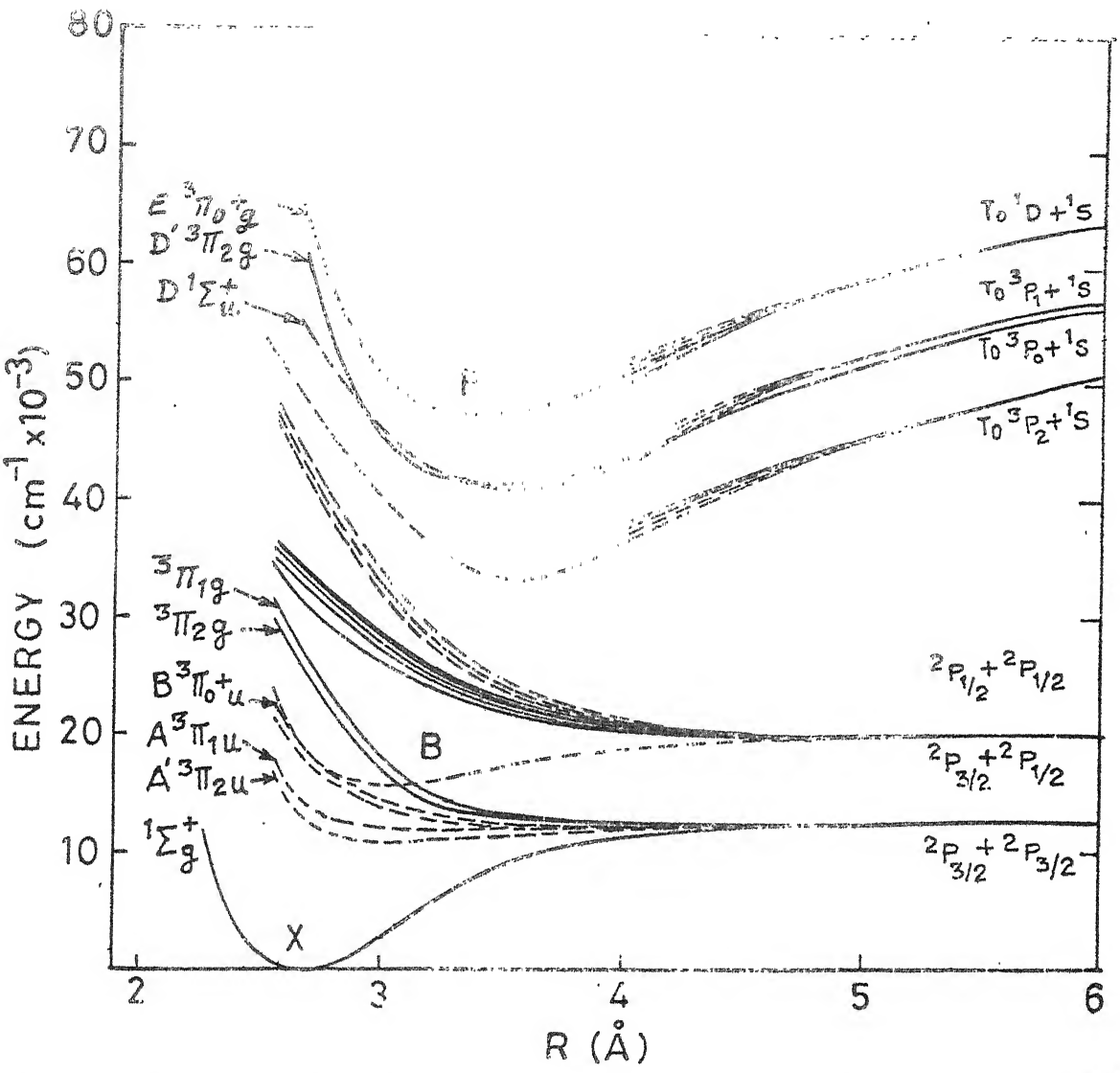

FIG. 1.1 A SIMPLIFIED POTENTIAL ENERGY DIAGRAM OF I_2.[15,16] SIMILAR POTENTIAL ENERGY CURVES ARE EXPECTED FOR Br_2

CHAPTER 2

EXPERIMENTAL TECHNIQUES

A brief description of the experimental techniques used at this Institute for this work is given in this chapter. The experimental set-ups used by Professor Venkateswarlu to record transient absorption spectrum of Br_2 and emission spectrum of $^{81}Br_2$ at Herzberg Institute of Astrophysics, National Research Council, Ottawa, Canada is described in chapter 3 and chapter 4.

2.1 Preparation of Discharge Tube

The discharge tube was made of quartz and was 30 cms in length and 2.5 cms in diameter. Polished quartz windows were fused to the ends and tungsten rods connected to the tube through graded seal were used as electrodes. The discharge tube was connected to the vacuum system as shown in Fig. 2.1. A combination of a silicone oil diffusion pump and a rotary pump was used to maintain the system at a pressure below 10^{-5} torr. The discharge tube was first continuously degassed for about 12 hours by a heating tape

wound round the tube and the whole system was degassed several times by heating it with the flame of a torch. After closing the stop-cock T2, the top of the tube at the extreme left (Fig. 2.1) was cut open. Analar grade bromine was poured into the tube and then the tube was sealed at C1. Bromine was kept at liquid nitrogen temperature so that its vapour pressure becomes negligible. A liquid nitrogen trap was used to save the vacuum unit from possible bromine contamination. The system was brought back to a pressure below 10^{-5} torr by connecting it to the vacuum system through T2. The discharge tube was again degassed by heating it several times with the flame of the torch. The whole system was also degassed with the help of the flame. After attaining a steady pressure below 10^{-5} torr the stop-cock T2 was closed and argon marked spectrally pure and obtained from Oxygen Acetylene Company was introduced at a desired pressure. Then the system was sealed at C3. Bromine was then allowed to enter the discharge tube after passing through a tube containing layers of P_2O_5 separated by glass wool. The relative pressures of argon and bromine were adjusted by observing the spectrum in the visible region through a hand spectroscope. The intensity of the spectrum of bromine in the visible region was found to decrease with the increase of argon pressure.

2.2 Preparation of Sample Tube

The sample tube for laser induced resonance fluorescence studies was also made of a quartz tube having an internal diameter of 2.5 cms with polished quartz windows fused at the ends of the tube. A side tube was attached to the cell so that the vapor pressure of bromine in the cell could be varied by changing the temperature of the side tube. The tube was filled with bromine as described above in section 2.1.

2.3 Recording of Transformer Discharge Spectrum

Bromine in the presence of argon was excited by an uncondensed transformer discharge. The spectrum was photographed on a Jarrell Ash 3.4 m Ebert Spectrograph (Fig. 2.2) in the second order at a reciprocal dispersion of about 2.5 Å/mm. Kodak (type 103-O) plates were used to photograph the spectrum. The plates were developed by Kodak D-76 developer and were then fixed in fast fixer. The exposure time varied from 1 to 2 hours for a slit width of 50 microns. Reference lines were obtained from an iron-neon hollow cathod lamp. The spectrum was measured using a Carl-Zeiss Abbe Comparator having a least count of one micron. The wave numbers of all the band heads were obtained using a large number of reference lines by least squares method programmed in FORTRAN-10 on DEC system 1090 computer of our Institute.

2.4 Set-up for Recording Laser Induced Fluorescence

A combination of Spectra Physics model 165-09 5 watt cw Ar^+ laser and Spex-1403 spectrophotometer was used to record the resonance fluorescence spectra of Br_2. The optical diagram of the system is shown in Fig. 2.3.

The Ar^+ laser was operated by a 265 exciter which contains all the necessary electronic circuits to create, sustain and monitor the ion discharge in the plasma tube, to monitor and control the output power, and to supply and regulate the solenoid current of the laser. The laser head, the plasma tube and the power supply unit of the 265 exciter were cooled continuously by the flow of distilled and deionised water chilled at a constant temperature ($20^{\circ}C$) by a Neslab HX 500 chiller plant. Tap water was used to dissipate the chiller heat. The beam deflector at the output end of the laser tube deflects the laser beam into the UVISIR illuminator after passing through a laser mate. A fused silica lens focusses the laser beam at the focus of an elliptical collecting mirror, which in turn refocusses the fluorescence beam on the entrance slit of the Spex-1403 double monochromator fitted with holographic gratings having 1800 lines/mm. A thermoelectrically cooled RCA C31034 photomultiplier tube was used to detect the spectra. The signal from the photomultiplier tube was recorded in the photon-counting mode on a linear strip chart recorder coupled to the monochromator through a compudrive. The block diagram of the whole set-up is shown in Fig. 2.4.

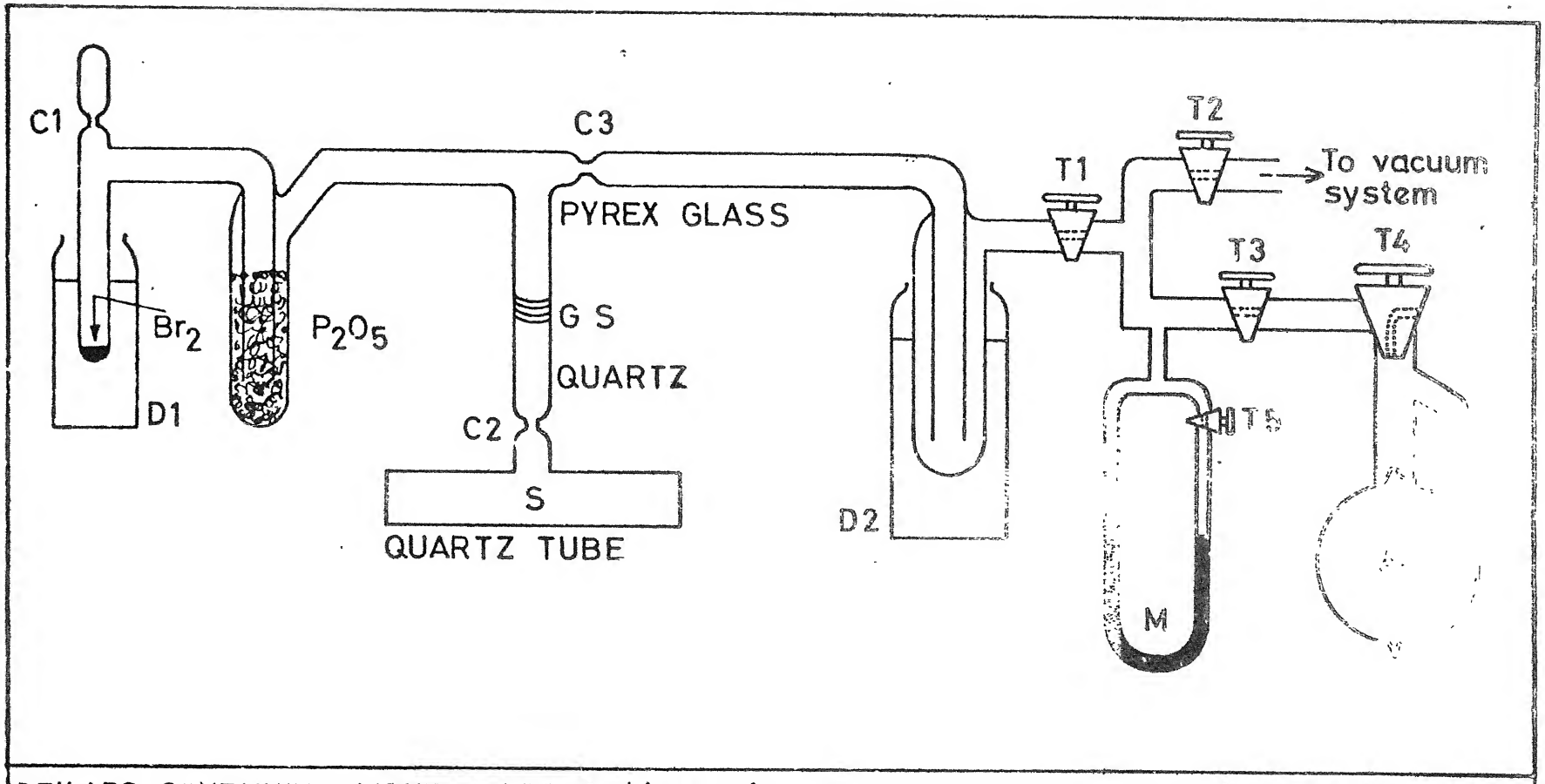

DEWARS CONTAINING LIQUID NITROGEN (D1,D2); CONSTRICTIONS (C1,C2,C3); GRADED SEAL (G.S.); SAMPLE TUBE OR DISCHARGE TUBE (S); STOPCOCKS(T1,T2,T3,T4,T5); MANOMETER(M).

FIG. 2.1 DESIGN FOR FILLING UP DISCHARGE/SAMPLE TUBE.

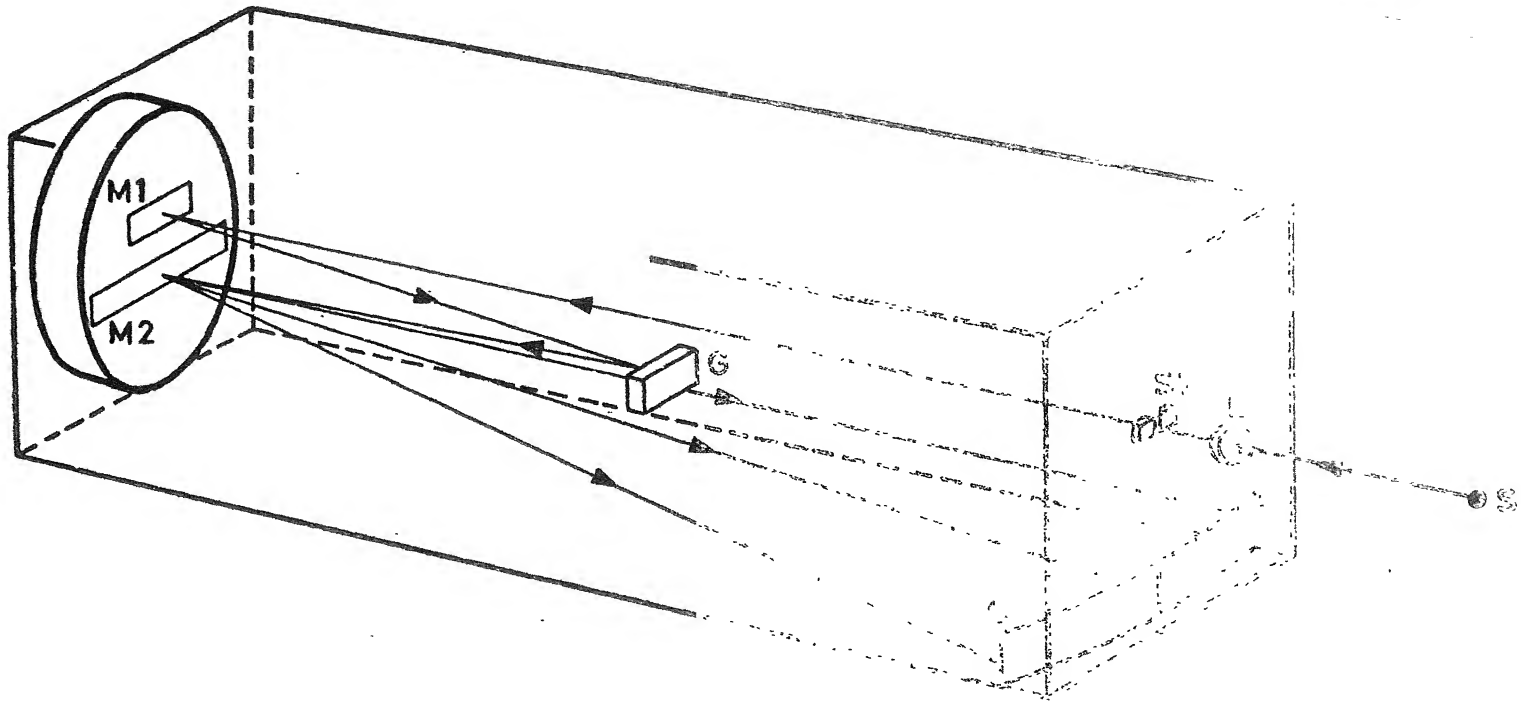

SOURCE (S) ; CYLINDRICAL QUARTZ LENS (L) ; ENTRANCE SLIT (S_1) ; CONCAVE MIRRORS (M_1, M_2) ; GRATING (G) ; CAMERA (C).

FIG. 2.2 OPTICAL DIAGRAM OF JARRELL ASH 3.4 METER EBERT SPECTROGRAPH.

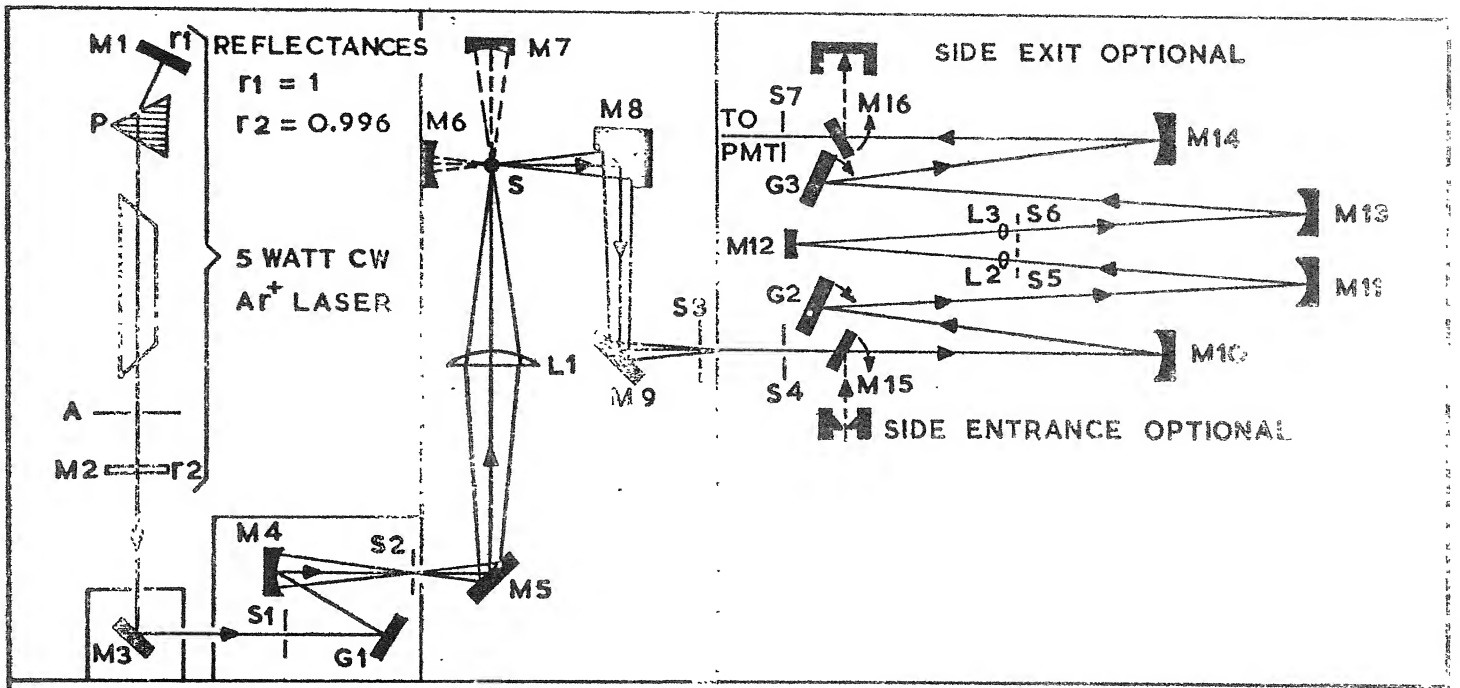

PRISM (P) ; APERTURE (A) ; PLANE MIRRORS (M1, M2, M3, M5, M9, M15, M16) ; CONCAVE MIRRORS (M4, M6, M7, M10, M11, M12, M13, M14) ; ELLIPTICAL COLLECTOR MIRROR (M8) ; SLITS (S1, S2, S3, S4, S5, S6, S7) ; PLANE GRATINGS (G1, G2, G3) ; FUSED SILICA CONDENSER LENS (L1) ; SAMPLE (S) ; OPTICAL FILTERS (L2, L3).

FIG. 2.3 OPTICAL DIAGRAM OF SPECTRA PHYSICS LASER AND SPEX 1403 SPECTROPHOTOMETER.

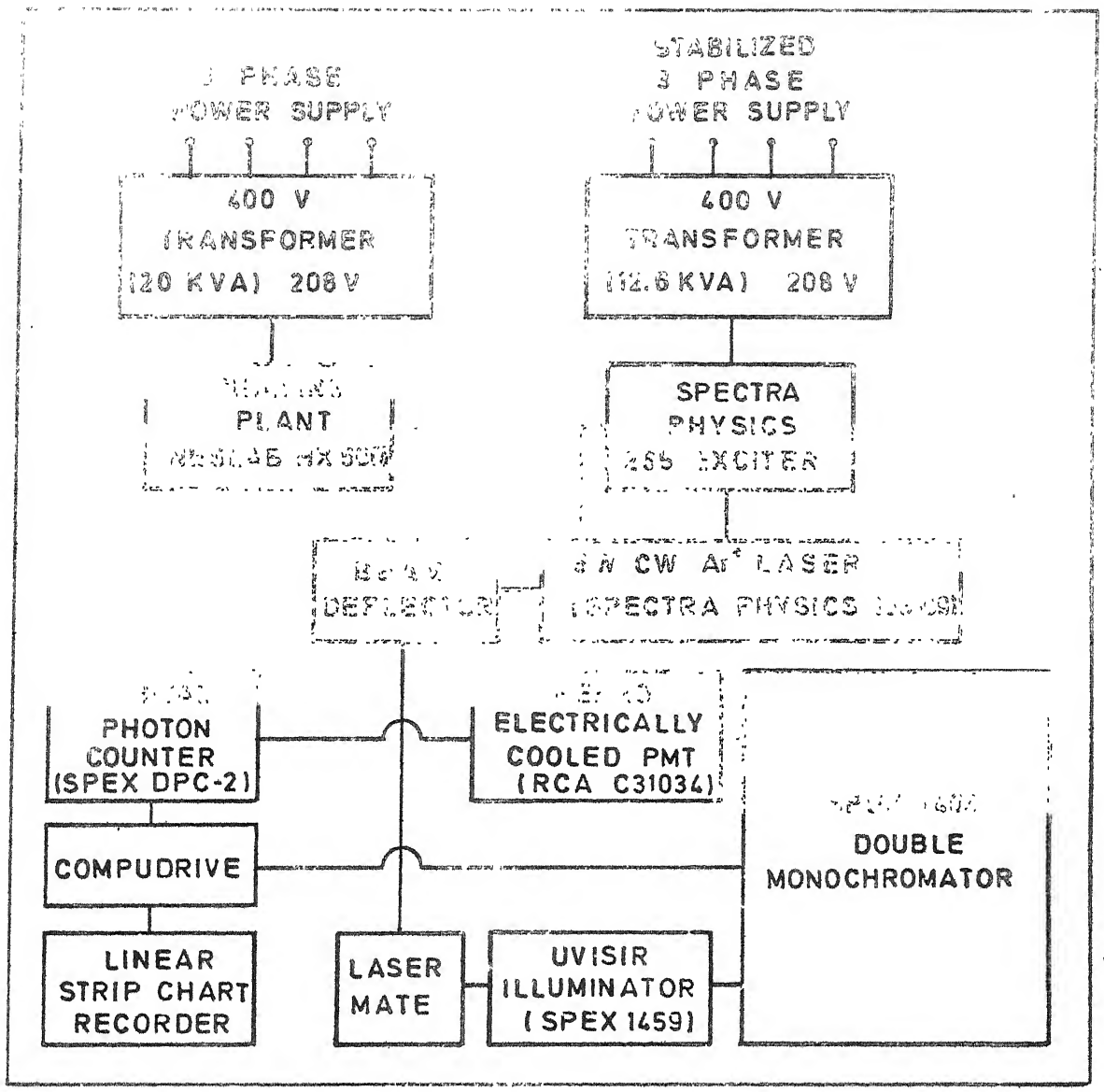

FIG.2.4 BLOCK DIAGRAM OF THE EXPERIMENTAL SET-UP USED TO STUDY LASER INDUCED RESONANCE FLUORESCENCE IN DIATOMIC BROMINE MOLECULE.

CHAPTER 3

VIBRATIONAL ANALYSIS OF 2950-2400 Å BAND SYSTEM OF Br_2

3.1 Introduction

Systematic and extensive studies of diatomic halogen molecules, both homopolar[17-37] and heteropolar[38-41], is being done by our research group for a number of years at Banaras, Aligarh, Ottawa and Kanpur. Though the halogens are one of the extensively studied class of molecules, they still continue to attract the attention of various research groups because of their possible potential use in the development of powerful lasers in different spectral regions. Laser oscillations have recently been observed in the ultraviolet region at 1570 Å in fluorine (F_2)[42,43], at 2590 Å in chlorine (Cl_2)[44,45], at 2920 Å in bromine (Br_2)[46,47] and at 3420 Å in iodine (I_2)[48-50].

The emission spectrum of Br_2 vapor was known to consist of red-degraded bands[51,52] in the region 6700-4400 Å and a number of groups of diffuse bands and continua[21,24] in the region 4200-2000Å. Cameron and Elliot[53] excited bromine in

presence of nitrogen and reported that the continuum at 2900 Å is superposed by a set of diffuse bands with a separation of about 147 cm^{-1}.

The 2950-2670 Å emission system of Br_2 excited in the presence of argon (Ar), by uncondensed transformer discharge, was first analysed and reported by Venkateswarlu and Verma[26]. They also reported another emission system in the same discharge at 3150 Å [27]. Venkateswarlu and Verma interpreted the 2950-2670 Å emission system as terminating on the $B\ ^3\Pi_{0_u^+}$ state. Briggs and Norrish[54] recorded transient absorption in the same region by flash photolysis of bromine in presence of nitrogen. Venkateswara Rao+, a former member of our research group, while working in Mulliken's laboratory at Chicago during 1963-65 reanalysed the transient absorption data[54] of Briggs and Norrish. According to his analysis the transient absorption bands of bromine could be represented by the following equation[55]:

$$\nu = 35526.1 + (151.23\ v' - 0.3903 v'^2 + 0.00041\ v'^3) - (155.1\ v'' - 1.51\ v''^2) \qquad (3.1)$$

where $1 \leq v' \leq 44$ and $0 \leq v'' \leq 6$. It was further suggested by him that the lower state of the system is very likely the

+ Thanks are due to Dr Y Venkateswara Rao for showing me the manuscript of his work on the transient absorption spectra of Cl_2 and Br_2 alongwith Professor Robert S Mulliken's comments on it.

the metastable state $(\sigma_g)^2 (\pi_u)^4 (\pi_g)^3 (\sigma_u)^1 \ ^3\Pi_{2u}$. However, Wieland et al[56] reanalysed the emission as well as the transient absorption bands and put them into a single vibrational scheme with $^3\Pi_{o^+_u}$ as the lower state. But subsequently, Tellinghuisen[57] reexamined the vibrational structure of 2950-2800 Å emission system obtained by tesla discharge through isotopically enriched $^{79}Br_2$ in the presence of Ar and attributed this system to be D'(1432 $^3\Pi_{2g}$) $\longrightarrow$ A'(2431 $^3\Pi_{2u}$) transition. The upper state was labelled as an ion-pair state which tends to $Br^+ + Br^-$. Afterwards, Sur and Tellinghuisen reported[58] the rotational analysis and a further extension of the vibrational analysis to cover more bands in the region 2950-2800 Å using isotopically enriched $^{79}Br_2$ and $^{81}Br_2$, and confirmed the earlier assignment made by Tellinghuisen.

In this chapter vibrational analysis of the emission bands of isotopically enriched $^{81}Br_2$ and natural bromine in the region 2950-2600 Å, and the transient absorption bands of Br_2 in the region 2870-2410 Å obtained by flash photolysis is reported. The emission and the transient absorption bands are found to correspond to the same system. The transient absorption spectrum has greatly helped in extending the vibrational analysis to higher vibrational levels of the upper state.

3.2 Experimental Details

The vibrational band system emitted by Br_2 in presence of argon in the region 2950-2600 Å was photographed at IIT Kanpur on a Jarrell-Ash 3.4m Ebert grating spectrograph

in the second order at a reciprocal dispersion of about 2.5 Å/mm. Uncondensed transformer discharge was used to excite the system as described in Chapter 2. The spectrum was recorded on Kodak 103-O plate. Reference lines were obtained from an iron-neon hollow cathode lamp. After every three hours of discharge fresh quantities of Br_2 and Ar were introduced into the discharge tube.

A few hundred milligrames of $Na^{81}Br$ procured from Oak Ridge National Laboratory was oxidized by heating it in an excess of dry chromium trioxide. $^{81}Br_2$(~ 90%) was collected at liquid nitrogen temperature on a vacuum line. $^{81}Br_2$ thus obtained was transferred at a desired pressure to a quartz discharge tube fitted with fused-in quartz windows. Relative pressures of $^{81}Br_2$ and Ar in the discharge tube were varied to obtain optimum relative pressures. It was found that 2 to 4 Torr of $^{81}Br_2$ in 250 Torr of Ar gives the best emission of the 2950-2600 Å system. The emission spectrum of $^{81}Br_2$ was obtained by external excitation of $^{81}Br_2$ (2 Torr of $^{81}Br_2$ in 250 Torr of Ar) by a radio frequency (r.f.) oscillator. The spectrum was photographed on a 7.3 m Ebert vacuum grating spectrograph in the second order at a reciprocal dispersion of about 2.3 Å/mm. Kodak 103-O plates were used to record the spectrum. An iron-neon hollow cathode lamp was used to get the reference lines.

The plates were measured at IIT Kanpur using a Carl-Zeiss Abbe comparator having a least count of one micron. The standard wavelengths were taken from tables of Crosswhitte[59,60]. The wavelengths and wave numbers of all the band heads were obtained using a large number of standard lines by least squares method programmed in FORTRAN 10 on DEC-1090 computer of this Institute. The vacuum corrections of Eldén[61] were applied. The accuracy of the measurements is limited by the widths of the spectral features observed, but for the sharper features the measurements are accurate to ~ 0.5 cm^{-1}.

The transient absorption spectrum of Br_2 in presence of nitrogen was photographed using the second order of a 6.6m Eagle spectrograph at a reciprocal dispersion of about 1.2 Å/mm. The absorption cell was equiped with multiple reflection mirrors. Partial pressures of Br_2 and N_2, and also the time delay between the maximum of the photolysis flash and the maximum of the continuum were varied to record transient absorption spectrum. It was found that 10 Torr of Br_2 in 290 Torr of N_2 gives the best transient absorption spectrum with a time delay of about 8 μs. The photolysis flash consisted of one 20 cm lamp fired by a 72 μF condenser charged to 5.5 KV. A Lyman flash lamp was used as the source of continuum. Up to 200 Joules per flash were dissipated in the lamp. Four traversals of the absorption cell were used and about 80 flashes were necessary to give a good exposure.

The mixture of Br_2 and N_2 was replaced by a fresh one after every 10 flashes. An iron hollow cathode lamp filled with neon was used to provide a reference spectrum. The r.f. discharge spectrum and the transient absorption spectrum were photographed by Professor Venkateswarlu at Herzberg Institute of Astrophysics, NRC, Ottawa, Canada. The plates containing the transient absorption spectrum were measured at Ottawa on a photoelectric comparator of the Tomkins-Fred type[62].

3.3 Vibrational Analysis

The band systems in the emission spectrum of Br_2 and $^{81}Br_2$ are shown in Fig 3.1 and Fig 3.2 respectively. The transient absorption band system of photoflashed Br_2 is shown in Fig 3.3. Air wavelengths of few lines of the reference spectrum are mentioned in the Figures. Most of the band heads are sharp and red degraded. However, there are some violet degraded and spike-like features in the long wavelength region. These features may be due to the dependence of the rotational and distortion constants of the levels on vibrational quantum number v.

Bromine has three isotopic species $^{81}Br_2$, $^{79}Br^{81}Br$ and $^{79}Br_2$ with ratio of natural abundances as 1:2:1. Band heads due to different isotopic species were found in the vibrational spectrum of Br_2. The vibrational assignments, intensities (estimated in visual scale 0-10), vacuum wavenumbers of the

observed band heads and their deviations($\Delta\nu$) from the calculated positions of the band heads for the three isotopic species in the emission and the transient absorption band systems are mentioned in Table 3.1 and Table 3.2 respectively. The band heads having deviations upto 3.6 cm^{-1} for the emission spectrum and upto 5 cm^{-1} for the transient absorption spectrum were used to get the vibrational constants for the upper and lower states. The band heads reported by Briggs and Norrish[54] were also fitted in the vibrational scheme. Except 6 band heads at 34951 ,39462,39849,40353,40857 and 40975 cm^{-1} all other 44 band heads could be fitted with deviations ($\Delta\nu$) below 6 cm^{-1} which is the stated[54] accuracy of their measurement. The vibrational assignments, vacuum wavenumbers and deviations of the transient absorption band system reported by Briggs and Norrish[54] are given in Table 3.3.

The Deslandres array (Fig 3.4) of the bands of $^{79}Br^{81}Br$ shows a reasonable correlation of the emission and transient absorption spectrum. The intensity distribution and Condon parabola of the emission system of $^{79}Br^{81}Br$ are shown in Fig 3.5. The v' =0 progression is unbroken and accounts for a large fraction of the total intensity. v' = 1 progression has comparatively weaker intensity and so on. The final vibrational constants were obtained by simultaneous least squares fit of all the band heads of the three isotopic species to the following polynomial in $\rho(v'+ 1/2)$ and $\rho(v'' +1/2)$:

$$\nu = \Delta T_e + \sum_{i=1}^{m} C'_{vi}[\rho(v'+\tfrac{1}{2})]^i - \sum_{j=1}^{n} C''_{vj}[\rho(v''+\tfrac{1}{2})]^j \quad (3.1)$$

where ρ is the usual isotopic ratio[5], $(\mu/\mu')^{\frac{1}{2}}$.

Equation (3.1) representing the vibrational band system corresponding to two electronic states can be expressed by a single matrix equation as

$$\underline{Y} = \underline{X}\,\underline{B} + \underline{E} \quad (3.2)$$

where $\underline{Y}$ is a column vector containing the M (= total number of band heads of the three isotopic species) known positions of the band heads (ν). $\underline{E}$ is the column vector containing M unknown measurement errors. For m = 3 and n = 4, $\underline{B}$ will be a column vector containing the required vibrational constants $\Delta T_e, C'_{v1}, C'_{v2}, C'_{v3}, C''_{v1}, C''_{v2}, C''_{v3}$ and C''_{v4}. $\underline{X}$ is a M×8 known coefficient matrix having 8 elements of each row as $1, \rho(v'+1/2), \rho^2(v'+1/2)^2, \rho^3(v'+1/2)^3, -\rho(v''+\frac{1}{2}), -\rho^2(v''+1/2)^2, -\rho^3(v''+1/2)^3$ and $-\rho^4(v''+1/2)^4$.

The least squares values $\underline{B}$ of the vibrational constants are[63-65]

$$\underline{B} = (\underline{X}^T\,\underline{X})^{-1}\,\underline{X}^T\,\underline{Y} \quad (3.3)$$

and the corresponding variance-covariance matrix is

$$\underline{V} = \sigma^2(\underline{X}^T\,\underline{X})^{-1} \quad (3.4)$$

with the estimated variance as

$$\sigma^2 = (\underline{Y} - \underline{X}\,\underline{B})^T(\underline{Y} - \underline{X}\,\underline{B})/(M-8). \quad (3.5)$$

The difference between observed and calculated positions ($\Delta\nu$) are obtained from ($\underline{Y} - \underline{X}\,\underline{B}$). The above simultaneous fit of the band heads will distribute the errors in measurement of the band heads among the two electronic states so that the errors in the values of individual constants of both the states get minimized simultaneously. The precision of the estimates of $\underline{B}$ is indicated by their standard errors, which are the square roots of diagonal elements of the variance-covariance matrix associated with $\underline{B}$.

To calculate the vibrational constants the matrix $\underline{X}$ was generated in the computer program (written in FORTRAN) from the known values of ρ, v' and v'' corresponding to different band heads and then $\underline{B}$, $\underline{V}$, σ and ($\underline{Y} - \underline{X}\,\underline{B}$) were calculated using DEC -1090 computer. To get the vibrational constants of $^{81}Br_2$, $\underline{B}$ was calculated taking ρ as 1.000000, 1.006309 and 1.012579 for $^{81}Br_2$, $^{79}Br^{81}Br$ and $^{79}Br_2$ respectively. Taking ρ as 0.993730 for $^{81}Br_2$, 1.000000 for $^{79}Br^{81}Br$ and 1.006231 for $^{79}Br_2$, $\underline{B}$ for $^{79}Br^{81}Br$ was calculated. Similarly $\underline{B}$ for $^{79}Br_2$ was calculated taking ρ as 0.987577 for $^{81}Br_2$, 0.993808 for $^{79}Br^{81}Br$ and 1.000000 for $^{79}Br_2$.

3.4 Results and Discussion

The vibrational constants for $^{81}Br_2$, $^{79}Br^{81}Br$ and $^{79}Br_2$ obtained in this work are given in Table 3.4. The σ of the

fit was about 1.3 cm^{-1}. In the same table the vibrational constants for $^{79}Br_2$ have also been compared with those of Ref.(58) obtained by analysing about 80 band heads in the emission spectra of different isotopic species of Br_2 with v' varying between 0 to 6. Though the value of ΔT_e in the present work is almost the same as that of Ref.(58), the other constants differ. This is due to the fact that the present analysis includes more bands than that used in Ref.(58). The use of transient absorption data of photo-flashed Br_2 has also helped to extend the analysis to include the transitions involving lower state vibrational levels down to v'' = 0 and upper state vibrational levels up to v' = 46.

The emission spectrum completely overlaps the transient absorption spectrum and the wavenumbers of a large number of emission and absorption bands agree within our experimental accuracy. All the bands were also found to fit into a single vibrational scheme. These facts show that the emission and the transient absorption bands arise out of one and the same transition.

On comparing the lower state vibrational quanta ($\Delta G''_{v+\frac{1}{2}}$ values) with those of the known[37,66-68] X $^1\Sigma_g^+$, A $^3\Pi_{1u}$ and B $^3\Pi_{0_u^+}$ states of Br_2 it is inferred that the lower state is not one of them. Again, in the flash photolysis experiment it has been observed that the transient absorption spectrum could be obtained even with a

time delay as high as 50μs. It is, therefore, expected that the transient absorption of photoflashed Br_2 should preferably originate from a metastable state of Br_2. So, among the low lying valence states which may be stable, $A'\,^3\Pi_{2u}$ arising out of the configuration $(\sigma_g)^2(\pi_u)^4(\pi_g)^3(\sigma_u)^1$ which in Mulliken's notation is abbreviated as 2431 may be assigned to the present system, the higher state of the transition being one of the low lying ion pair states (D'). This designation is also consistent with the absence of intensity alternation in the rotational structure of the bands as discussed in Chapter 4.

3.5 Conclusion

In this work it could be shown that the emission system of Br_2 as well as the transient absorption system of photoflashed Br_2 correspond to the same system. The lower state of the system has been identified as $A'\,^3\Pi_{2u}$. The vibrational analysis has been extended over a greater region to include the transitions involving lower state vibrational levels down to $v'' = 0$ and upper state vibrational level up to $v' = 46$.

TABLE 3.1 Vibrational Assignments, Relative Intensities, Vacuum Wavenumbers and Deviations (observed-calculated) of the Bandheads in the 2900 Å Emission System of Br_2

v',v''	$^{81}Br_2$			$^{79}Br^{81}Br$			$^{79}Br_2$		
	I*	ν (cm^{-1})	$\Delta\nu$ (cm^{-1})	I*	ν (cm^{-1})	$\Delta\nu$ (cm^{-1})	I*	ν (cm^{-1})	$\Delta\nu$ (cm^{-1})
2,18				1	33862.9	-2.8			
1,16				1	33867.6	-1.1			
4,23				1	33874.7	-0.7			
2,17				1	33938.4	-0.1	1	33930.6	-2.0
1,15				2	33952.5	-0.2			
2,16				3	34015.4	-1.4	2	34009.5	-1.3
3,18	2	34017.6	-0.4						
1,14				3	34041.0	-1.4	1	34034.3	-1.1
3,17	3	34091.0	0.1	5	34082.4	-3.4			
0,12				6	34091.0	1.0	5	34082.4	0.0
2,15							6	34091.0	-3.6
5,21				2	34120.5	0.7			
1,13	7	34142.3	-2.3	7	34135.5	-2.2	4	34131.3	0.4
3,16				4	34162.7	-1.5			
4,18	3	34163.5	-0.3						
2,14	8	34193.7	-2.9	9	34190.3	-0.1	8	34185.8	1.4
0,11	9	34201.9	-2.1	10	34198.0	1.4			
6,22	2	34216.8	2.4						
4,17	5	34237.3	0.6						
1,12	9	34244.1	-1.4						
3,15	8	34250.9	-2.5	9	34247.5	-0.6	9	34242.6	-0.4
6,21	4	34267.9	1.5	3	34268.3	3.3			
7,24	4	34267.9	-0.3	3	34268.3	-0.5			
2,13	3	34292.5	0.7	3	34284.2	-1.6			
5,18	6	34307.1	-1.7						

* I = Estimated intensity in visual scale 0-10.

Table 3.1 Continued

v',v''	$^{81}Br_2$			$^{79}Br^{81}Br$			$^{79}Br_2$		
	I	ν (cm^{-1})	$\Delta\nu$ (cm^{-1})	I	ν (cm^{-1})	$\Delta\nu$ (cm^{-1})	I	ν (cm^{-1})	$\Delta\nu$ (cm^{-1})
0,10	10	34314.0	-1.9	10	34308.2	-0.6			
4,16	10	34314.0	-1.1	10	34308.2	-2.6			
6,20	5	34326.4	2.9						
3,14				4	34336.1	-1.7			
1,11				4	34347.1	1.7			
5,17	8	34379.8	-1.9	7	34380.9	2.5			
2,12	5	34389.4	-3.2						
4,15	4	34398.9	-0.2						
0, 9	10	34434.4	1.3	9	34428.1	1.7			
6,18	8	34452.5	-0.6						
5,16				6	34455.6	-1.2			
8,23				6	34455.6	0.8			
7,20	6	34466.8	-0.3	6	34469.7	3.5			
4,14	3	34489.3	0.6	4	34483.1	-1.3			
2,11				3	34496.0	2.6			
7,19	5	34530.2	0.9	4	34526.5	-1.6			
5,15				3	34539.9	-0.8			
0,8	4	34555.4	-0.2	5	34551.1	1.7			
8,21				4	34556.9	3.6			
9,24				4	34556.9	1.3			
1,9				2	34577.1	1.9	2	34572.9	3.4
4,13				2	34582.1	2.3			
7,18				5	34595.9	0.5			
9,23				5	34595.9	-2.0			
8,20				4	34612.1	2.1			
3,11	2	34643.9	-1.6						
9,22	2	34643.9	0.7						
8,19	4	34671.3	-0.9	2	34673.0	1.1			
0,7				4	34680.1	2.6	2	34673.0	1.1
4,12				4	34680.1	-0.7			
6,15	3	34688.2	-0.3						
1,8	5	34704.5	1.1	3	34698.9	0.8	5	34693.8	0.9

Table 3.1 Continued

v',v''	$^{81}Br_2$			$^{79}Br^{81}Br$			$^{79}Br_2$		
	I	ν (cm^{-1})	$\Delta\nu$ (cm^{-1})	I	ν (cm^{-1})	$\Delta\nu$ (cm^{-1})	I	ν (cm^{-1})	$\Delta\nu$ (cm^{-1})
9,21				3	34698.9	2.6			
10,24				3	34698.9	0.9			
2,9				2	34722.8	-0.4			
8,18				3	34740.7	1.5			
10,23				3	34740.7	0.5			
3,10	0	34757.7	0.4	2	34754.7	1.7			
9,20				2	34754.7	1.7			
0,6				5	34812.5	1.9			
8,17				5	34812.5	0.6			
2,8	1	34852.5	1.9	2	34848.4	2.2			
3,9	1	34874.3	-0.3	2	34872.2	1.6			
6,13	1	34874.3	0.9						
11,23				4	34883.8	2.0			
9,18	3	34883.7	1.8						
10,20	1	34896.9	3.2	1	34893.8	-1.6			
4,10				1	34897.8	-1.8			
9,17				2	34954.1	-0.9			
10,19	2	34959.3	3.4						
6,12	3	34976.2	2.0	5	34974.5	2.5			
2,7	3	34976.2	-2.0	5	34974.5	0.2			
8,15				5	34974.5	0.3			
12,24	3	34976.2	0.6						
11,21				2	34982.6	2.3			
7,13	1	35014.7	-2.3						
12,23				4	35021.6	-1.0			
4,9	1	35023.6	3.3						
10,18	1	35023.6	0.2						
9,16	0	35031.5	-1.7						
5,10				3	35045.0	-0.6			
12,22				4	35071.6	2.1			

Table 3.1 Continued

v',v''	$^{81}Br_2$			$^{79}Br^{81}Br$			$^{79}Br_2$		
	I	ν (cm^{-1})	$\Delta\nu$ (cm^{-1})	I	ν (cm^{-1})	$\Delta\nu$ (cm^{-1})	I	ν (cm^{-1})	$\Delta\nu$ (cm^{-1})
13,25	0	35074.0	-2.6						
6,11				2	35081.6	3.0			
10,17	1	35094.0	-2.3	1	35095.8	-1.5			
1,5	1	35098.6	-2.1	1	35095.8	-1.5			
11,19	1	35098.6	2.0						
2,6	2	35111.8	1.1	4	35106.8	-0.7			
13,24	2	35111.8	-3.1						
3,7	2	35123.9	-0.7	3	35124.9	3.2			
12,21				3	35124.9	3.6			
4,8				1	35143.4	3.2			
8,13				1	35160.6	1.4			
13,23				1	35160.6	-2.2			
9,14	1	35208.9	2.0						
7,11	1	35222.5	-1.7	1	35224.8	1.7			
11,17	1	35238.1	1.1						
12,19	1	35238.1	1.4						
3,6				3	35257.2	2.4			
10,15				3	35257.2	-2.4			
14,24				3	35257.2	-2.7	1	35267.5	1.1
4,7	0	35269.4	-1.0	1	35267.5	-0.8			
5,8	0	35286.4	-1.4						
9,13	1	35304.0	1.9						
12,18	1	35304.0	-0.2	4	35305.8	-1.2			
11,16	1	35315.2	-0.3						
13,20	1	35315.2	1.4						
7,10	1	35335.7	-0.4	3	35337.6	2.3			
10,14	1	35349.6	1.2						
15,25	1	35349.6	-3.4						
8,11	1	35370.7	3.6						
12,17	3	35376.5	-0.6						

Table 3.1 Continued

v^{i},v^{ii}	$^{81}Br_2$			$^{79}Br^{81}Br$			$^{79}Br_2$		
	I	ν (cm^{-1})	$\Delta\nu$ (cm^{-1})	I	ν (cm^{-1})	$\Delta\nu$ (cm^{-1})	I	ν (cm^{-1})	$\Delta\nu$ (cm^{-1})
13,19	3	35376.5	0.5						
2,4				1	35388.3	0.5			
4,6	2	35402.0	-0.9	3	35402.4	0.9			
9,12	2	35402.0	-0.9	3	35402.4	-0.9			
5,7	0	35415.6	0.2						
6,8	2	35433.5	1.3	1	35430.2	-1.2			
15,23	2	35433.5	-0.5	1	35442.9	2.1			
10,13				1	35442.9	-1.7			
12,16				3	35457.5	-0.6			
14,20				3	35457.5	0.2			
8,10	1	35480.3	1.3						
15,22	1	35480.3	-0.9						
11,14	2	35490.3	1.2						
16,25				2	35495.9	-2.7			
13,17	0	35514.3	-2.1						
14,19	0	35514.3	-0.2						
3,4	1	35534.7	-1.3						
15,21	1	35534.7	1.5	3	35541.6	2.3			
12,15				3	35541.6	-0.5			
4,5	1	35541.3	1.2						
6,7	0	35559.9	0.2						
16,23	1	35573.3	2.2	1	35581.1	2.4			
7,8	1	35578.7	2.9						
11,13	0	35586.3	1.9						
8,9				3	35597.5	0.8			
13,16				3	35597.5	-0.7			
15,20				3	35597.5	1.5			
14,17				2	35659.7	0.4			
15,19				2	35659.7	1.8			

Table 3.1 Continued

v',v''	$^{81}Br_2$			$^{79}Br^{81}Br$			$^{79}Br_2$		
	I	ν (cm^{-1})	$\Delta\nu$ (cm^{-1})	I	ν (cm^{-1})	$\Delta\nu$ (cm^{-1})	I	ν (cm^{-1})	$\Delta\nu$ (cm^{-1})
16,21	1	35671.8	1.5						
17,24				1	35672.0	-1.6			
5,5				4	35687.7	2.4			
11,12				4	35687.7	0.5			
7,7	1	35705.7	2.3	1	35706.7	2.7			
17,23	1	35705.7	-1.7	1	35714.2	-1.6			
14,16				1	35734.0	-3.6			
16,20				1	35734.0	0.1			
17,22	1	35757.3	2.7	1	35765.5	2.9			
10,10				1	35765.5	1.1			
16,19	1	35788.3	-1.2	1	35797.4	1.6			
11,11				1	35797.4	3.5			
15,17				1	35797.4	-0.5			
14,15				2	35818.9	-2.7			
3,2				3	35830.1	-2.4			
6,5	2	35832.1	2.7	3	35830.1	-0.4			
12,12				3	35830.1	2.0			
18,23				1	35852.2	0.0	1	35858.3	-3.1
9,8	1	35862.2	1.3						
13,13	1	35862.2	-1.5	1	35868.2	1.0			
17,20	1	35862.2	-1.5						
15,16				1	35877.7	1.4			
14,14	0	35908.2	1.2						
18,21	1	35941.2	-1.1						
4,2	1	35975.4	-2.0						
5,3				3	35975.8	1.4			
7,5	1	35975.4	2.3	3	35975.8	0.8			
19,23				0	35988.8	1.0	0	35999.5	1.7
18,20	0	35996.0	-3.3						
17,18				0	35999.5	-0.7			

Table 3.1 Continued

v',v''	$^{81}Br_2$			$^{79}Br^{81}Br$			$^{79}Br_2$		
	I	ν (cm^{-1})	$\Delta\nu$ (cm^{-1})	I	ν (cm^{-1})	$\Delta\nu$ (cm^{-1})	I	ν (cm^{-1})	$\Delta\nu$ (cm^{-1})
10,8	0	36005.3	2.9						
16,15	1	35092.1	-0.2						
14,12				1	36104.2	-3.4			
8,5				3	36121.1	2.3			
20,23	1	36112.3	0.3	3	36121.1	-1.6	1	36130.6	-2.8
18,18				1	36137.3	0.7			
15,13	1	36139.5	-0.6						
11,8				1	36149.4	2.8			
17,16				1	36149.4	-1.9			
16,14	1	36181.1	-0.9						
14,11	1	36212.3	2.8	1	36214.4	0.2			
20,21	1	36212.3	1.1						
21,24				1	36214.4	-0.2			
17,15				1	36234.1	-1.2			
15,12				2	36246.9	0.7			
7,3				3	36264.3	0.2			
9,5				3	36264.3	2.5			
10,6	2	36263.4	0.9						
19,18	2	36263.4	-0.4	1	36271.7	-0.5	1	36280.9	0.3
16,13				1	36280.0	-3.1			
21,22	0	36295.7	3.1						
15,11				1	36353.6	0.7			
21,21				1	36353.6	-1.7			
18,15	2	36361.3	-3.0						
8,3	2	36402.7	-0.8	2	36406.8	-1.1			
11,6	2	36402.7	-0.5						
20,18				2	36406.8	-0.3			
21,18	0	36528.5	-2.8						
10,4	1	36538.8	-2.5						
11,5	1	36538.8	-1.6						

Table 3.1 Continued

v',v''	$^{81}Br_2$			$^{79}Br^{81}Br$			$^{79}Br_2$		
	I	ν (cm^{-1})	$\Delta\nu$ (cm^{-1})	I	ν (cm^{-1})	$\Delta\nu$ (cm^{-1})	I	ν (cm^{-1})	$\Delta\nu$ (cm^{-1})
9,3				3	36552.3	1.3			
12,6				3	36552.3	3.6			
21,17				1	36611.4	-2.5			
17,11	0	36621.9	1.1						
18,12				0	36659.6	2.0			
11,4				2	36686.9	-1.3			
12,5				2	36686.9	0.3			
10,3	1	36687.6	0.4	1	36695.2	1.9			
14,7	1	36687.6	-1.0	1	36695.2	0.1			
21,13	0	36952.5	1.0						
8,1				1	36709.8	-3.1			
11,3				2	36836.5	1.6			
15,7				2	36836.5	2.7			
21,14				0	36866.7	0.8			
13,4				1	36970.7	1.5			
16,7				1	36970.7	-1.0			
15,5				1	37102.2	-2.6			
16,6				1	37102.2	-2.6			
12,2				1	37127.5	1.1			
10,0				0	37155.2	-0.7			
15,3				0	37395.7	1.8			
16,3				0	37531.6	-0.2			
15,2	0	37531.8	-1.7	1	37544.6	0.0			
20,6				1	37647.5	-1.3	1	37660.9	0.4
21,7				1	37647.5	-2.3			
18,4				1	37660.9	2.3			
15,0	0	37846.5	2.9	1	37858.0	1.5			
18,2	0	37944.2	1.6						
17,1				1	37976.9	3.0			
16,0				0	37992.8	-1.6			
19,2				0	38091.3	-0.3			
21,1				0	38515.2	0.3			

TABLE 3.2 Vibrational Assignments, Relative intensities, Vacuum Wavenumbers and Deviations (observed-calculated) of the Bandheads in the Transient Absorption System of Br_2 near 2900 Å.

v',v''	$^{81}Br_2$			$^{79}Br^{81}Br$			$^{79}Br_2$		
	I*	ν (cm^{-1})	$\Delta\nu$ (cm^{-1})	I*	ν (cm^{-1})	$\Delta\nu$ (cm^{-1})	I*	ν (cm^{-1})	$\Delta\nu$ (cm^{-1})
1,7	1	34832.4	1.4						
1,6							1	34954.9	-0.4
2,7				1	34973.4	-0.9			
5,10	1	35052.5	4.4						
2,6				2	35104.9	-2.6			
3,6				3	35253.2	-1.6			
2,4				3	35385.7	-2.1			
4,6				2	35401.3	-0.2			
13,17							2	35523.9	0.5
4,5				5	35539.8	0.5			
5,6				2	35546.0	-1.4			
10,11				2	35651.8	-0.5			
4,4				5	35680.9	-0.9			
5,5				2	35685.3	0.0			
14,15				3	35818.2	-3.4			
4,3				6	35827.5	-1.0			
18,23	1	35843.8	0.8						
18,22	2	35889.8	-0.4						
6,4				9	35972.8	-0.1			
16,15	3	36091.7	-0.6						
6,3				8	36117.2	-2.4			
15,12				3	36246.9	0.7			
9,5				10	36261.8	0.0			
16,12	3	36378.7	0.7						
8,3				5	36407.1	-0.8			
17,12	3	36516.4	2.0						
10,4	7	36542.6	1.3						

* I = Estimated intensity in the visual scale 0-10

Table 3.2 Continued

v',v''	$^{81}Br_2$			$^{79}Br^{81}Br$			$^{79}Br_2$		
	I	ν) (cm^{-1})	$\Delta\nu$) (cm^{-1})	I	ν) (cm^{-1})	$\Delta\nu$) (cm^{-1})	I	ν) (cm^{-1})	$\Delta\nu$) (cm^{-1})
9,3				6	36551.0	0.0			
18,12				3	36659.6	2.0	1	36666.2	1.1
11,4				6	36687.2	-1.0			
10,3				2	36692.9	-0.4	1	36701.0	1.7
19,12							1	36800.4	-1.2
20,13				3	36827.2	0.1	6	36834.0	-2.1
11,3				6	36834.0	-0.9			
10,2				3	36841.6	-2.4			
12,3	3	36966.5	-1.5	5	36976.5	0.7	3	36983.4	-0.1
9,0							1	37020.9	-0.6
19,10							1	37020.9	-0.1
22,13				1	37093.1	-1.5			
14,4				4	37107.4	-1.2	2	37116.1	-1.0
12,2	2	37116.1	-1.7	2	37125.5	-0.9			
23,13	1	37211.4	-4.6						
15,4				4	37245.1	-2.1	3	37254.2	-2.3
13,2				4	37265.9	-0.6			
15,3	1	37382.1	-1.6	4	37394.7	0.8	3	37403.7	-0.3
14,2							2	37415.8	-0.3
13,1							1	37431.2	0.0
24,12				1	37456.8	-3.1			
27,16	0	37464.1	-2.7	1	37481.3	0.7			
25,13							2	37499.7	-2.7
18,5				1	37516.1	-0.1			
16,3				2	37531.4	-0.4			
15,2				4	37543.4	-1.2			
14,1				2	37559.9	-0.4	0	37570.4	-1.0
16,2	1	37670.9	0.3	5	37680.5	-2.0	2	37691.9	-2.3
15,1				2	37696.7	-2.2	1	37708.2	-2.6
17,2	2	37805.9	-1.1	5	37818.5	-1.1			

Table 3.2 Continued

v',v''	$^{81}Br_2$			$^{79}Br^{81}Br$			$^{79}Br_2$		
	I	ν (cm^{-1})	$\Delta\nu$ (cm^{-1})	I	ν (cm^{-1})	$\Delta\nu$ (cm^{-1})	I	ν (cm^{-1})	$\Delta\nu$ (cm^{-1})
16,1				4	37834.8	-2.0	1	37846.4	-3.1
18,2	1	37940.8	-1.8	6	37954.2	-1.8			
17,1				6	37972.6	-1.3			
16,0				0	37997.8	3.4			
25,8				1	38049.8	-0.5	1	38066.4	2.0
19,2	2	38075.8	-1.7	3	38089.9	-1.7			
18,1				6	38109.5	-0.8	3	38121.8	-2.7
23,5							0	38200.6	-0.6
21,3				2	38210.3	0.4	3	38222.1	-2.5
19,1	4	38231.6	0.7	7	38244.8	-1.1	3	38257.6	-3.3
18,0				0	38268.0	0.1			
23,4				1	38329.7	0.6			
34,16	1	38346.8	0.6						
20,1	3	38363.0	-2.0	6	38381.0	0.2	1	38397.6	1.1
19,0							1	38416.8	-2.7
27,7				1	38438.8	0.7			
30,10				2	38450.7	-2.3			
21,1	3	38497.5	-0.8	6	38516.2	1.3	2	38533.3	2.0
20,0				1	38541.4	3.0			
33,12				1	38610.0	-0.6			
22,1	3	38631.3	0.4	6	38649.6	1.4	1	38664.1	-1.3
23,1	1	38763.6	0.8	4	38781.2	0.4			
29,6	1	38810.4	0.7	0	38827.7	-0.7			
24,1	1	38897.8	3.9	3	38913.8	1.2			
23,0				1	38938.4	0.0			
29,5				0	38964.5	-1.2			
27,3							0	39012.4	-4.7
25,1				3	39045.1	1.5	1	39067.1	4.2

Table 3.2 Continued

v',v''	$^{81}Br_2$			$^{79}Br^{81}Br$			$^{79}Br_2$		
	I	ν) (cm^{-1})	$\Delta\nu$) (cm^{-1})	I	ν) (cm^{-1})	$\Delta\nu$) (cm^{-1})	I	ν) (cm^{-1})	$\Delta\nu$) (cm^{-1})
24,0				3	39072.3	2.1	2	39090.7	0.9
28,3				0	39124.7	-2.2			
35,9	1	39176.7	2.9						
25,0				3	39203.9	2.7	2	39224.4	2.9
28,2				0	39278.2	0.6			
26,0	1	39312.7	2.3						

TABLE 3.3 Vibrational Assignments Vacuum Wavenumbers and Deviations (observed-calculated) of the Bandheads of Transient Absorption System of Br_2 reported by Briggs and Norrish[54].

v',v''	$^{79}Br^{81}Br$		$^{79}Br_2$	
	$\tilde{\nu}$ (cm^{-1})	$\Delta\tilde{\nu}$ (cm^{-1})	$\tilde{\nu}$ (cm^{-1})	$\Delta\tilde{\nu}$ (cm^{-1})
0,6			34804	-1.6
1,5	35100	2.7		
2,5	35249	3.7		
2,4	35384	-3.8		
3,4	35534	-1.1		
4,4	35680	-1.8		
5,4	35824	-3.7		
6,4	35968	-4.9		
7,4	36118	0.6		
8,4	36259	-2.2		
8,3	36406	-1.9		
9,3	36548	-3.0		
10,3	36692	-1.3		
11,3	36834	-0.9		
12,3	36975	-0.8		
13,3	37117	1.1		
14,3	37254	-1.3		
14,2	37410	4.1		
15,2	37543	-1.6		
16,2	37679	-3.5		
17,2	37820	0.4		
18,2	37953	-3.0		
19,2	38090	-1.6		
20,2	38231	4.5		
20,1	38381	0.2		

TABLE 3.4 Vibrational Constants (cm^{-1}) of D' and A' States of Bromine

	Present Work			Ref.(58)
	$^{81}Br_2$	$^{79}Br^{81}Br$	$^{79}Br_2$	$^{79}Br_2$
ΔT_e	35705.55(36)	35705.55(36)	35705.55(36)	35705.97(78)
Upper State (D')				
C'_{v1} (ω'_e)	148.53(4)	149.46(4)	150.39(4)	150.863(10)
C'_{v2} ($-\omega'_e x'_e$)	-0.3441(25)	-0.3485(25)	-0.3529(25)	-0.3842(14)
C'_{v3} ($\omega'_e y'_e$)	$-5.385(396) \times 10^{-4}$	$-5.482(404) \times 10^{-4}$	$-5.588(411) \times 10^{-4}$	
Lower State (A')				
C''_{v1} (ω''_e)	159.57(15)	160.58(15)	161.58(15)	165.172(379)
C''_{v2} ($-\omega''_e x''_e$)	-1.349(24)	-1.368(24)	-1.384(25)	-2.504(71)
C''_{v3} ($\omega''_e y''_e$)	$-6.608(145) \times 10^{-2}$	$-6.727(148) \times 10^{-2}$	$-6.859(151) \times 10^{-2}$	0.05689(64)
C''_{v4} ($\omega''_e z''_e$)	$1.121(29) \times 10^{-3}$	$1.149(30) \times 10^{-3}$	$1.179(30) \times 10^{-3}$	$-4.624(276) \times 10^{-3}$

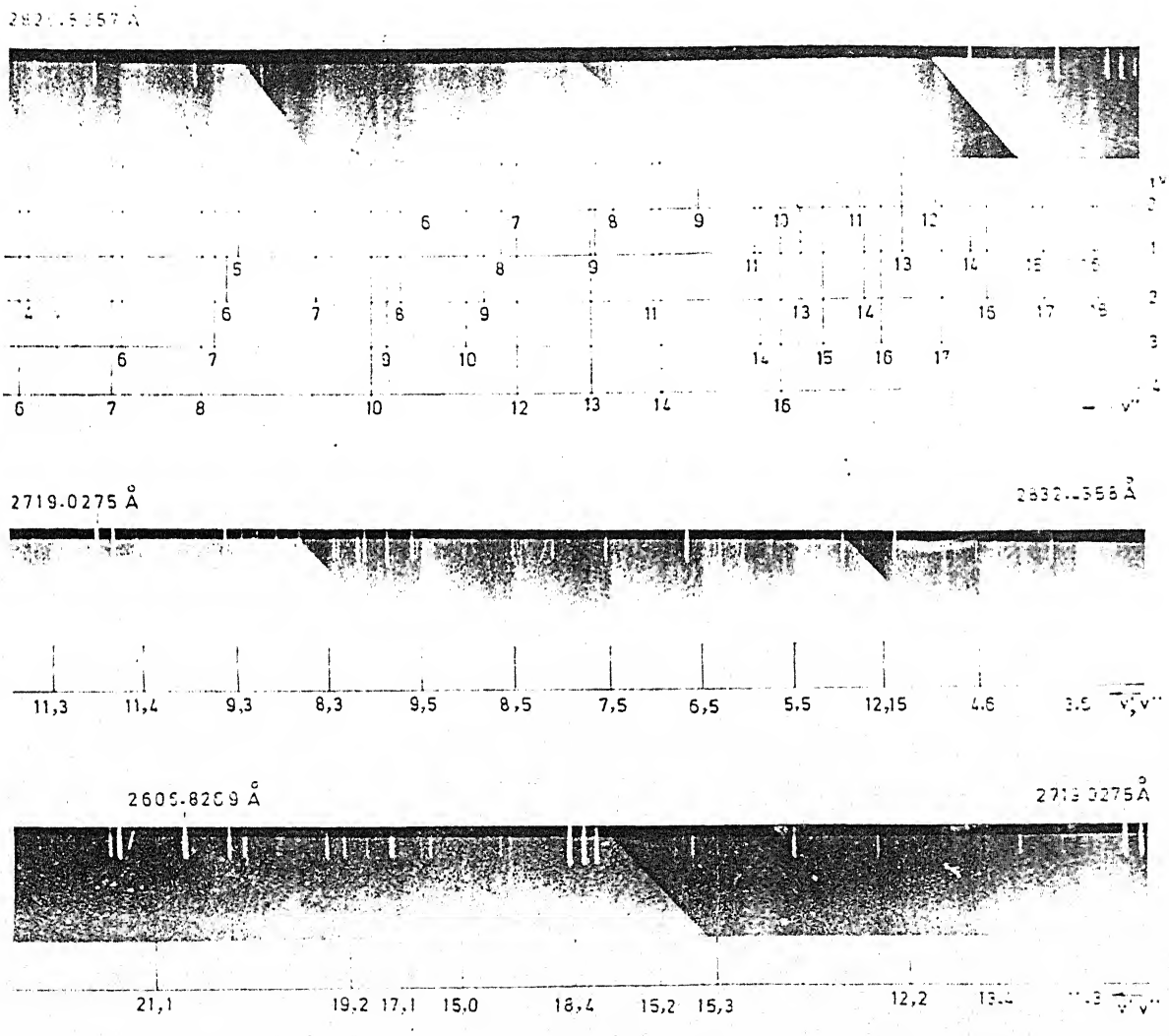

FIG. 3.1 D'—A' EMISSION BAND SYSTEM OF Br_2

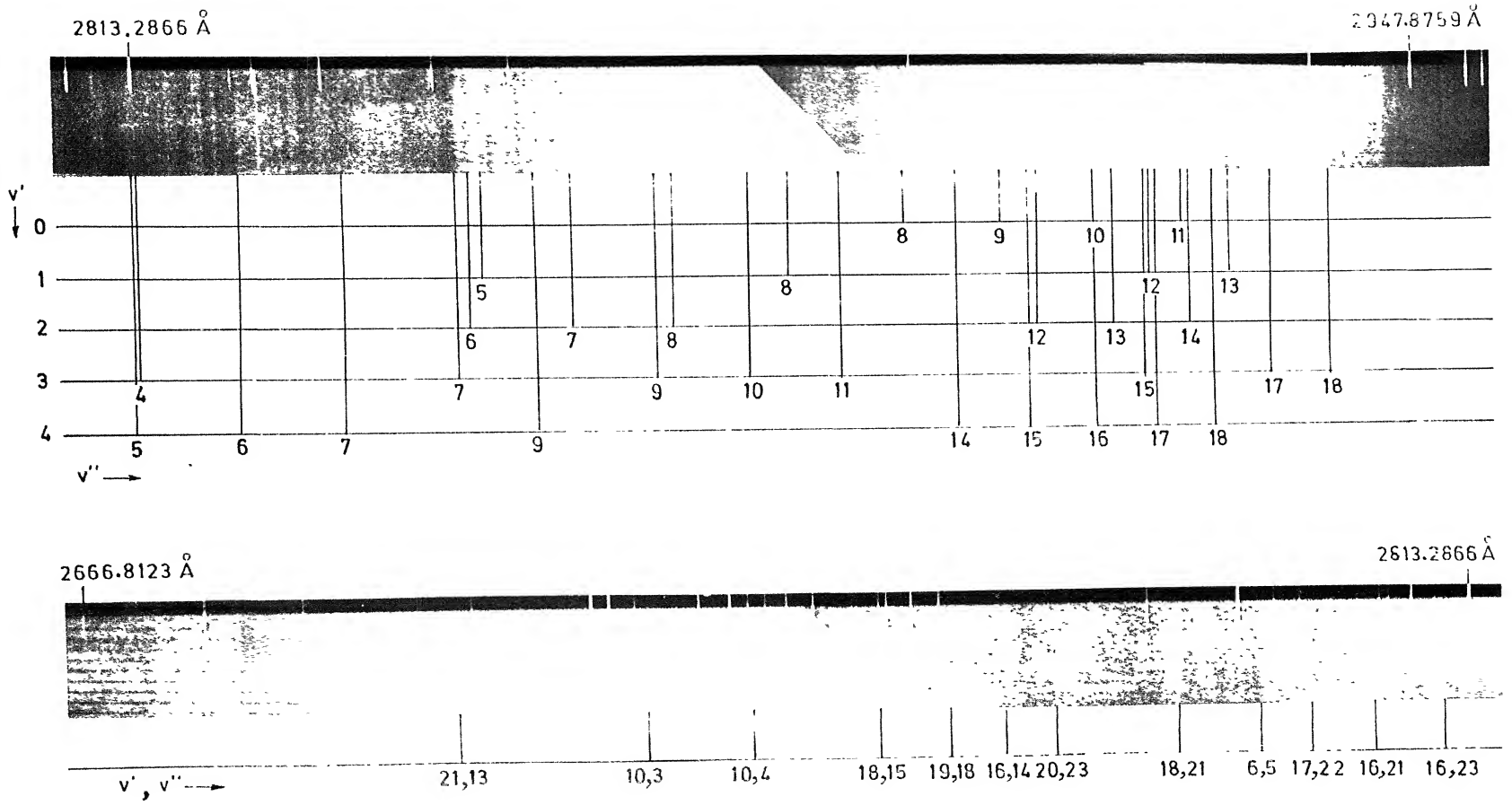

FIG 3.2 $D' \rightarrow A'$ EMISSION BAND SYSTEM OF $^{81}Br_2$

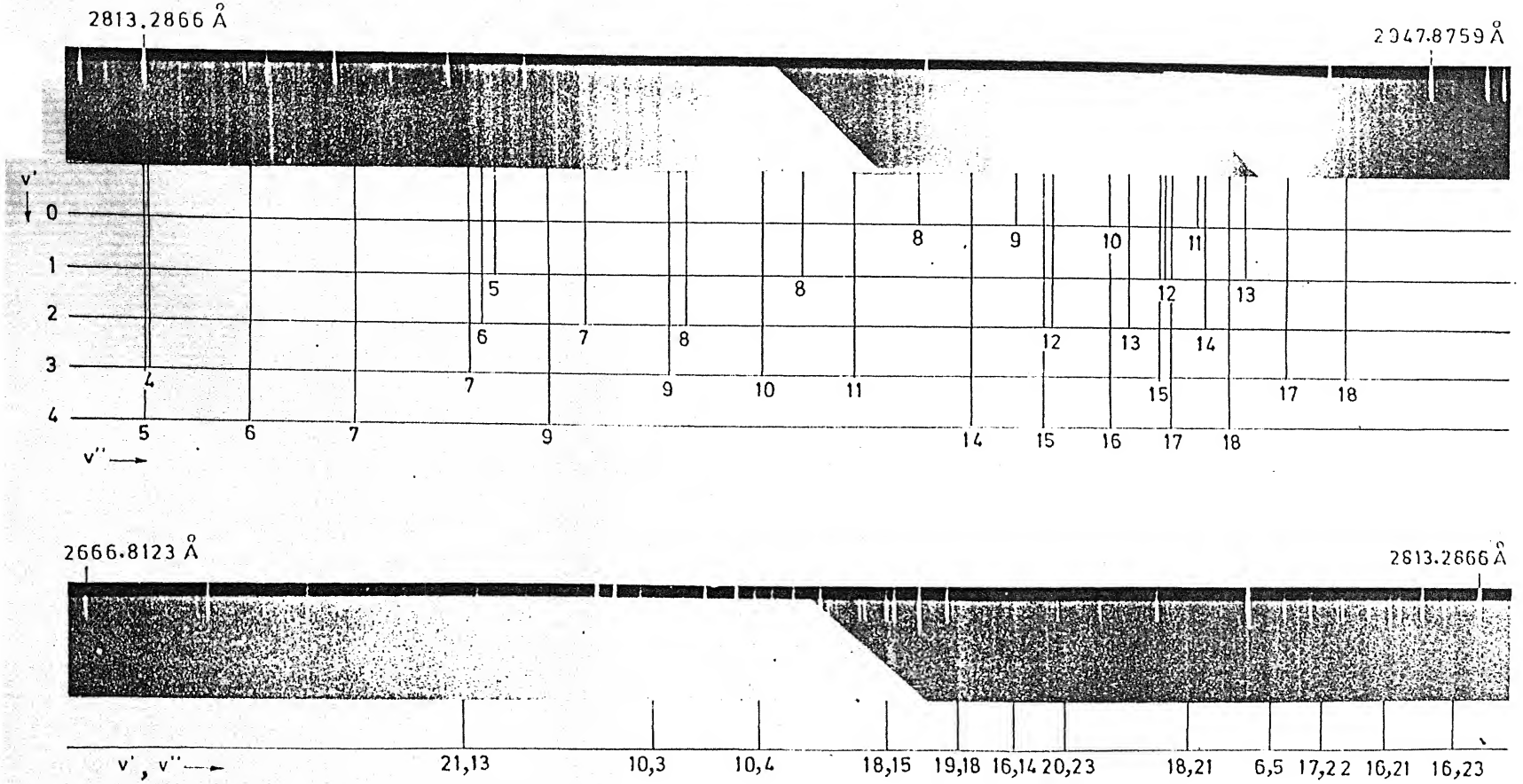

FIG. 3.2 D'—A' EMISSION BAND SYSTEM OF $^{81}Br_2$

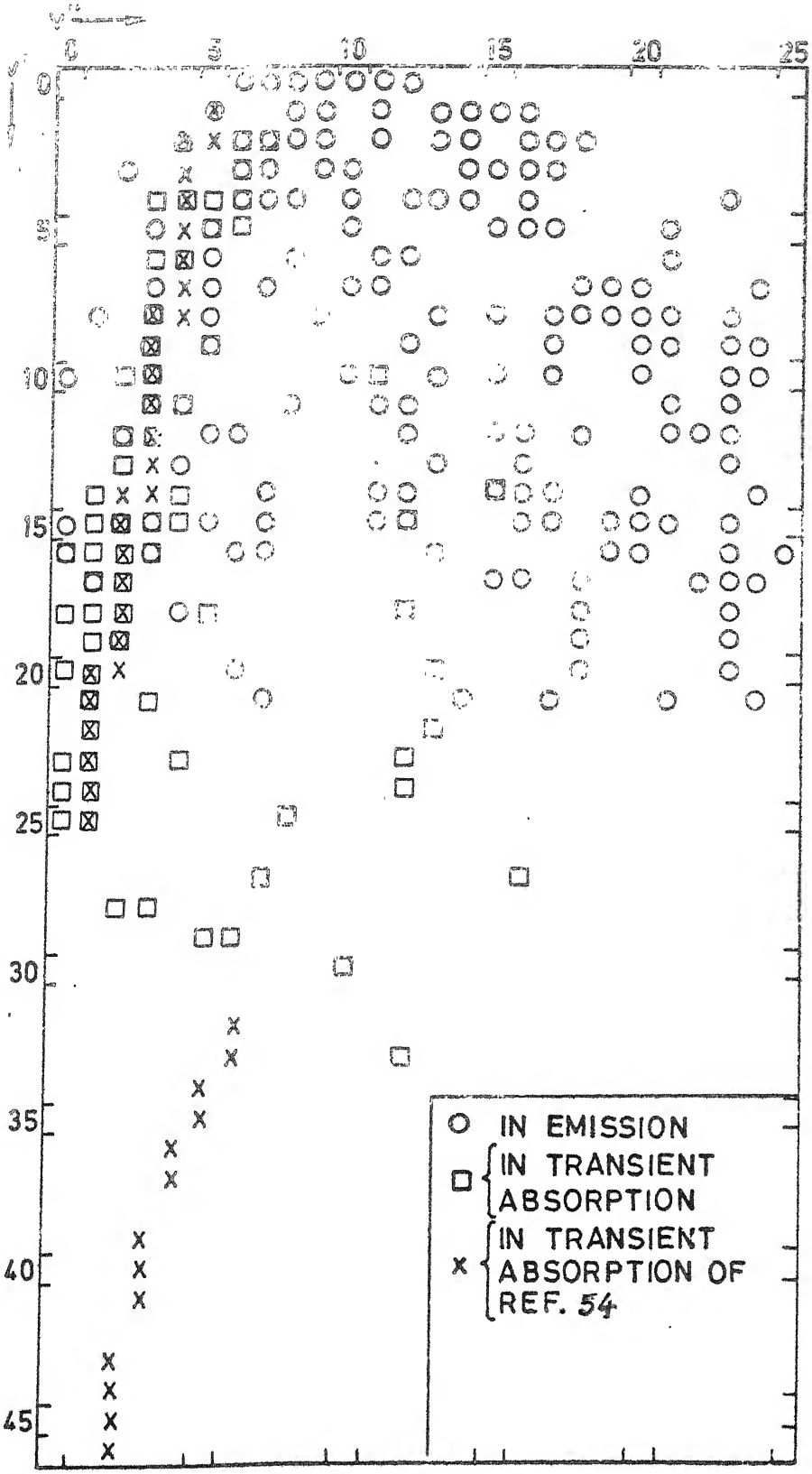

FIG. 3.4 DESLANDRES ARRAY OF D′—A′ BANDS OF ^{79}Br ^{81}Br

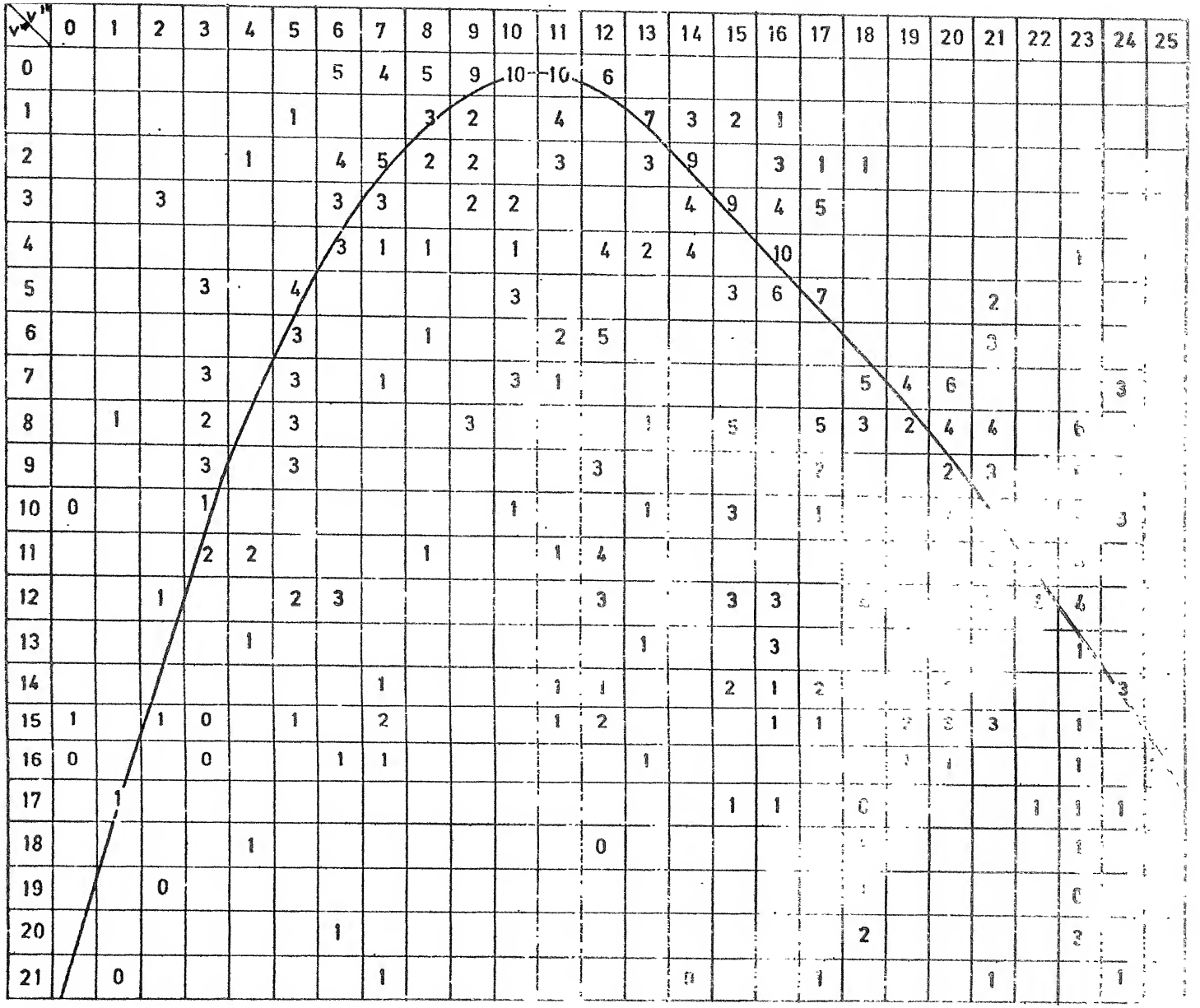

FIG. 3.5 THE INTENSITY DISTRIBUTION AND CONDON PARABOLA OF THE D'→A' EMISSION BAND SYSTEM OF $^{79}Br\ ^{81}Br$

CHAPTER 4

ROTATIONAL ANALYSIS OF D' → A' EMISSION SYSTEM OF $^{81}Br_2$

4.1 Introduction

The rotational structure of natural Br_2 is complex because of the overlap of the rotational transitions in the three isotopic species $^{81}Br_2$, $^{79}Br^{81}Br$ and $^{79}Br_2$ whose abundances are in the ratio 1:2:1. Therefore, the rotational structure of the separated isotopic species $^{81}Br_2$ has been studied. While the rotational analysis of the 2900 Å emission system of $^{81}Br_2$ was in progress in our laboratory Sur and Tellinghuisen reported[58] the results of their rotational analysis of 11 bands of $^{79}Br_2$ and 3 bands of $^{81}Br_2$. They recorded the spectrum of isotopically enriched $^{79}Br_2$ and $^{81}Br_2$ on a Jobin-Yvon HR1500 1.5 m Czerny-Turner spectrometer in the first order with a reciprocal dispersion of about

1.5 Å/mm. In this Chapter rotational analysis of 8 bands (0-8,0-9,0-10,0-11,1-8,1-12,3-5 and 4-5) of $^{81}Br_2$ recorded at a much higher dispersion and greater resolution is reported.

4.2 Experimental Details

Preparation of $^{81}Br_2$ from $Na^{81}Br_2$ has been described in Section 3.2 of Chapter 3. By varying the relative pressures of $^{81}Br_2$ and Ar in the quartz discharge tube, fitted with fused quartz windows, it was found that 2 to 4 Torr of $^{81}Br_2$ in 250 Torr of Ar gives the best emission spectrum. The emission spectrum of $^{81}Br_2$ in presence of Ar was excited by a radio frequency oscillator. The spectrum was photographed on a 7.3 m Ebert vacuum grating spectrograph in the 20th order and 21st order at reciprocal dispersion varying between 0.11 Å/mm to 0.09 Å/mm. Kodak 103-0 plates were used to record the spectrum. The exposure time varied from 10 minutes to 50 minutes depending upon the intensity and the region of the spectrum. Reference spectrum was obtained from an iron-neon hollow-cathode lamp. The spectrum was recorded by Professor Venkateswarlu at Herzberg Institute of Astrophysics, NRC, Ottawa, Canada, as such high resolution facilities are not available in this country. The spectral lines were measured at this Institute on a Carl-Zeiss Abbe comparator having a least count of one micron. The wavelengths and vacuum wavenumbers of all the rotational lines were obtained using a large number of lines of the reference

spectrum which were fitted to 4th and 5th order polynomials by least squares method programmed in FORTRAN on DEC-1090 computer of IIT Kanpur. The vacuum corrections of Eldén[61] were applied. The accuracy of the measurement is about ± 0.02 cm^{-1} for sharp lines.

4.3 Rotational Analysis

4.3.1 Rotational Structure

The rotational structures of the 8 bands studied (0-8, 0-9, 0-10, 0-11, 1-8, 1-12, 3-5, and 4-5) are shown in Figures 4.1, 4.2, 4.3 and 4.4. The rotational lines are resolved down to comparatively low values of J ranging from 4 to 9 in 6 of the 8 bands analysed. Band heads are formed in R branch and $\nu_R(J)$ coincides with $\nu_P(J-n)$, n varying from 6 to 10 for different bands. However, this overlapping occurs only upto relatively low $J(\leq 27)$ in 5 of the 8 bands. In the region of high J where P and R branches are resolved the R branch could easily be identified since the distance between consecutive R lines decreasesfaster than that between consecutive P lines because of the distortion effect which is proportional to $[J(J+1) - \Omega^2]^2$. In spite of the fact that Br_2 has a nuclear spin of (3/2) $\hbar$ no appreciable and systematic intensity alternation could be noticed in the rotational structure.

Since Br_2 is a comparatively large and heavy molecule, it tends to Hund's coupling case (c). So the rotational lines of a v' - v'' band will follow, as described in Chapter 1, the relationship

$$\nu = \nu_0 + B_v' K' - D_v' K'^2 - B_v'' K'' + D_v'' K''^2 \qquad (4.1)$$

where ν_0 is the origin of (v'-v'') band, $K = J(J+1) - \Omega^2$, B_v is the rotational constant and D_v is the first centrifugal distortion constant. Assuming the lower state to be $^3\Pi_{2u}$ and the transition as $2g \rightarrow 2u$ the value of Ω has been taken as 2.

The $^3\Pi - {}^3\Pi$ transitions can have four sub-bands corresponding to $0_g^+ - 0_u^+$, $0_g^- - 0_u^-$, $1_g - 1_u$ and $2_g - 2_u$ components. Each of the sub-bands consists of a strong R branch and a strong P branch. In the case of $1_g - 1_u$ and $2_g - 2_u$ sub-bands, there will also be a weak Q branch whose intensity is approximately proportional to

$$(1/J)\ \mathrm{Exp}\ [-F_v(J)\ hc/kT)]$$

where

$$F_v(J) = B_v K - D_v K^2 . \qquad (4.2)$$

So the intensity of the Q branch will fall off rapidly with increasing J. No Q branch could be noticed in the rotational structure of any of the bands.

4.3.2 Determination of J Numbering

Initially approximate rotational assignments of P and R branches were made by combination differences. From Equations (1.20) and (1.22) the following combination relations can be written after neglecting the effects due to centrifugal distortion(for low values of J):

$$\Delta_2 F'(J) = \nu_R(J) - \nu_P(J)$$

$$= F'_v (J+1) - F'_v (J-1)$$

$$\simeq 4 B'_v (J+\tfrac{1}{2}) \qquad (4.3)$$

$$\Delta_2 F'' (J) = \nu_R(J-1) - \nu_P(J+1)$$

$$= F''_v (J+1) - F''_v (J-1)$$

$$\simeq 4B''_v (J+\tfrac{1}{2}) \qquad (4.4)$$

By trial and error the relative J numbering was so adjusted that the $\Delta_2 F'$ values for all the bands with common upper level agree within the experimental errors. Similarly $\Delta_2 F''$ values should agree, within the experimental errors, for all bands having a common lower level. A graph of $\Delta_2 F(J)$ against $(J + \frac{1}{2})$ should be a straight line except for a slight departure at high J values due to the centrifugal distortion term D_v. The absolute J numbering could be obtained by laterally shifting the curve so that it passes through the point $J = -\frac{1}{2}$. Both the relative and absolute J

numberings were checked by band-by-band fit of the rotational lines as described in Section 4.4.1

4.4 Calculation of Rotational Constants

The rotational constants B_v and D_v of various levels can be calculated by least-squares fit of the data to the relation[5]

$$\Delta_2 F = (4 B_v - 6 D_v)(J + \tfrac{1}{2}) - 8 D_v (J + \tfrac{1}{2})^3. \qquad (4.5)$$

Then the constants $C_{r1}, C_{r2}, \ldots$ and $C_{d1}, C_{d2}, \ldots$ can be calculated using the least-squares fits of B_v and D_v values corresponding to different v values to Equations (1.15) and (1.16).

Now, the least-squares fit of the combination differences gives correlated[63-65] values for B_v' and B_v'' since the combination difference approach implicitly assumes that all the experimental errors are associated with one of the states. But in actual practice the errors are distributed between each pair of the states. So the calculated values of the rotational constants for a state must be dependent on the rotational constants of the other state. These correlated errors can be largely eliminated by merging[65] the results obtained by different individual band-by-band fits with proper statistical regard to different measurement precision and correlation.

4.4.1 Band-by-Band Least Squares Fits

In a particular band corresponding to an upper and a lower vibrational level and a series of rotational levels the fit of the band, under the assumption that the experimental errors of the lines in the band are randomly scattered with variance σ^2 and zero covariance, is the usual unweighted and uncorrelated least-squares solution of the over-determined matrix equation[65]

$$\underline{Y} = \underline{U}\,\underline{\beta} + \underline{\varepsilon} \qquad (4.6)$$

where $\underline{Y}$ is the column vector containing m (= total number of P and R lines) known measured line positions, and $\underline{\beta}$ and $\underline{\varepsilon}$ are the column vectors containing the five desired molecular constants ν_0, B'', B', D'', D', and m unknown measurement errors respectively. $\underline{U}$ is the known m x 5 coefficient matrix given by

$$\underline{U} = \begin{bmatrix} 1 & -K'' & K'_P & K''^2 & -K'^2_P \\ \vdots & & & & \\ \text{upto ml terms} & & & & \\ 1 & -K'' & K'_R & K''^2 & -K'^2_R \\ \vdots & & & & \\ \text{upto (m - ml) terms} & & & & \end{bmatrix} \qquad (4.7)$$

where ml is the number of P lines and $K''=[J(J+1) - \Omega^2]$, $K'_P = [(J-1)J - \Omega^2]$ and $K'_R = [(J+1)(J+2) - \Omega^2]$.

The resulting least-squares values $\underline{\beta}$ of the molecular constants are[65]

$$\underline{\beta} = (\underline{U}^T \underline{U})^{-1} \underline{U}^T \underline{Y} \qquad (4.8)$$

and the corresponding variance-covariance matrix is

$$\underline{V} = \sigma^2 (\underline{U}^T \underline{U})^{-1}$$

with estimated variance as

$$\sigma^2 = (\underline{Y} - \underline{U}\,\underline{\beta})^T (\underline{Y} - \underline{U}\,\underline{\beta})/(m-5) \qquad (4.9)$$

$(\underline{Y} - \underline{U}\,\underline{\beta})$ gives the deviation ($\Delta\nu$) of the observed line position from the calculated line position. Vacuum wavenumbers and the deviations of the rotational lines of the eight bands analysed are tabulated in Tables 4.2 to 4.9.

The band-by-band least squares fit of a particular band gives five estimated molecular constants $\underline{\beta}$ and the corresponding 5 x 5 variance - covariance matrix $\underline{V}$. In the computer program of band-by-band least squares fit the relative as well as the absolute J numberings could be changed to get best fit with minimum variance.

4.4.2 Merged Least Squares Fit

In the case of bands sharing an upper or a lower vibrational level the constants from the band-by-band least squares fits are merged to get the final constants. As for example, the band-by-band least-squares fits of 0-8, 0-9, 0-10,

0-11, 1-8, 1-12 give 30 values for the constants. Out of these 30 values there will be four values each for B_0' and D_0' obtained from 0-8, 0-9, 0-10 and 0-11 bands and two values each for B_1', D_1', B_8'' and D_8'' obtained from 1-8, 1-12 and 0-8 bands . These multiple values of different constants are not identical, as expected, due to the random measurement errors and different number of lines in each band. Thus we have to merge the 30 values from the six band-by-band fits to get the best, that is minimum variance, linear and unbiased (MVLU) values of the 20 molecular constants using the following method which accounts for the different precisions of the values and the non-zero correlation between them.

The merging of the 30 redundant values into 20 non-redundant values can be accomplished by a least squares solution to the over-determined 30 equations:

$$\underline{Y}^m = \underline{X}\,\underline{\beta}^m + \underline{\delta} \qquad (4.10)$$

which can be written in the form as shown in Table 4.1. The 30 elements of Y^m are the 30 constants obtained by individual band-by-band fits of the six bands. $\underline{\beta}^m$ represents the 20 non-redundant values of the unknown constants (ν_{0-8}, B_8'', B_0', D_8'', D_0', ν_{0-9}, B_9'', D_9'', ν_{0-10}, B_{10}'', D_{10}'', ν_{0-11}, B_{11}'', D_{11}'', ν_{1-8}, B_1', D_1', ν_{0-12}, B_{12}'' and D_{12}'') as shown in Table 4.1. For example, the 2nd and 22nd individual equations in the matrix Eq (4.10) (explained in Table 4.1) are

$$B''_{0-8} = B''_{8} + \delta_2 \tag{4.11}$$

$$B''_{1-8} = B''_{8} + \delta_{22} \tag{4.12}$$

The least-squares solution of Eq (4.10) yields the values for the molecular constants $\underline{\beta}^m$ that minimize the sum of the squares of the unknown $\underline{\delta}$, subject to known interrelations among the $\underline{\delta}$. These interrelations arise due to the fact that the variance-covariance matrices ($\underline{V}$) associated with $\underline{\beta}$ do not, in general, have equal diagonal elements and zero off-diagonal elements. So, we use the weighted and correlated least-squares formalism to get the molecular constants given by the elements of the column vector[65]

$$\underline{\beta}^m = (\underline{X}^T \underline{\Phi}^{-1} \underline{X})^{-1} \underline{X}^T \underline{\Phi}^{-1} \underline{Y}^m \tag{4.13}$$

where $\underline{\Phi}$ is the non-diagonal 30 x 30 matrix composed of the individual variance-covariance matrices $\underline{V}$ (0-8), $\underline{V}$(0-9), $\underline{V}$(0-10), $\underline{V}$(0-11), $\underline{V}$(1-8) and $\underline{V}$(1-12) as shown below:

$$\underline{\Phi} = \begin{bmatrix} \underline{V}(0\text{-}8) & \underline{0} & \underline{0} & \underline{0} & \underline{0} & \underline{0} \\ \underline{0} & \underline{V}(0\text{-}9) & \underline{0} & \underline{0} & \underline{0} & \underline{0} \\ \underline{0} & \underline{0} & \underline{V}(0\text{-}10) & \underline{0} & \underline{0} & \underline{0} \\ \underline{0} & \underline{0} & \underline{0} & \underline{V}(0\text{-}11) & \underline{0} & \underline{0} \\ \underline{0} & \underline{0} & \underline{0} & \underline{0} & \underline{V}(1\text{-}8) & \underline{0} \\ \underline{0} & \underline{0} & \underline{0} & \underline{0} & \underline{0} & \underline{V}(1\text{-}12) \end{bmatrix} \tag{4.14}$$

The precision of the estimates $\underline{\beta}^m$ is indicated by their standard errors which are the square roots of the diagonal elements of the variance-covariance matrix associated with $\underline{\beta}^m$:

$$\underline{V}^m = \sigma_m^2 \left(\underline{X}^T \underline{\Phi}^{-1} \underline{X} \right)^{-1} \qquad (4.15)$$

The variance σ_m^2 of the merged fit is given by

$$\sigma_m^2 = (\underline{Y}^m - \underline{X}\,\underline{\beta}^m)^T \underline{\Phi}^{-1} (\underline{Y}^m - \underline{X}\,\underline{\beta}^m)/f_m \qquad (4.16)$$

where the degrees of freedom (f_m) for the merged fit are given by $f_m = 30 - 20 = 10$. Similarly, the 10 redundant constants obtained from band-by-band least squares fits of 3-5 and 4-5 bands were also merged to get the 8 non-redundant constants.

The final rotational constants (C_{v1}, C_{v2},... and C_{d1}, C_{d2},...) of upper and lower states were obtained from the least squares fits of B_v', D_v', B_v'' and D_v'' to the standard polynomial representations:

$$B_v = \sum_{j=1}^{m} C_{rj}(v + \tfrac{1}{2})^{j-1}, \qquad (4.17)$$

$$D_v = \sum_{k=1}^{p} C_{dk}(v+\tfrac{1}{2})^{k-1} \qquad (4.18)$$

The equilibrium internuclear distance R_e is calculated for the upper and lower states from the equation

$$C_{r1} = h/8\,\pi^2\, c\, \mu\, R_e^2 \qquad (4.19)$$

4.5 Results and Discussion

The rotational constants for different vibrational levels of the upper and lower states were calculated after merging the results of separate band-by-band least squares fits by a program in FORTRAN on DEC-1090 computer. The results are tabulated in Table 4.10. The final rotational constants obtained for the upper (D') and the lower (A') states of $^{81}Br_2$ are given in Table 4.11. These constants reproduce most of the measured line positions within ± 0.1 cm^{-1}. Of the 8 bands of $^{81}Br_2$ which have been analysed here the 0-8, 0-9 and 1-8 bands were analysed and reported[58] by Sur and Tellinghuisen while the results of the analyses of the remaining 5 bands of $^{81}Br_2$, namely 0-10, 0-11, 1-12, 3-5 and 4-5, are presented for the first time.

As mentioned earlier, the P and R branches are resolved down to fairly low values of J in most of the bands and the rotational structure extends to high J values. In addition to these, the constants obtained from band-by-band fits were merged to obtain the best (MVLU) values. So, the constants presented in Table 4.9 are expected to be fairly reliable.

Just as the vibrational constants of the lower state of this system of bands differ from the corresponding known[37,66-68] constants of $X\ ^1\Sigma_g^+$, $A'\ ^3\Pi_{1u}$ and $B\ ^3\Pi_{0_u^+}$ states (see Chapter 3) so its rotational constants also do not agree with the corresponding constants of these states, thereby showing that

the lower state of the system is different from them.

If the lower state of the system was $^3\Pi_{0_u^+}$ then an intensity alternation with the ratio of intensities of successive lines (having higher and lower intensities) as 5:3 should have been observed in the rotational structures of the bands. The absence of the intensity alternation in the rotational lines containing unresolved Λ/Ω - doublets of the 8 bands studied does not contradict to the assignment of $^2g - {}^2u$ to the transition giving rise to the band system. However, further work with still higher dispersion and greater resolution is needed to find out the lowest value of J in the rotational structure as well as to check the presence of Q branch so that the value of Ω of the states in the system can be ascertained unambiguously.

TABLE 4.1 DETAILS OF THE EQUATIONS FOR MERGED LEAST SQUARES FIT OF 0–8, 0–9, 0–10, 0–11, 1–8 AND 1–12 BANDS

$$
\begin{bmatrix} \nu_{0-8} \\ B''_{0-8} \\ B'_{0-8} \\ D''_{0-8} \\ D'_{0-8} \\ \nu_{0-9} \\ B''_{0-9} \\ B'_{0-9} \\ D''_{0-9} \\ D'_{0-9} \\ \nu_{0-10} \\ B''_{0-10} \\ B'_{0-10} \\ D''_{0-10} \\ D'_{0-10} \\ \nu_{0-11} \\ B''_{0-11} \\ B'_{0-11} \\ D''_{0-11} \\ D'_{0-11} \\ \nu_{1-8} \\ B''_{1-8} \\ B'_{1-8} \\ D''_{1-8} \\ D'_{1-8} \\ \nu_{1-12} \\ B''_{1-12} \\ B'_{1-12} \\ D''_{1-12} \\ D'_{1-12} \end{bmatrix}
=
\begin{bmatrix}
1&0&0&0&0&0&0&0&0&0&0&0&0&0&0&0&0&0&0&0 \\
0&1&0&0&0&0&0&0&0&0&0&0&0&0&0&0&0&0&0&0 \\
0&0&1&0&0&0&0&0&0&0&0&0&0&0&0&0&0&0&0&0 \\
0&0&0&1&0&0&0&0&0&0&0&0&0&0&0&0&0&0&0&0 \\
0&0&0&0&1&0&0&0&0&0&0&0&0&0&0&0&0&0&0&0 \\
0&0&0&0&0&1&0&0&0&0&0&0&0&0&0&0&0&0&0&0 \\
0&0&0&0&0&0&1&0&0&0&0&0&0&0&0&0&0&0&0&0 \\
0&0&1&0&0&0&0&0&0&0&0&0&0&0&0&0&0&0&0&0 \\
0&0&0&0&0&0&0&1&0&0&0&0&0&0&0&0&0&0&0&0 \\
0&0&0&0&1&0&0&0&0&0&0&0&0&0&0&0&0&0&0&0 \\
0&0&0&0&0&0&0&0&1&0&0&0&0&0&0&0&0&0&0&0 \\
0&0&0&0&0&0&0&0&0&1&0&0&0&0&0&0&0&0&0&0 \\
0&0&1&0&0&0&0&0&0&0&0&0&0&0&0&0&0&0&0&0 \\
0&0&0&0&0&0&0&0&0&0&1&0&0&0&0&0&0&0&0&0 \\
0&0&0&0&1&0&0&0&0&0&0&0&0&0&0&0&0&0&0&0 \\
0&0&0&0&0&0&0&0&0&0&0&1&0&0&0&0&0&0&0&0 \\
0&0&0&0&0&0&0&0&0&0&0&0&1&0&0&0&0&0&0&0 \\
0&0&1&0&0&0&0&0&0&0&0&0&0&0&0&0&0&0&0&0 \\
0&0&0&0&0&0&0&0&0&0&0&0&0&1&0&0&0&0&0&0 \\
0&0&0&0&1&0&0&0&0&0&0&0&0&0&0&0&0&0&0&0 \\
0&0&0&0&0&0&0&0&0&0&0&0&0&0&1&0&0&0&0&0 \\
0&1&0&0&0&0&0&0&0&0&0&0&0&0&0&0&0&0&0&0 \\
0&0&0&0&0&0&0&0&0&0&0&0&0&0&0&1&0&0&0&0 \\
0&0&0&1&0&0&0&0&0&0&0&0&0&0&0&0&0&0&0&0 \\
0&0&0&0&0&0&0&0&0&0&0&0&0&0&0&0&1&0&0&0 \\
0&0&0&0&0&0&0&0&0&0&0&0&0&0&0&0&0&1&0&0 \\
0&0&0&0&0&0&0&0&0&0&0&0&0&0&0&0&0&0&1&0 \\
0&0&0&0&0&0&0&0&0&0&0&0&0&0&0&1&0&0&0&0 \\
0&0&0&0&0&0&0&0&0&0&0&0&0&0&0&0&0&0&0&1 \\
0&0&0&0&0&0&0&0&0&0&0&0&0&0&0&0&1&0&0&0
\end{bmatrix}
\begin{bmatrix} \nu_{0-8} \\ B''_{8} \\ B'_{0} \\ D''_{8} \\ D'_{0} \\ \nu_{0-9} \\ B''_{9} \\ D''_{9} \\ \nu_{0-10} \\ B''_{10} \\ D''_{10} \\ \nu_{0-11} \\ B''_{11} \\ D''_{11} \\ \nu_{1-8} \\ B'_{1} \\ D'_{1} \\ \nu_{0-12} \\ B''_{12} \\ D''_{12} \end{bmatrix}
+
\begin{bmatrix} \delta_1 \\ \delta_2 \\ \delta_3 \\ \delta_4 \\ \delta_5 \\ \delta_6 \\ \delta_7 \\ \delta_8 \\ \delta_9 \\ \delta_{10} \\ \delta_{11} \\ \delta_{12} \\ \delta_{13} \\ \delta_{14} \\ \delta_{15} \\ \delta_{16} \\ \delta_{17} \\ \delta_{18} \\ \delta_{19} \\ \delta_{20} \\ \delta_{21} \\ \delta_{22} \\ \delta_{23} \\ \delta_{24} \\ \delta_{25} \\ \delta_{26} \\ \delta_{27} \\ \delta_{28} \\ \delta_{29} \\ \delta_{30} \end{bmatrix}
$$

TABLE 4.2 Vacuum Wavenumbers (cm^{-1}) and Deviations (cm^{-1}) of the Rotational Lines in the (0-8) Band of $^{81}Br_2$

J	ν_P	$\Delta\nu_P$	ν_R	$\Delta\nu_R$
9	34553.93	-0.01		
10	34553.59	-0.04		
11	34553.29	0.00		
12	34552.97	0.03		
13	34552.62	0.06		
14	34552.11	-0.05		
15	34551.80	0.06		
16	34551.47	0.18	34553.93	-0.08
17	34550.96	0.14	34553.59	-0.12
18	34550.39	0.06	34553.29	-0.09
19	34549.93	0.11	34552.97	-0.07
20	34549.38	0.10	34552.62	-0.04
21	34548.90	0.18	34552.11	-0.16
22			34551.80	-0.05
23	34547.57	0.03	34551.47	0.05
24	34546.99	0.08	34550.96	0.01
25	34546.42	0.16	34550.39	-0.08
26	34545.50	-0.09	34549.93	-0.03
27	34544.82	-0.08	34549.38	-0.06
28	34544.15	-0.03	34548.90	0.02
29	34543.48	0.03		
30	34542.65	-0.03	34547.57	-0.14
31	34541.92	0.02	34546.99	-0.11
32	34541.04	-0.06	34546.42	-0.04
33	34540.29	0.02	34545.76	-0.03
34			34545.14	0.03
35	34538.49	-0.06	34544.42	0.02
36	34537.54	-0.11	34543.66	-0.01
37	34536.66	-0.08	34542.89	-0.03
38	34535.82	0.02	34542.14	-0.01
39	34534.84	0.00	34541.36	0.01
40	34533.86	0.00	34540.53	0.00
41	34532.80	-0.05	34539.85	0.16
42	34531.78	-0.04	34538.80	-0.03
43	34530.87	0.09	34537.97	0.02
44	34529.75	0.04	34537.02	-0.02
45	34528.66	0.05	34536.12	0.01
46	34527.49	-0.01	34535.17	0.01
47	34526.38	0.02	34534.18	-0.01
48	34525.20	-0.01	34533.24	0.04
49	34524.04	0.01	34532.16	-0.03
50	34522.84	0.01	34531.14	-0.01
51	34521.63	0.02	34530.10	0.01
52	34520.35	-0.01	34529.03	0.02
53	34519.13	0.03	34527.92	0.01

Table 4.2 Continued

J	ν_P	$\Delta\nu_P$	ν_R	$\Delta\nu_R$
54	34517.86	0.05	34526.75	-0.04
55	34516.54	0.04	34525.66	0.01
56	34515.23	0.06	34524.45	-0.03
57	34513.86	0.04	34523.26	-0.03
58	34512.41	-0.04	34522.11	0.02
59	34511.04	-0.02	34520.80	-0.06
60	34509.64	0.00	34519.61	0.00
61	34508.25	0.04	34518.41	0.07
62	34506.75	0.00	34517.11	0.07
63	34505.24	-0.04	34515.78	0.05
64	34503.77	-0.01	34514.44	0.04
65	34502.25	-0.01	34513.09	0.05
66	34500.73	0.01	34511.70	0.03
67	34499.15	-0.01	34510.24	-0.03
68	34497.62	0.04	34508.85	0.00
69	34496.05	0.07	34507.43	0.02
70	34494.36	0.01	34505.94	-0.02
71	34492.73	0.02	34504.48	0.00
72	34490.91	-0.14	34502.98	0.00
73	34489.39	0.03	34501.46	0.00
74	34487.67	0.01	34499.92	0.00
75	34485.92	-0.02	34498.35	-0.01
76	34484.17	-0.02	34496.72	-0.06
77	34482.44	0.01	34495.17	-0.01
78	34480.58	-0.07	34493.56	0.00
79	34478.79	-0.05	34491.93	0.01
80	34477.00	-0.02	34490.22	-0.04
81	34475.20	0.03	34488.54	-0.03
82	34473.25	-0.06	34486.91	0.04
83	34471.43	0.00	34485.18	0.02
84	34469.52	-0.01	34483.43	0.01
85	34467.66	0.06	34481.69	0.03
86	34465.65	-0.01	34479.86	-0.02
87	34463.57	-0.13	34478.09	0.01
88	34461.76	0,04	34476.28	0.02
89	34459.73	0.01	34474.45	0.02
90	34457.72	0.02	34472.56	-0.01
91	34455.69	0.02	34470.70	0.00
92	34453.62	0.01	34468.82	0.01
93	34451.56	0.02	34466.90	0.01
94	34449.47	0.03	34464.90	-0.06
95	34447.29	-0.04	34463.07	0.06
96	34445.20	0.00	34461.01	-0.03
97	34443.03	-0.02	34459.07	0.01
98	34440.86	-0.02	34457.07	0.02
99	34438.69	-0.01	34455.05	0.02
100	34436.55	0.06	34452.99	0.00

Table 4.2 Continued

J	ν_P	$\Delta\nu_P$	ν_R	$\Delta\nu_R$
101	34434.16	-0.11	34450.97	0.04
102	34431.96	-0.07	34448.84	-0.01
103	34429.72	-0.05	34446.76	0.01
104	34427.47	-0.02	34444.65	0.01
105	34425.22	0.02	34442.46	-0.05
106	34422.84	-0.05	34440.38	0.02
107	34420.75	0.19	34438.18	-0.01
108	34418.21	0.00	34436.06	0.06
109	34415.83	-0.02	34433.82	0.02
110	34413.39	-0.08	34431.61	0.03
111	34411.09	0.02	34429.29	-0.06
112	34408.64	-0.01	34427.10	0.01
113	34406.16	-0.06	34424.66	-0.16
114	34403.73	-0.04	34422.51	-0.02
115	34401.32	0.02	34420.27	0.04
116	34398.83	0.01	34417.93	0.02
117	34396.31	-0.01	34415.59	0.02
118	34393.82	0.01		
119	34391.25	-0.02	34410.86	0.02
120	34388.57	-0.16	34408.36	-0.10
121	34386.26	0.10	34406.16	0.11
122	34383.60	0.02	34403.73	0.10
123	34381.05	0.07	34401.32	0.12
124	34378.46	0.09	34398.83	0.08
125	34375.63	-0.11	34396.31	0.03
126	34373.24	0.14	34393.82	0.02
127	34370.54	0.10	34391.25	-0.05
128	34367.87	0.10		
129	34365.26	0.18	34386.26	0.00
130	34362.36	-0.01	34383.60	-0.11
131	34359.55	-0.11	34381.05	-0.11
132	34356.80	-0.12	34378.46	-0.12
133	34354.10	-0.07	34375.81	-0.18
134	34351.29	-0.12	34373.46	0.07
135	34348.56	-0.07	34370.76	-0.01
136	34346.01	0.17	34368.11	-0.03
137			34365.56	0.07
138			34362.91	0.08
139			34360.19	0.03
140			34357.43	-0.04
141			34354.80	0.03
142			34352.10	0.05
143			34349.29	-0.03

TABLE 4.3 Vacuum Wavenumbers (cm^{-1}) and Deviations (cm^{-1}) of the Rotational Lines in the (0-9) Band of $^{81}Br_2$

J	ν_P	$\Delta\nu_P$	ν_R	$\Delta\nu_R$
4	34432.71	0.11		
5	34432.52	0.11		
6	34432.30	0.10		
7	34431.96	-0.01		
8	34431.61	-0.10		
9	34431.35	-0.09		
10	34431.04	-0.10		
11	34430.75	-0.08		
12	34430.44	-0.05	34432.71	0.15
13	34430.07	-0.06	34432.52	0.16
14	34429.72	-0.03	34432.30	0.15
15	34429.29	-0.06	34431.96	0.05
16	34428.88	-0.05	34431.61	-0.05
17	34428.37	-0.12	34431.35	-0.03
18	34427.95	-0.07	34431.04	-0.04
19	34427.48	-0.06	34430.75	-0.01
20	34427.10	0.07	34430.44	0.02
21	34426.45	-0.06	34430.07	0.01
22	34425.87	-0.09	34429.72	0.04
23	34425.22	-0.17	34429.29	0.02
24	34424.66	-0.14	34428.88	0.03
25	34424.12	-0.07	34428.37	-0.03
26	34423.47	-0.09	34427.95	0.02
27	34422.84	-0.06	34427.48	0.03
28	34422.15	-0.08	34427.10	0.16
29	34421.47	-0.07	34426.45	0.04
30	34420.75	-0.07	34425.87	0.01
31	34419.99	-0.09	34425.22	-0.07
32	34419.30	-0.03	34424.66	-0.04
33	34418.51	-0.04	34424.12	0.04
34	34417.68	-0.07	34423.47	0.02
35	34416.86	-0.07	34422.84	0.04
36	34416.07	-0.02	34422.15	0.03
37	34415.15	-0.09	34421.47	0.04
38	34414.30	-0.05	34420.75	0.04
39	34413.39	-0.06	34419.99	0.01
40	34412.50	-0.03	34419.30	0.08
41	34411.53	-0.06	34418.51	0.07
42	34410.58	-0.05	34417.68	0.03
43	34409.59	-0.06	34416.86	0.03
44	34408.64	0.00	34416.07	0.08
45	34407.58	-0.04	34415.15	0.02
46	34406.52	-0.06	34414.30	0.04
47	34405.47	-0.05	34413.39	0.03
48	34404.40	-0.03	34412.50	0.06
49	34403.29	-0.04	34411.53	0.03
50	34402.17	-0.04	34410.58	0.04

Table 4.3 Continued

J	ν_P	$\Delta\nu_P$	ν_R	$\Delta\nu_R$
51	34401.04	-0.02	34409.59	0.03
52	34399.88	-0.02	34408.64	0.07
53	34398.83	0.11	34407.58	0.03
54	34397.50	-0.02	34406.52	0.01
55	34396.31	0.02	34405.47	0.02
56	34395.05	0.00	34404.40	0.02
57	34393.82	0.03	34403.29	0.01
58	34392.52	0.01	34402.17	0.01
59	34391.25	0.04	34401.04	0.01
60	34389.92	0.03	34399.88	0.01
61	34388.57	0.02	34398.83	0.13
62	34387.22	0.03	34397.50	0.00
63	34385.85	0.04	34396.31	0.02
64	34384.48	0.06	34395.05	-0.01
65	34383.07	0.07	34393.82	0.02
66	34381.69	0.12	34392.52	-0.01
67	34380.18	0.07	34391.25	0.01
68	34378.77	0.13	34389.92	-0.01
69	34377.16	0.01	34388.57	-0.04
70	34375.63	-0.01	34387.22	-0.04
71	34374.14	0.03	34385.85	-0.05
72	34372.56	0.00	34384.48	-0.03
73	34371.03	0.04	34383.07	-0.04
74	34369.45	0.04	34381.69	0.00
75	34367.87	0.07	34380.18	-0.07
76	34366.26	0.08	34378.77	-0.02
77	34364.62	0.08	34377.29	-0.03
78	34362.91	0.02	34375.81	-0.01
79	34361.24	0.03	34374.32	0.01
80	34359.55	0.03	34372.81	0.03
81	34357.86	0.06	34371.22	-0.01
82	34356.12	0.05	34369.68	0.02
83	34354.36	0.03	34368.11	0.03
84	34352.62	0.06	34366.49	0.01
85	34350.79	0.01	34364.91	0.05
86	34348.99	0.01	34363.18	-0.04
87	34347.17	0.01	34361.58	0.01
88	34345.37	0.02	34359.91	0.01
89	34343.51	0.04	34358.22	0.01
90	34341.63	0.03	34356.53	0.03
91	34339.74	0.02	34354.80	0.02
92	34337.86	0.04	34353.06	0.02
93	34335.91	0.02	34351.29	0.01

Table 4.3 Continued

J	ν_P	$\Delta\nu_P$	ν_R	$\Delta\nu_R$
94	34333.97	0.01	34349.53	0.02
95	34331.99	-0.01	34347.73	0.01
96	34330.04	0.01	34346.01	0.10
97	34327.99	-0.06	34344.07	-0.02
98	34326.05	0.00	34342.28	0.03
99	34324.03	0.00	34340.37	-0.02
100	34322.01	0.02	34338.50	-0.02
101	34319.98	0.04	34336.60	-0.03
102	34317.87	0.00	34334.66	-0.07
103	34315.79	0.00	34332.72	-0.09
104	34313.66	-0.03	34330.85	-0.02
105	34311.59	0.01	34328.90	-0.02
106	34309.48	0.03	34326.93	-0.02
107	34307.39	0.09	34324.97	0.00
108	34305.16	0.02	34322.92	-0.05
109	34303.01	0.05	34320.88	-0.08
110	34300.80	0.03	34318.91	-0.02
111	34298.45	-0.12	34316.87	-0.01
112	34296.34	0.00	34314.84	0.02
113	34294.18	0.07	34312.78	0.03
114	34291.92	0.06	34310.68	0.02
115	34289.63	0.04	34308.59	0.03
116	34287.41	0.10	34306.49	0.05
117	34284.99	-0.03	34304.30	-0.01
118	34282.64	-0.07	34302.25	0.08
119	34280.27	-0.12	34300.04	0.03
120	34278.03	-0.03	34297.79	-0.04
121	34275.54	-0.17	34295.66	0.02
122	34273.19	-0.15	34293.32	-0.12
123	34270.99	0.02	34291.33	0.10
124	34268.51	-0.07	34288.84	-0.16
125	34266.12	-0.05	34286.81	0.05
126	34263.61	-0.15	34284.60	0.10
127	34261.20	-0.13	34282.08	-0.15
128	34258.83	-0.05	34279.78	-0.17
129	34256.34	-0.09	34277.45	0.12
130	34253.94	-0.02	34275.28	-0.07
131	34251.54	0.06	34272.87	-0.16
132	34248.95	-0.04	34270.73	0.03
133	34246.51	0.03	34268.27	-0.09

Table 4.3 Continued

J	ν_P	$\Delta\nu_P$	ν_R	$\Delta\nu_R$
134	34243.90	-0.06	34266.12	0.12
135	34241.40	-0.04	34263.61	-0.02
136	34238.83	-0.06	34261.20	-0.05
137	34236.25	-0.09	34258.83	-0.03
138	34233.72	-0.06	34256.34	-0.12
139	34231.26	0.06	34253.94	-0.10
140	34228.68	0.07	34251.54	-0.07
141	34226.14	0.12	34249.27	0.09
142	34223.41	0.00	34246.74	0.01
143	34220.89	0.10	34244.28	0.01
144	34218.24	0.08	34241.82	0.02
145	34215.57	0.05	34239.34	0.02
146	34212.92	0.06	34236.92	0.09
147			34234.39	0.07
148			34231.90	0.09
149			34229.26	-0.03
150			34226.66	-0.10
151			34224.38	0.16
152			34221.72	0.05
153			34219.15	0.05

TABLE 4.4 Vacuum Wavenumbers (cm^{-1}) and Deviations (cm^{-1}) of the Rotational Lines in the (0-10) Band of $^{81}Br_2$

J	ν_P	$\Delta\nu_P$	ν_R	$\Delta\nu_R$
15	34312.13	0.14		
16	34311.59	0.00		
17	34311.17	-0.01		
18	34310.86	0.12		
19	34310.31	0.02		
20	34309.75	-0.06		
21	34309.25	-0.07		
23	34308.25	-0.03	34312.13	-0.02
24	34307.72	-0.01	34311.77	0.00
25	34307.11	-0.05	34311.34	-0.02
26	34306.49	-0.08		
27	34306.07	0.11	34310.55	0.05
28	34305.46	0.13	34310.02	-0.01
29	34304.65	-0.04	34309.48	-0.07
30	34303.98	-0.04	34308.99	-0.06
31	34303.33	-0.01	34308.59	0.06
32	34302.62	-0.01	34307.98	-0.01
33	34301.87	-0.04	34307.39	-0.04
34	34301.20	0.03	34306.80	-0.06
35	34300.40	-0.01	34306.22	-0.04
36	34299.64	0.01	34305.64	0.00
37	34298.71	-0.12	34305.01	0.00
38	34298.18	0.17	34304.30	-0.06
39	34297.16	-0.01	34303.67	-0.02
40	34296.34	0.02	34303.01	0.01
41	34295.43	-0.02	34302.25	-0.04
42	34294.55	0.00	34301.53	-0.03
43	34293.67	0.03	34300.80	-0.01
44	34292.69	-0.02	34300.19	0.14
45	34291.74	-0.02	34299.27	0.01
46	34290.78	-0.02	34298.45	-0.01
47	34289.79	-0.02	34297.62	-0.02
48	34288.84	0.03	34296.81	0.01
49	34287.78	-0.01	34296.10	0.15
50	34286.81	0.06	34295.08	0.01
51	34285.69	0.00	34294.18	0.00
52	34284.60	-0.02	34293.32	0.05
53	34283.53	0.01	34292.32	-0.02
54	34282.41	0.00	34291.33	-0.06
55	34281.30	0.02	34290.42	0.00

Table 4.4 Continued

J	ν_P	$\Delta\nu_P$	ν_R	$\Delta\nu_R$
56	34280.10	-0.03	34289.43	-0.01
57	34278.95	-0.02	34288.44	0.00
58	34277.78	0.00	34287.41	-0.01
59	34276.57	-0.01	34286.37	-0.01
60	34275.35	-0.01	34285.35	0.02
61	34274.14	0.01	34284.25	-0.01
62	34272.87	0.00	34283.15	-0.02
63	34271.58	-0.02	34282.08	0.02
64	34270.32	0.01	34280.93	-0.01
65	34269.01	0.00	34279.78	-0.02
66	34267.70	0.01	34278.66	0.02
67	34266.34	-0.01	34277.45	-0.01
68	34264.99	0.00	34276.24	-0.03
69	34263.61	0.00	34275.05	-0.01
70	34262.28	0.06	34273.84	0.01
71	34260.81	-0.01	34272.61	0.02
72	34259.41	0.02	34271.31	-0.01
73	34257.96	0.01	34270.05	0.00
74	34256.65	0.16	34268.75	0.00
75	34255.05	0.03	34267.46	0.02
76	34253.49	-0.04	34266.12	0.00
77	34252.01	-0.01	34264.78	0.01
78	34250.45	-0.05	34263.38	-0.03
79	34248.95	-0.01	34262.06	0.02
80	34247.40	0.00	34260.66	0.01
81	34245.84	0.01	34259.22	-0.02
82	34244.28	0.04	34257.80	-0.01
83	34242.68	0.04	34256.34	-0.03
84	34240.99	-0.03	34254.91	-0.01
85	34239.34	-0.05	34253.49	0.04
86	34237.70	-0.04	34252.01	0.05
87	34236.04	-0.03	34250.45	-0.01
88	34234.39	0.00	34248.95	0.01
89	34232.70	0.01	34247.40	-0.01
90	34230.97	-0.01	34245.84	-0.02
91	34229.26	0.00	34244.28	-0.02
92	34227.53	0.01	34242.68	-0.04
93	34225.82	0.06	34240.99	-0.14
94	34224.01	0.02	34239.48	-0.04
95	34222.18	-0.03	34237.93	0.03
96	34220.39	-0.02	34236.25	-0.01
97	34218.61	0.02	34234.60	-0.01
98	34216.72	-0.04	34232.90	-0.05

Table 4.4 Continued

J	ν_P	$\Delta\nu_P$	ν_R	$\Delta\nu_R$
99	34214.90	-0.02	34231.26	-0.01
100	34213.09	0.03	34229.52	-0.05
101	34211.23	0.04	34227.84	-0.03
102	34209.32	0.01	34226.14	0.00
103	34207.40	-0.01	34224.38	-0.03
104	34205.44	-0.06	34222.65	-0.01
105	34203.58	0.01	34220.89	-0.01
106	34201.50	-0.14	34219.15	0.03
107	34199.60	-0.08	34217.37	0.04
108	34197.77	0.05	34215.57	0.04
109	34195.84	0.10	34213.76	0.04
110	34193.68	-0.07	34211.96	0.07
111	34191.82	0.07	34210.13	0.08
112	34189.79	0.06	34208.22	0.03
113	34187.64	-0.06	34206.37	0.04
114	34185.55	-0.11	34204.51	0.06
115	34183.69	0.08	34202.61	0.05
116	34181.47	-0.07	34200.73	0.08
117	34179.36	-0.11	34198.80	0.06
118	34177.52	0.14	34196.86	0.05
119	34175.21	-0.07	34194.96	0.09
120	34173.20	0.04	34192.87	-0.05
121	34171.15	0.11	34190.98	0.02
122			34188.91	-0.07
123			34186.92	-0.08
124			34184.90	-0.10
125			34183.07	0.07
126			34180.93	-0.05
127			34178.96	0.01
128			34176.82	-0.09
129			34174.83	-0.03

TABLE 4.5 Vacuum Wavenumbers (cm^{-1}) and Deviations (cm^{-1}) of the Rotational Lines in the (0-11) Band of $^{81}Br_2$

J	ν_P	$\Delta\nu_P$	ν_R	$\Delta\nu_R$
6	34202.34	0.02		
7	34202.14	0.03		
8	34201.94	0.06		
9	34201.68	0.04		
10	34201.50	0.12		
11	34201.04	-0.06		
12	34200.88	0.08		
13	34200.47	-0.02		
14	34200.09	-0.06		
15	34199.91	0.11	34202.34	-0.02
16	34199.60	0.16	34202.14	-0.02
17	34199.21	0.16	34201.94	0.00
18	34198.60	-0.05	34201.68	-0.02
19	34198.20	-0.03	34201.50	0.06
20	34197.77	-0.02	34201.04	-0.13
21	34197.41	0.08	34200.88	0.00
22	34196.86	0.00	34200.47	-0.10
23	34196.40	0.03	34200.09	-0.15
24	34195.84	-0.02	34199.91	0.01
25	34195.35	0.02	34199.60	0.06
26	34194.70	-0.08	34199.21	0.05
27	34194.17	-0.05	34198.60	-0.16
28	34193.68	0.04	34198.20	-0.15
29	34193.05	0.00	34197.77	-0.15
30	34192.43	0.00	34197.41	-0.06
31	34191.82	0.02	34197.03	0.03
32	34191.12	-0.03	34196.51	-0.01
33	34190.48	-0.01	34196.06	0.04
34	34189.79	-0.02	34195.51	0.01
35	34189.13	0.02	34194.96	0.00
36	34188.45	0.06	34194.44	0.03
37	34187.77	0.11	34193.82	-0.02
38	34186.92	0.02	34193.27	0.02
39	34186.14	0.00	34192.66	0.01
40	34185.36	0.01	34192.04	0.01
41	34184.58	0.03	34191.37	-0.02
42	34183.69	-0.04	34190.72	-0.02
43	34182.83	-0.06	34190.04	-0.03
44	34182.02	-0.02	34189.35	-0.03
45	34181.17	0.00	34188.67	-0.01
46	34180.31	0.02	34187.96	0.00

Table 4.5 Continued

J	ν_P	$\Delta\nu_P$	ν_R	$\Delta\nu_R$
47	34179.36	-0.03	34187.20	-0.02
48	34178.52	0.05	34186.43	-0.03
49	34177.52	-0.01	34185.74	0.05
50	34176.59	0.01	34184.90	-0.01
51	34175.62	0.01	34184.10	0.00
52	34174.60	-0.03	34183.29	0.01
53	34173.64	0.01	34182.41	-0.04
54	34172.61	0.00	34181.65	0.05
55	34171.58	0.00	34180.65	-0.08
56	34170.53	0.00	34179.87	0.03
57	34169.46	-0.01	34178.96	0.02
58	34168.38	-0.01	34178.02	-0.01
59	34167.28	-0.01	34177.16	0.06
60	34166.22	0.04	34176.15	0.00
61	34165.07	0.01	34175.21	0.02
62	34163.93	0.02	34174.17	-0.04
63	34162.70	-0.05	34173.20	-0.01
64	34161.58	0.00	34172.19	-0.01
65	34160.38	-0.01	34171.15	-0.03
66	34159.20	0.01	34170.14	0.00
67	34158.01	0.04	34169.09	0.01
68	34156.69	-0.05	34168.00	-0.01
69	34155.48	-0.01	34166.99	0.06
70	34154.22	0.00	34165.89	0.06
71	34152.96	0.02	34164.74	0.03
72	34151.65	0.00	34163.65	0.07
73	34150.34	0.00	34162.42	-0.02
74	34149.03	0.01	34161.28	0.00
75	34147.63	-0.05	34160.06	-0.05
76	34146.27	-0.06	34158.93	0.01
77	34144.95	-0.02	34157.71	-0.01
78	34143.58	-0.01	34156.49	-0.01
79	34142.21	0.02	34155.24	-0.03
80	34140.78	0.00	34154.02	-0.01
81	34139.43	0.07	34152.77	0.00
82	34137.95	0.02	34151.47	-0.02
83	34136.45	-0.03	34150.32	0.11
84	34135.02	0.00	34148.90	-0.01
85	34133.55	0.01	34147.63	0.03
86	34132.05	0.00	34146.27	0.00
87	34130.54	-0.01	34144.95	0.02
88	34129.02	-0.01	34143.58	0.00

Table 4.5 Continued

J	ν_P	$\Delta\nu_P$	ν_R	$\Delta\nu_R$
89	34127.54	0.04	34142.21	0.00
90	34125.96	0.00	34140.78	-0.05
91	34124.41	0.00	34139.43	-0.01
92	34122.86	0.02	34138.06	0.02
93	34121.25	-0.01	34136.62	0.00
94	34119.69	0.02	34135.21	0.02
95	34118.07	0.01	34133.76	0.01
96	34116.45	0.00	34132.28	-0.01
97	34114.78	-0.04	34130.87	0.04
98	34113.15	-0.03		
99			34127.94	0.08
100			34126.38	0.02
101			34124.90	0.06
102			34123.40	0.08
103			34121.62	-0.16
104			34120.04	-0.19
105			34118.51	-0.16
106			34117.16	0.06
107			34115.56	0.04
108			34113.95	0.02
109			34112.41	0.08

TABLE 4.6 Vacuum Wavenumbers (cm^{-1}) and Deviations (cm^{-1}) of the Rotational Lines in the (1-8) Band of $^{81}Br_2$

J	ν_P	$\Delta\nu_P$	ν_R	$\Delta\nu_R$
7	34702.70	0.04		
8	34702.50	0.11		
9	34702.10	-0.01		
10	34701.78	-0.01		
11	34701.44	-0.02		
12	34701.02	-0.08		
13	34700.61	-0.11		
14	34700.35	0.04	34702.70	0.00
15	34699.88	-0.01	34702.50	0.06
16	34699.46	0.02	34702.10	-0.05
17	34698.99	0.03	34701.78	-0.06
18	34698.51	0.04	34701.44	-0.07
19	34698.04	0.09	34701.02	-0.14
20	34697.45	0.04	34700.61	-0.17
21	34696.92	0.07	34700.35	-0.03
22	34696.32	0.06	34699.88	-0.08
23	34695.71	0.06	34699.46	-0.05
24	34694.99	-0.03	34698.99	-0.05
25	34694.36	0.00	34698.51	-0.04
26	34693.65	-0.03	34698.04	0.00
27	34693.05	0.07	34697.45	-0.05
28	34692.35	0.09	34696.92	-0.03
29	34691.49	-0.02	34696.32	-0.04
30	34690.76	0.01	34695.71	-0.05
31	34689.96	0.01	34695.15	0.02
32	34689.15	0.01	34694.52	0.04
33	34688.27	-0.03	34693.78	-0.03
34	34687.42	-0.03	34693.28	0.16
35	34686.54	-0.02	34692.59	0.19
36			34691.68	0.02
37	34684.67	-0.06		
38	34683.74	-0.05	34690.09	-0.02
39	34682.81	0.00	34689.33	0.02
40	34681.85	0.03	34688.47	-0.01
41	34680.83	0.02	34687.66	0.03
42	34679.76	-0.01	34686.85	0.10
43	34678.60	-0.11	34685.80	-0.06
44	34677.58	-0.05	34684.96	0.02
45	34676.54	0.02	34684.01	0.01
46	34675.42	0.02	34683.02	-0.02
47	34674.22	-0.03	34682.09	0.04

Table 4.6 Continued

J	ν_P	$\Delta\nu_P$	ν_R	$\Delta\nu_R$
48	34673.11	0.03	34681.06	0.01
49	34671.91	0.02	34680.03	0.01
50	34670.70	0.03	34678.97	0.00
51	34669.44	0.00	34677.92	0.02
52	34668.16	-0.02	34676.83	0.03
53	34666.83	-0.07	34675.69	0.00
54	34665.57	-0.03	34674.55	0.00
55	34664.30	0.02	34673.41	0.02
56	34663.09	0.16	34672.18	-0.03
57	34661.53	-0.04	34671.00	-0.01
58	34660.18	0.00	34669.80	0.02
59	34658.79	0.02	34668.50	-0.04
60	34657.40	0.06	34667.28	0.01
61	34655.90	0.01	34665.99	0.01
62	34654.41	0.00	34664.71	0.03
63	34652.85	-0.07	34663.37	0.03
64	34651.40	0.00	34662.03	0.04
65	34649.86	-0.01	34660.65	0.03
66	34648.30	-0.01	34659.21	-0.02
67	34646.72	-0.01	34657.80	-0.01
68	34645.14	0.01	34656.35	-0.02
69	34643.51	0.00	34654.91	-0.01
70	34641.85	-0.02	34653.49	0.05
71	34640.21	0.00	34651.96	0.02
72	34638.53	0.00	34650.42	0.00
73	34636.81	-0.01	34648.85	-0.03
74	34635.13	0.03	34647.34	0.02
75	34633.35	0.00	34645.75	0.01
76	34631.63	0.04	34644.10	-0.04
77	34629.77	-0.03	34642.68	0.17
78	34627.98	-0.02	34640.87	0.00
79	34626.17	0.00	34639.22	0.01
80	34624.34	0.01	34637.53	0.00
81	34622.44	-0.02	34635.87	0.05
82	34620.56	-0.01	34634.08	-0.02
83	34618.67	0.00	34632.35	-0.01
84	34616.75	0.01	34630.60	0.01
85	34614.83	0.03	34628.83	0.02
86	34612.83	0.00	34627.00	-0.01
87	34610.86	0.01	34625.16	-0.03
88	34608.87	0.03	34623.28	-0.07
89	34606.79	-0.03	34621.50	0.02
90	34604.75	-0.02	34619.61	0.01

Table 4.6 Continued

J	ν_P	$\Delta\nu_P$	ν_R	$\Delta\nu_R$
91	34602.67	-0.04	34617.73	0.03
92	34600.63	0.00	34615.78	-0.01
93	34598.50	-0.03	34613.84	-0.01
94	34596.42	0.01	34611.91	0.02
95	34594.28	0.01	34609.85	-0.06
96	34592.08	-0.03	34607.90	-0.02
97	34589.94	0.01	34605.89	-0.01
98	34587.73	-0.01	34603.82	-0.05
99	34585.53	0.00	34601.75	-0.07
100	34583.27	-0.02	34599.73	-0.02
101	34581.03	-0.01	34597.64	-0.02
102	34578.81	0.04	34595.55	0.00
103	34576.50	0.02	34593.41	-0.02
104	34574.16	-0.02	34591.29	0.01
105	34571.85	0.00	34589.11	-0.01
106	34569.47	-0.04	34586.90	-0.04
107	34567.16	0.01	34584.77	0.03
108	34564.76	-0.02	34582.53	0.00
109	34562.38	0.00	34580.24	-0.05
110	34560.04	0.07	34578.00	-0.04
111	34557.57	0.03	34575.74	-0.03
112	34555.08	-0.01	34573.47	-0.02
113	34552.61	-0.01	34571.19	0.01
114	34550.14	0.00	34568.90	0.04
115			34566.62	0.09
116			34564.14	-0.03
117			34561.82	0.02
118			34559.34	-0.07
119			34557.04	0.03
120			34554.71	0.13
121			34552.13	-0.01

TABLE 4.7 Vacuum Wavenumbers (cm^{-1}) and Deviations (cm^{-1}) of the Rotational Lines in the (1-12) Band of $^{81}Br_2$

J	ν_P	$\Delta\nu_P$	ν_R	$\Delta\nu_R$
8	34243.30	-0.05		
9	34143.11	-0.01		
10	34242.90	0.03		
11	34242.68	0.07		
12	34242.36	0.03		
13	34242.13	0.10		
14	34241.82	0.10		
15	34241.40	0.01		
16	34240.99	-0.05		
17	34240.77	0.09		
18	34240.37	0.07	34243.30	-0.07
19	34239.94	0.04	34243.11	-0.03
20	34239.48	-0.01	34242.90	0.01
21	34239.18	0.11	34242.68	0.05
22	34238.65	0.03	34242.36	0.01
23			34242.13	0.07
24	34237.70	0.01	34241.82	0.07
25	34237.15	-0.05	34241.40	-0.02
26	34236.72	0.03	34240.99	-0.09
27	34236.25	0.09	34240.77	0.05
28	34235.60	-0.02	34240.37	0.02
29	34235.05	-0.02	34239.94	-0.02
30	34234.39	-0.11	34239.48	-0.07
31	34233.72	0.05	34239.18	0.05
32	34233.31	0.00	34238.65	-0.04
33	34232.70	0.01		
34	34232.07	0.01	34237.70	-0.07
35	34231.47	0.06	34237.15	-0.13
36	34230.63	-0.11	34236.72	-0.06
37	34230.10	0.04	34236.25	-0.02
38	34229.26	-0.10	34235.79	0.06
39	34228.68	0.03	34235.20	0.01
40	34227.84	-0.09	34234.60	-0.03
41	34227.09	-0.09	34233.96	0.15
42	34226.38	-0.05	34233.44	-0.02
43	34225.59	-0.06	34232.90	0.05
44	34224.80	-0.07	34232.28	0.05
45	34224.01	-0.05	34231.67	0.08
46	34223.20	-0.05	34230.97	0.04
47	34222.39	-0.02	34230.39	0.12

Table 4.7 Continued

J	ν_P	$\Delta\nu_P$	ν_R	$\Delta\nu_R$
89	34175.21	-0.02	34190.04	0.14
90	34173.86	0.01	34188.91	0.00
91	34172.45	-0.01	34187.42	-0.02
92	34171.15	0.10	34186.14	-0.06
93	34169.64	0.00	34184.90	-0.05
94	34168.23	0.01	34183.69	0.01
95	34166.74	-0.05	34182.41	0.00
96	34165.33	-0.02	34181.17	0.04
97	34163.93	0.03	34179.87	0.03
98	34162.42	-0.02	34178.52	-0.02
99	34160.87	-0.10	34177.16	-0.07
100	34159.47	-0.02	34175.89	-0.02
101	34158.01	0.00	34174.60	0.02
102	34156.49	-0.02	34173.20	-0.04
103	34155.00	-0.01	34171.93	0.03
104	34153.48	-0.02	34170.53	-0.02
105			34169.09	-0.09
106			34167.80	-0.01
107			34166.48	0.05
108			34165.07	0.02
109			34163.65	-0.01
110			34162.28	0.03

TABLE 4.8 Vacuum Wavenumbers (cm^{-1}) and Deviations (cm^{-1}) of the Rotational Lines in the (3-5) Band of $^{81}Br_2$

J	ν_P	$\Delta\nu_P$	ν_R	$\Delta\nu_R$
5	35393.29	0.02		
6	35393.05	0.03		
7	35392.77	0.02		
8	35392.45	0.01		
9	35392.02	-0.09		
10	35391.58	-0.17		
11	35391.31	-0.06	35393.29	0.03
12	35390.92	-0.03	35393.05	0.04
13	35390.46	-0.05	35392.77	0.04
14	35390.11	0.07	35392.45	0.02
15	35389.55	0.01	35392.02	-0.07
16	35389.04	0.02	35391.58	-0.15
17	35388.46	-0.01	35391.31	-0.03
18	35387.89	0.00	35390.92	-0.01
19	35387.28	0.00	35390.46	-0.03
20	35386.53	-0.11	35390.11	0.10
21	35385.97	-0.01	35389.55	0.03
22	35385.27	-0.02	35389.04	0.05
23	35384.52	-0.05	35388.46	0.02
24	35383.91	0.08	35387.89	0.03
25	35383.04	-0.02	35387.28	0.03
26	35382.22	-0.04	35386.53	-0.08
27	35381.38	-0.05	35385.97	0.02
28	35380.50	-0.08	35385.27	0.01
29	35379.56	-0.13	35384.52	-0.02
30	35378.79	0.01	35383.91	0.12
31	35377.84	-0.01	35383.04	0.02
32	35376.88	0.00	35382.22	0.00
33	35375.62	0.12	35381.38	-0.01
34	35374.75	-0.12	35380.50	-0.04
35	35373.77	-0.06	35379.56	-0.09
36	35372.81	0.06	35378.79	0.04
37	35371.65	0.00	35377.84	0.03
38	35370.52	0.00	35376.88	0.04
39	35369.38	0.01	35375.62	0.16
40	35368.21	0.02	35374.75	-0.08
41	35366.99	0.01	35373.77	-0.02
42	35365.75	0.01	35372.81	0.09
43	35364.47	-0.01	35371.65	0.03
44	35363.21	0.02	35370.52	0.03

Table 4.8 Continued

J	ν_P	$\Delta\nu_P$	ν_R	$\Delta\nu_R$
45	35361.83	-0.04	35369.38	0.05
46	35360.53	0.00	35368.21	0.06
47	35359.18	0.03	35366.99	0.05
48	35357.74	-0.02	35365.75	0.04
49	35356.32	-0.01	35364.47	0.02
50	35354.79	-0.09	35363.21	0.05
51	35353.42	0.02	35361.83	-0.01
52	35351.89	0.00	35360.53	0.03
53	35350.35	-0.01	35359.18	0.05
54	35348.87	0.07	35357.74	0.01
55	35347.23	0.01	35356.32	0.01
56	35345.54	-0.07	35354.79	-0.07
57	35343.99	0.02	35353.42	0.04
58	35342.31	0.01	35351.89	0.01
59	35340.67	0.06	35350.35	0.00
60	35338.92	0.03	35348.87	0.07
61	35337.18	0.03	35347.23	0.02
62	35335.38	0.01	35345.54	-0.06
63	35333.61	0.03	35343.99	0.02
64	35331.77	0.02	35342.31	0.00
65	35329.89	-0.01	35340.67	0.05
66	35328.04	0.01	35338.92	0.02
67	35326.13	0.01	35337.18	0.02
68	35324.22	0.02	35335.38	-0.02
69	35322.30	0.06	35333.61	0.01
70	35320.30	0.04	35331.77	-0.01
71	35318.26	0.01	35329.89	-0.05
72	35316.20	-0.02	35328.04	-0.03
73	35314.19	0.03	35326.13	-0.04
74	35312.11	0.03	35324.22	-0.03
75	35310.02	0.05	35322.30	0.00
76	35307.88	0.05	35320.30	-0.02
77	35305.74	0.07	35318.26	-0.06
78	35303.63	0.15	35316.20	-0.09
79	35301.34	0.07	35314.19	-0.05
80	35299.10	0.07	35312.11	-0.05
81	35296.81	0.04	35310.02	-0.04
82	35294.52	0.04	35307.88	-0.05
83	35292.23	0.07	35305.74	-0.04
84	35289.78	-0.04	35303.63	0.03
85	35287.42	-0.04	35301.34	-0.05
86	35285.13	0.06	35299.10	-0.06
87	35282.57	-0.08	35296.81	-0.10

Table 4.8 Continued

J	ν_P	$\Delta\nu_P$	ν_R	$\Delta\nu_R$
88	35280.24	0.03	35294.52	-0.10
89	35277.62	-0.13	35292.23	-0.09
90	35275.23	-0.03	35290.11	0.12
91	35272.70	-0.04	35287.65	0.02
92	35270.09	-0.11		
93	35267.63	0.00	35282.81	-0.03
94	35265.06	0.02	35280.40	-0.01
95	35262.40	-0.03	35277.95	-0.01
96	35259.71	-0.08	35275.56	0.08
97	35257.13	0.00	35272.95	-0.02
98	35254.42	-0.02	35270.43	-0.01
99	35251.73	0.00	35267.89	0.00
100	35249.06	0.07	35265.31	0.00
101	35246.24	0.01	35262.72	0.01
102	35243.45	0.01	35260.06	-0.02
103	35240.65	0.02	35257.44	0.01
104	35237.75	-0.05	35254.89	0.14
105	35234.93	-0.01	35252.04	-0.01
106	35232.12	0.06	35249.33	0.00
107	35229.03	-0.13	35246.58	0.00
108	35226.42	0.19	35243.78	-0.03
109	35223.16	-0.11	35241.00	-0.01
110	35220.38	0.08	35238.08	-0.11
111	35217.24	-0.06	35235.31	-0.04
112	35214.19	-0.08		
113	35211.24	0.01	35229.55	-0.05
114			35226.67	-0.01
115			35223.79	0.05
116			35220.87	0.09
117			35217.84	0.04
118			35214.89	0.10
119			35211.81	0.05

TABLE 4.9 Vacuum Wavenumbers (cm^{-1}) and Deviations (cm^{-1}) of the Rotational Lines in the (4-5) Band of $^{81}Br_2$

J	ν_P	$\Delta\nu_P$	ν_R	$\Delta\nu_R$
15	35535.98	-0.17		
16	35535.50	-0.14		
18	35534.38	-0.14		
19	35533.76	-0.16		
20	35533.20	-0.09		
21	35532.46	-0.18	35535.98	-0.14
22	35531.90	-0.05	35535.50	-0.10
24			35534.38	-0.10
25	35529.66	-0.08	35533.76	-0.12
26	35528.83	-0.12	35533.20	-0.05
27			35532.46	-0.14
28	35527.24	-0.05	35531.90	-0.01
29	35526.52	0.10		
30	35525.44	-0.08		
31	35524.67	0.08	35529.66	-0.04
32			35528.83	-0.08
33	35522.62	-0.04	35527.91	-0.18
34	35521.53	-0.12	35527.24	0.00
35	35520.74	0.12	35526.52	0.15
36	35519.43	-0.12	35525.44	-0.03
37	35518.40	-0.07	35524.67	0.13
38	35517.43	0.08	35523.41	-0.18
39			35522.62	0.01
40	35515.01	-0.03	35521.53	-0.07
41	35513.88	0.04	35520.74	0.18
42	35512.79	0.17	35519.43	-0.07
43	35511.41	0.04	35518.40	-0.01
44	35510.26	0.17	35517.43	0.13
45	35508.94	0.16	35516.03	-0.12
46	35507.63	0.18	35515.01	0.03
47	35506.19	0.10	35513.88	0.09
48	35504.70	-0.01		
49	35503.45	0.16	35511.41	0.10
50	35501.92	0.06		
51	35500.56	0.17	35508.94	0.21
52	35498.83	-0.07		
53	35497.53	0.15	35506.19	0.15
54	35496.00	0.17	35504.70	0.05

Table 4.9 Continued

J	ν_P	$\Delta\nu_P$	ν_R	$\Delta\nu_R$
55	35494.35	0.09	35503.45	0.21
56			35501.92	0.12
57	35491.16	0.13		
58	35489.44	0.06	35498.83	-0.02
59	35487.63	-0.07	35497.53	0.20
60	35485.96	-0.04	35496.00	0.22
61	35484.40	0.14	35494.35	0.14
62	35482.55	0.04	35492.54	-0.07
63	35480.67	-0.05	35491.16	0.17
64	35478.85	-0.06	35489.44	0.10
65	35477.12	0.05	35487.63	-0.03
66	35475.22	0.02	35485.96	0.00
67	35473.29	-0.02	35484.40	0.18
68	35471.33	-0.07	35482.55	0.08
69	35469.47	0.02	35480.67	-0.01
70	35467.61	0.13	35478.85	-0.02
71	35465.42	-0.06	35477.12	0.08
72	35463.36	-0.10	35475.22	0.05
73	35461.42	0.01	35473.29	0.00
74	35459.25	-0.09	35471.33	-0.04
75	35457.19	-0.05	35469.47	0.04
76	35455.11	0.00	35467.61	0.15
77	35452.99	0.03	35465.42	-0.05
78	35450.73	-0.05	35463.36	-0.09
79	35448.51	-0.06	35461.42	0.02
80	35446.39	0.05	35459.25	-0.08
81	35444.03	-0.05	35457.19	-0.04
82	35441.77	-0.03	35455.11	0.00
83	35439.47	-0.02	35452.99	0.03
84	35437.11	-0.04	35450.73	-0.05
85	35434.75	-0.04	35448.51	-0.07
86	35432.36	-0.04	35446.39	0.04
87	35429.95	-0.04	35444.03	-0.07
88	35427.51	-0.04	35441.77	-0.05
89	35425.05	-0.04	35439.47	-0.05
90	35422.56	-0.04	35437.11	-0.07
91	35420.05	-0.03	35434.75	-0.08
92	35417.51	-0.03	35432.36	-0.09
93	35414.90	-0.08	35429.95	-0.09
94	35412.35	-0.04	35427.51	-0.10
95	35409.78	0.01	35425.05	-0.10

Table 4.9 Continued

J	ν_P	$\Delta\nu_P$	ν_R	$\Delta\nu_R$
96	35407.16	0.03	35422.56	-0.10
97	35404.47	0.01	35420.05	-0.10
98	35401.79	0.03	35417.51	-0.11
99			35414.90	-0.16
100	35396.32	0.02	35412.35	-0.12
101	35393.58	0.05	35409.78	-0.08
102	35390.71	-0.03	35407.16	-0.06
103	35387.89	-0.03	35404.47	-0.09
104	35385.01	-0.06	35401.79	-0.09
105	35382.22	0.02	35399.08	-0.08
106	35379.28	-0.03	35396.32	-0.11
107	35376.38	-0.01	35393.58	-0.08
108	35373.41	-0.03	35390.92	0.04
109	35370.52	0.04	35388.11	0.04
110	35367.54	0.06	35385.27	0.04
111	35364.47	0.01	35382.40	0.03
112	35361.53	0.11	35379.56	0.08
113			35376.72	0.15
114			35373.77	0.14
115			35370.76	0.09
116			35367.84	0.15
118			35361.83	0.19

TABLE 4.10 Rotational Constants (cm^{-1}) for Different Vibrational Levels of D' and A' States of $^{81}Br_2$ **

		Present Work		Calculated* from Ref.(58)	
	v	10^2B_v	10^8D_v	10^2B_v	10^8D_v
Upper State (D')					
	0	4.1283(58)	1.030(255)	4.1393	1.286
	1	4.1148(59)	1.065(263)	4.1247	1.287
	3	4.0862(297)	1.903(1690)	4.0957	1.289
	4	4.0565(297)	2.977(1695)	4.0812	1.290
Lower State (A')					
	5	5.4706(298)	4.688(1716)	5.5792	3.906
	8	5.2655(58)	4.815(260)	5.2741	4.711
	9	5.1903(59)	5.287(260)	5.1982	5.081
	10	5.1089(59)	5.689(265)	5.1180	5.515
	11	5.0231(59)	6.181(279)	5.0331	6.016
	12	4.9403(60)	7.368(284)	4.9429	6.589

*Calculated from Rotational Constants of $^{79}Br_2$ given in Ref (58).

** Band origins are

$v' - v''$	$\nu(cm^{-1})$
0-8	34555.66 (2)
0-9	34433.10 (2)
0-10	34315.54 (2)
0-11	34203.15 (2)
1-8	34703.83 (2)
1-12	34244.57 (2)
3-5	35394.04 (4)
4-5	35540.60 (7)

TABLE 4.11 Rotational Constants (cm^{-1}) for D' and A' States of $^{81}Br_2$

	D' State	A' State
$C_{r1}(B_e)$	4.1395×10^{-2}	5.7612×10^{-2}
$C_{r2}(-\alpha_e)$	-1.722×10^{-4}	-4.256×10^{-4}
$C_{r3}(\gamma_e)$		-1.860×10^{-5}
$C_{d1}(D_e)$	1.210×10^{-8}	8.329×10^{-8}
$C_{d2}(\beta_e)$	-3.93×10^{-9}	-1.11×10^{-8}
C_{d3}	1.73×10^{-9}	8.18×10^{-10}
$R_e(\text{Å})$	3.173	2.689

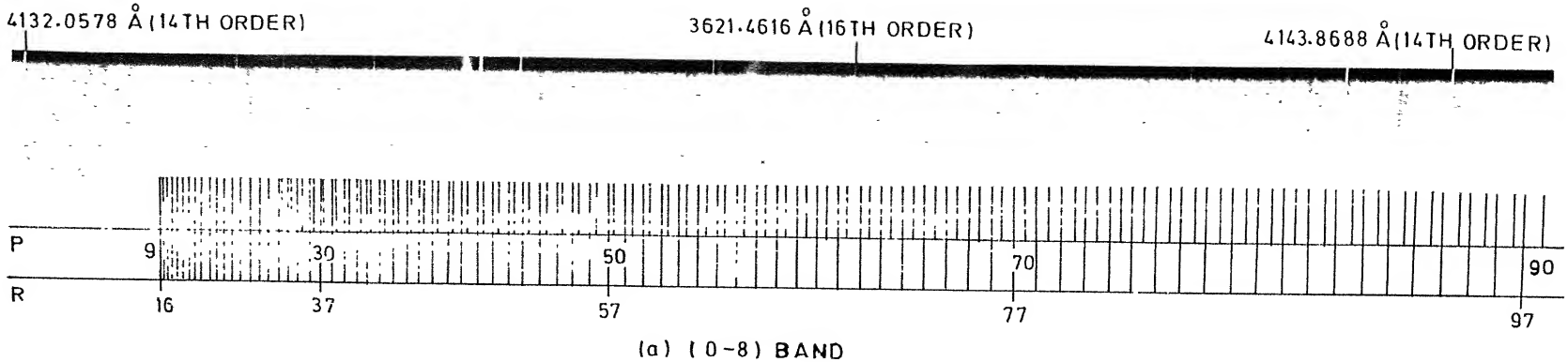

(a) (0-8) BAND

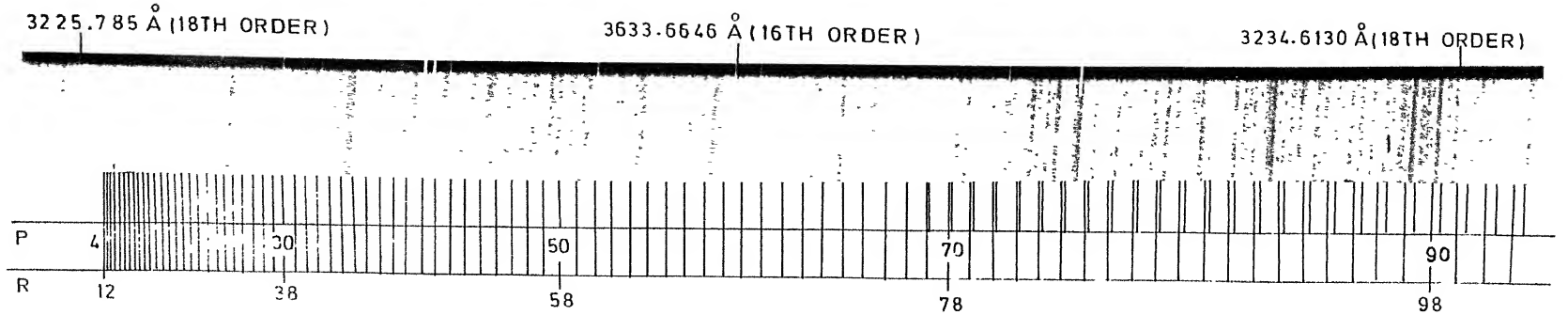

(b) (0-9) BAND

FIG. 4.1 ROTATIONAL STRUCTURE OF (0-8) AND (0-9) BANDS OF $^{81}Br_2$ PHOTOGRAPHED IN THE 20TH ORDER AT A RECIPROCAL DISPERSION OF ABOUT 0.11 Å/mm. AIR WAVELENGTH AND CORRESPONDING ORDER OF FEW LINES OF THE REFERENCE SPECTRUM HAVE BEEN MENTIONED.

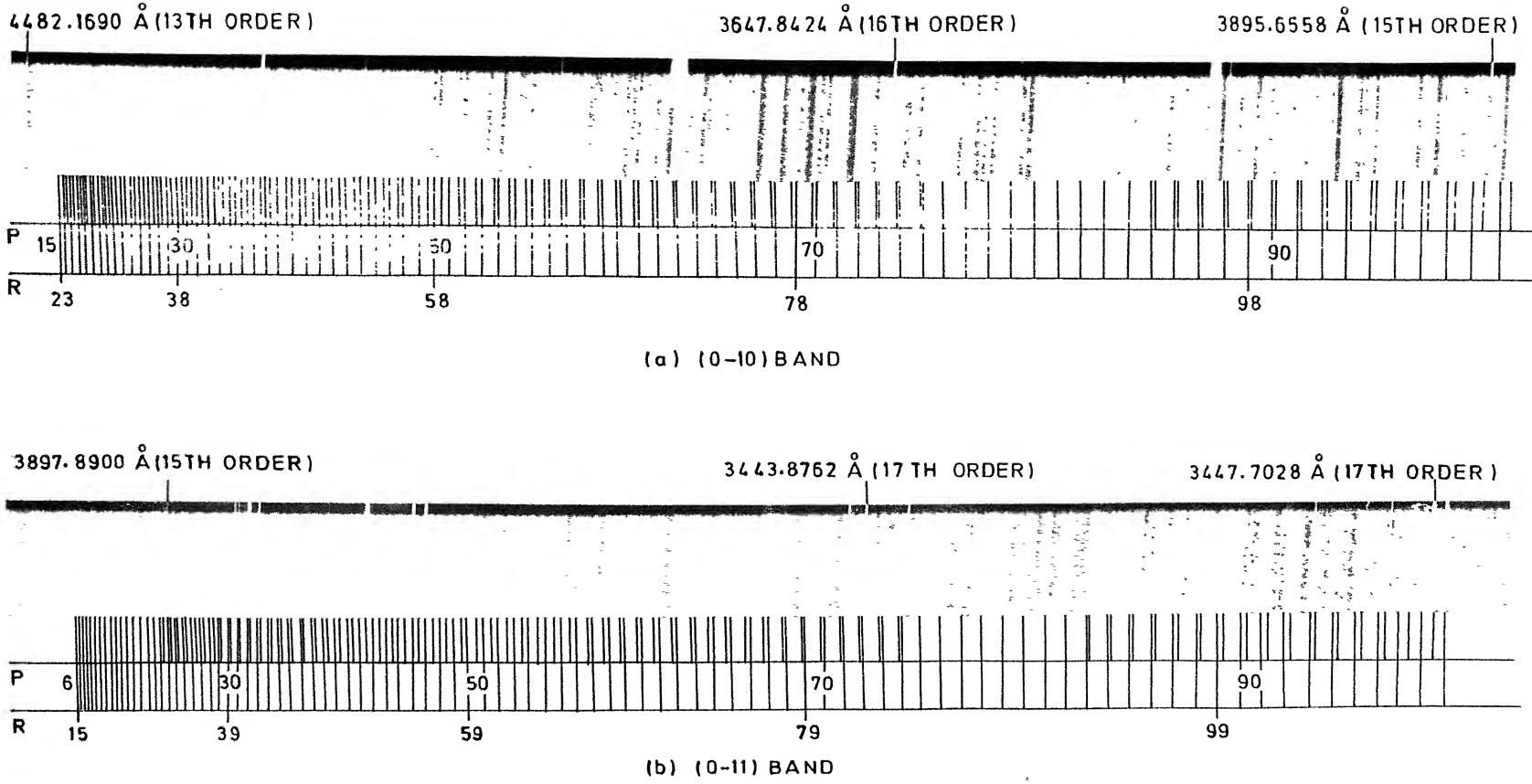

FIG. 4.2 ROTATIONAL STRUCTURE OF (0-10) AND (0-11) BANDS OF $^{81}Br_2$ PHOTOGRAPHED IN THE 20TH ORDER AT A RECIPROCAL DISPERSION OF ABOUT 0.11 Å /mm. AIR WAVELENGTH AND CORRESPONDING ORDER OF FEW LINES OF THE REFERENCE SPECTRUM HAVE BEEN MENTIONED.

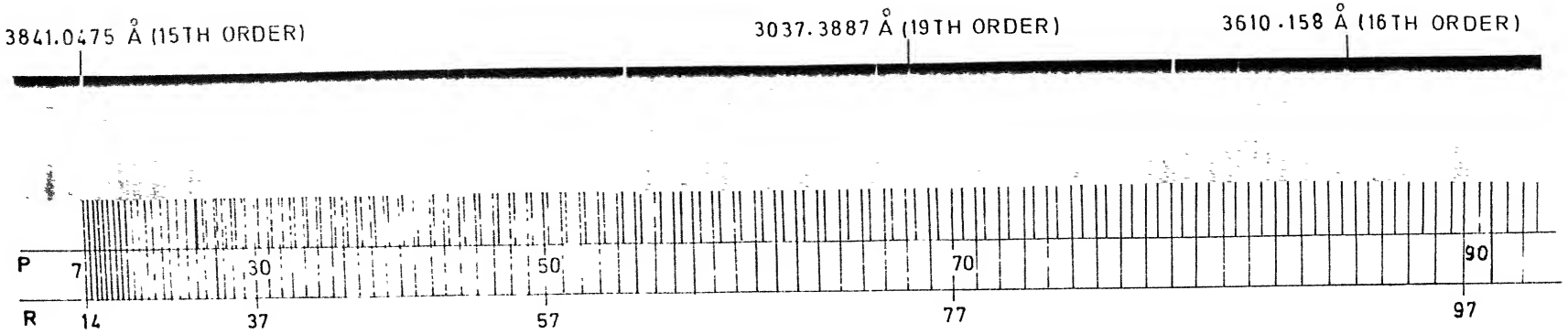

(a) (1-8) BAND

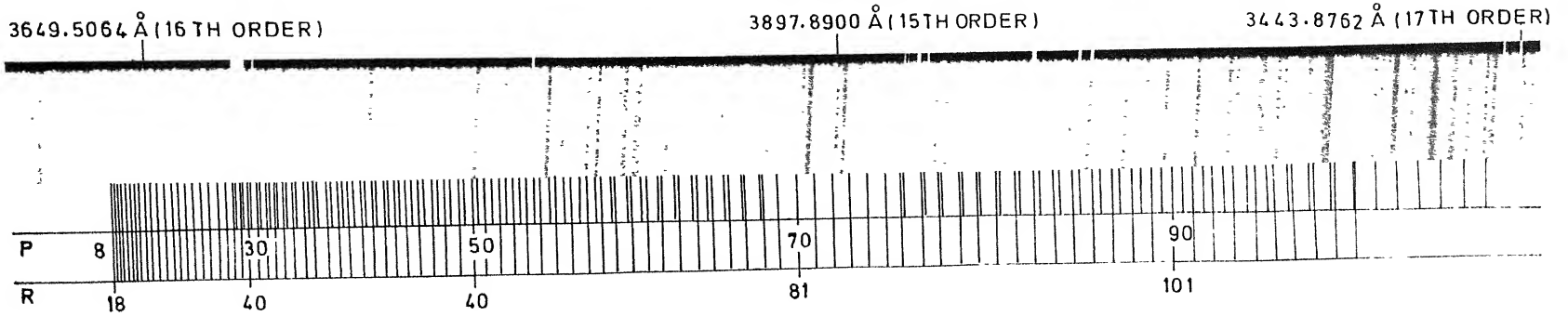

(b) (1-12) BAND

FIG. 4.3 ROTATIONAL STRUCTURE OF (1-8) AND (1-12) BANDS OF $^{81}Br_2$ PHOTOGRAPHED IN THE 20TH ORDER AT A RECIPROCAL DISPERSION OF ABOUT 0.11 Å/mm. AIR WAVELENGTH AND CORRESPONDING ORDER OF FEW LINES OF THE REFERENCE SPECTRUM HAVE BEEN MENTIONED.

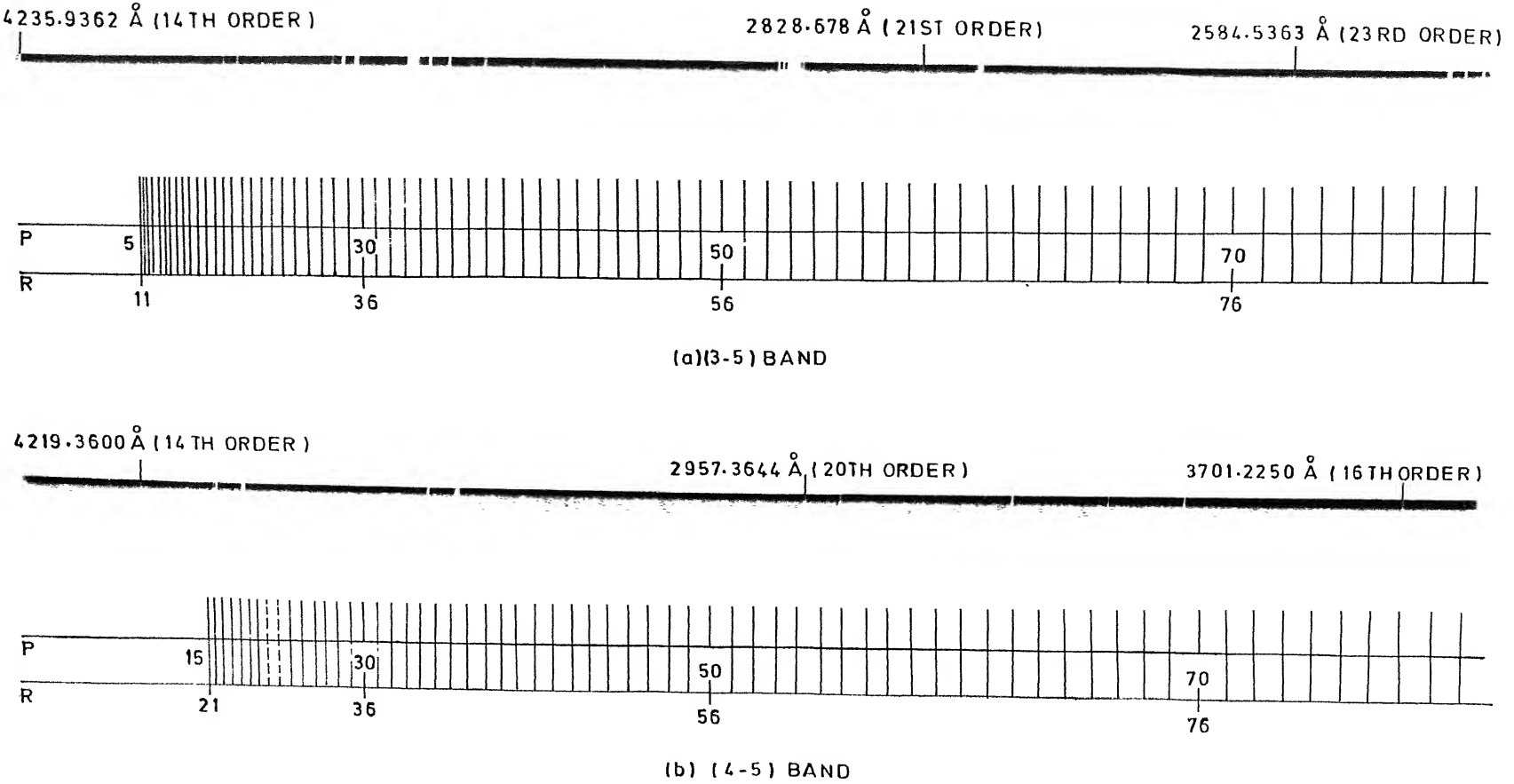

FIG. 4.4 ROTATIONAL STRUCTURE OF (3-5) AND (4-5) BANDS OF $^{81}Br_2$ PHOTOGRAPHED IN THE 21ST ORDER AT A RECIPROCAL DISPERSION OF ABOUT 0.09 Å/mm. AIR WAVELENGTH AND CORRESPONDING ORDER OF FEW LINES OF THE REFERENCE SPECTRUM HAVE BEEN MENTIONED.

CHAPTER 5

RKR POTENTIALS AND FRANCK-CONDON FACTORS CORRESPONDING TO D' - A' SYSTEM OF $^{81}Br_2$

5.1 Introduction

Several types of potential functions U which are useful for a semi-quantitative discussion of a particular electronic state of a diatomic molecule can be obtained[69,70] by using the spectroscopic data on energy levels. In the Rydberg-Klein-Rees (RKR) first order WKB method a more accurate potential function is derived from the experimental vibrational and rotational spectroscopic term values without imposing any assumed analytic form on the potential. The method was initially developed by Rydberg[71], and Klein[72] on the basis of Bohr-Sommerfeld quantization of the phase integral for the vibrational motion. Afterwards, Rees[73] developed analytical modifications to their graphical procedures. Vanderslice et al[74] made it compatible for use on high speed electronic computers. High order WKB

approximations have been discussed by different authors[75,76] but their effects have been found to be small even in the case of hydrogen[75].

Franck-Condon factors govern the main features of the vibrational intensity distribution in molecular electronic transition. Franck[77] qualitatively developed the main idea, which was later given a wave-mechanical basis by Condon[78]. According to this idea the intensity fluctuations in a band system arise primarily from the overlap of the wave functions characterizing the vibrational levels of the upper and lower electronic states. For high vibrational levels, the wave functions are rapidly varying oscillatory functions within the range of the classically allowed motion. So, the overlap integrals depend critically on the phase relation of the initial and final wave functions. This specifically nonclassical effect has been termed as "internal diffraction" by Condon[79].

The spectroscopic parameters obtained in Chapter 3 and Chapter 4 are used to calculate RKR potentials for both the states involved in the D' - A' system of bromine. These RKR turning points are then used to calculate the Franck-Condon factors for the band system.

5.2 Theory

In the usual RKR method, the "classical turning points" $R_{min} = R -$ and $R_{max} = R +$ for the vibrational level with

quantum number v can be calculated from the formula[80]

$$R \pm = (f/g + f^2) \pm f \qquad (5.1)$$

where f and g are the intermediate integrals given by

$$f_v = (\hbar/4\pi\ \mu c)^{\frac{1}{2}} \int_{v_{min}}^{v} [G(v) - G(v')]^{-\frac{1}{2}}\, dv', \qquad (5.2)$$

$$g_v = (\hbar/4\pi\ \mu c)^{-\frac{1}{2}} \int_{v_{min}}^{v} B(v')\, [G(v)-G(v')]^{-\frac{1}{2}}\, dv' \qquad (5.3)$$

where μ is the reduced mass. The vibrational term value G(v) and the rotational constant B(v) may be expressed, in the conventional way, as

$$G(v) = \sum_{i=1}^{m} C_{vi}(v+\tfrac{1}{2})^i, \qquad (5.4)$$

$$B(v) = \sum_{i=1}^{n} C_{ri}(v+\tfrac{1}{2})^{i-1}. \qquad (5.5)$$

The main problem of accurately evaluating the integrals in Eqs (5.2) and (5.3) is the singularity which occurs at the upper limit of integration. Various authors have discussed and used a variety of methods to treat this singularity[72-76,80-92]. The lower limit of integration v_{min} is the value of v at the potential minimum. In Klein's treatment[72] $v_{min} = -\frac{1}{2}$. A slight adjustment of the value of v_{min} corresponding to Dunham's Y_{00} correction[93] improves the quantum mechanical consistency of the curve. With the inclusion of this correction which is generally small, v_{min} is approximately given by[94]

$$v_{min} \approx -\tfrac{1}{2} - Y_{00}/C_{v1}, \qquad (5.6)$$

where

$$Y_{00} = (C_{r1} + C_{v2})/4 - C_{r2}C_{v1}/12\, C_{r1} + (C_{r2}C_{v1})^2/144\, C_{r1}^3, \quad (5.7)$$

and the corresponding corrected energy of level v is $G(v) + Y_{00}$.

In this work the Klein f and g integrals were evaluated by fast and accurate 4-point Gauss-Mehler quadrature method with appropriate weight function[90,92,95,96]. The quadrature procedure can be written as[92]

$$\frac{2}{b-a} \int_a^b f(v)\, dv = \int_{-1}^{1} F(x)\, dx$$

$$= \int_{-1}^{1} w(x)\, F_w(x)\, dx$$

$$\approx \sum_{i=1}^{p} H_i\, F_w(x_i). \quad (5.8)$$

The first transformation from the inteval (a,b) onto the interval (-1,1) is obtained by the substitution $v = \frac{1}{2}(b+a) + \frac{1}{2}x(b-a)$. In the next step w(x) is an arbitrary weight function which can be chosen to offset the singularities in f and g at the upper limit v. The integral can then be approximated by a sum over p points, were $\{x_i\}$ and $\{H_i\}$ can be extracted from appropriate Jacobi polynomials[92,95]. Here the integration interval was successively subdivided into 1,2,4,8,16 and 32 segments, each of which was estimated with a 4-point quadrature. Only the last segment

containing the singularity was evaluated with the $(1-x)^{-\frac{1}{2}}$-weighted quadrature whereas all other segments were evaluated with the usual Gauss-Legendre formula.

The intensity emitted in the radiative transition $(v',J') \longrightarrow (v'', J'')$ is given by[5,80]

$$I_{v''J''}^{v'J'} = \left(\frac{64\pi^4 c}{3}\right)\left(\frac{S_{J''}^{J'} N_{v'J'}}{(2J'+1)}\right)\nu^4 |\langle \psi_{v'J'} | \mu_e(R) | \psi_{v''J''} \rangle|^2, \tag{5.9}$$

where $S_{J''}^{J'}$ is the rotational line strength given by the Hönl-London formula, $N_{v'J'}$ is the population of the upper level, ν is the frequency of the emitted line in wave numbers (cm^{-1}), and ψ_{vJ} is the rotational-vibrational wave function characterizing the (v,J) state and $\mu_e(R)$ is the electronic transition moment function.

Now, it can reasonably be supposed that $\mu_e(R)$ will be a slowly varying function of R over a small range of R in which the vibrational wave functions have appreciable value. By replacing $\mu_e(R)$ in the last factor in Eq(5.9) by an average or effective value $\bar{\mu}_e$ it can be taken outside the integral to give

$$|\langle \psi_{v'J'} | \mu_e(R) | \psi_{v''J''} \rangle|^2 = |\bar{\mu}_e|^2 |\langle \psi_{v'J'} | \psi_{v''J''} \rangle|^2, \tag{5.10}$$

where the square of the overlap integral is known as the Franck-Condon factor (FCF) and is generally denoted by q.

In the R-centroid approximation, $|\bar{\mu}_e|^2$ is given by $|\mu_e(\bar{R})|^2$, $\bar{R}$ being the R-centroid, so that[97]

$$|\mu_e(\bar{R})|^2 = \frac{|\langle \psi_{v'J'} | \mu_e(R) | \psi_{v''J''} \rangle|^2}{|\langle \psi_{v'J'} | \psi_{v''J''} \rangle|^2} \qquad (5.11)$$

$$\bar{R} = \frac{\langle \psi_{v'J'} | R | \psi_{v''J''} \rangle}{|\langle \psi_{v'J'} | \psi_{v''J''} \rangle|^2} \qquad (5.12)$$

The radial wave functions in the Franck-Condon overlap integral are the solutions of the one dimensional Schrödinger equation for effective potential

$$U_J(R) = U_o(R) + K\hbar/(4c\,\mu\,R^2) \qquad (5.13)$$

where $U_o(R)$ is the rotationless potential and the second term on the right hand side is the centrifugal term, $K = [J(J+1) - \Omega^2]$, μ is the molecular reduced mass. The wave functions are implicit functions of the rotational quantum numbers.

The Schrodinger equation for the motion of a diatomic molecule can be expressed into its angular and radial parts and its solution may be expressed in the form[98,99]

$$\psi = R^{-1}\, P(R)\, Y_{J\wedge M}(\Theta, \Phi, \phi), \qquad (5.14)$$

where R, Θ, Φ are the spherical polar coordinates of one nucleus relative to the other one, and ϕ is an additional coordinate giving the angular orientation of the electronic charge cloud about the internuclear axis. The $Y_{J\wedge M}$'s are the hypergeometric functions, $\wedge$ is the quantum number for

the z-component of electronic angular momentum. The P(R) is the solution of the one-dimensional radial Schröndinger equation

$$P^{(2)}(R) = [U(R) - E]\, P(R), \qquad (5.15)$$

$$P^{(n)} = d^n P/dR^n,$$

where U(R) is the radial internuclear potential as discussed in section 1.2 of Chapter 1. The boundary conditions for (5.15) are: P(0) = 0, and P(R) is bounded.

The radial wave functions were computed by numerical solution of the radial Schrödinger equation (5.15) using the Numerov method in a manner similar to that introduced by Cooley[99] and later developed by Zare and Cashion[100]. Values of the potential at equally spaced intervals on the abscissa required for this method were generated from the known RKR potential by Lagrangian interpolation. After computing the wave functions, the overlap integrals and R-centroids were evaluated using Simpson's method.

5.3 Calculations

The vibrational and rotational constants reported in Chapter 3 and Chapter 4 were used to calculate the RKR curves [rotationless $U_o(R)$] for the D' and A' states of $^{81}Br_2$. The calculations of the turning points were performed by 4-point Gauss-Mehler quadrature method[95] using a program written

in FORTRAN-10 on DEC 1090 computer. These RKR potentials for both the electronic states were then used to obtain the exact vibrational wavefunctions by direct numerical solution of radial Schrödinger equation. Franck-Condon factors and R-centroids were calculated on DEC 1090 computer using a slightly modified version of the program due to Zare and Cashion.[100] The integrations were performed between the limits 2.1 Å and 4.1 Å with step size of 0.001 Å. A further decrease of the step size to 0.0005 Å did not change the larger values ($>10^{-2}$) of FCFs appreciably. The FCFs are expected to be reliable to one or two digits in the fourth significant figure for the larger values.

5.4 Results and Discussion

The G(v)'s and RKR turning points computed for D' and A' curves of $^{81}Br_2$ are given in Table 5.1 and Table 5.2 respectively. The potential energy curves are shown in Fig 5.1. Near the dissociation limit of A' curve a flaring out of the turning points of the inner or repulsive branch of the curve was noticed. This misbehavior may be due to slight inadequacies in the rotational constants near dissociation. The errors introduced in the RKR turning points due to inaccurate rotational constants are small for lower vibrational levels but rapidly build up for higher vibrational levels.

To demonstrate the reliability of the values of FCFs and R-centroids comparisons of experimental and calculated values of vibrational term values and rotational constants for both D' and A' states are given in Table 5.3 and Table 5.4 respectively. The entries in column 2 refer to the experimental data for G(v) and those in column 3 refer the eigenvalues (E_v) obtained by numerical solution of the radial Schrödinger equation. Column 4 gives the difference between them. Similarly column 7 gives the difference between the spectroscopic values of B(v) and those (B_{cal}) calculated from the expectation values of $1/R^2$. The values of FCFs calculated agree with those reported by Sur and Tellinghuisen[58] for $0 \leq v' \leq 5$ for D' - A' system of $^{81}Br_2$.

The FCFs and $\bar{R}$s for the D' - A' system of $^{81}Br_2$ computed for $0 \leq v'' \leq 22$ and $0 \leq v' \leq 10$, and $J' = J'' = 0$ are tabulated in Table 5.5. The FCFs qualitatively agree with the intensity distribution of D' - A' emission band system of Br_2 mentioned in Chapter 3.

Table 5.1 Results of the Calculations for the Potential Energy Curve for D' State of $^{81}Br_2$

v'	G(v') (cm^{-1})	R_{min} (Å)	R_{max} (Å)
0	74.22	3.1006	3.2506
1	222.06	3.0517	3.3119
2	369.21	3.0197	3.3563
3	515.66	2.9947	3.3938
4	661.41	2.9738	3.4272
5	806.46	2.9557	3.4580
6	950.80	2.9396	3.4867
7	1094.43	2.9251	3.5140
8	1237.35	2.9118	3.5401
9	1379.56	2.8996	3.5651
10	1521.04	2.8882	3.5894
11	1661.81	2.8776	3.6130
12	1801.85	2.8677	3.6360
13	1941.16	2.8583	3.6585
14	2079.74	2.8495	3.6805
15	2217.58	2.8410	3.7022

Table 5.2 Results of the Calculations for the Potential Energy Curve for A' State of $^{81}Br_2$

v''	G(v'') (cm^{-1})	R_{min} (Å)	R_{max} (Å)
0	79.38	2.6210	2.7660
1	236.05	2.5760	2.8293
2	389.45	2.5474	2.8774
3	539.25	2.5256	2.9200
4	685.13	2.5078	2.9599
5	826.80	2.4927	2.9985
6	964.01	2.4795	3.0367
7	1096.51	2.4679	3.0749
8	1224.09	2.4575	3.1136
9	1346.59	2.4480	3.1531
10	1463.83	2.4394	3.1937
11	1575.70	2.4315	3.2356
12	1682.09	2.4242	3.2791
13	1782.94	2.4173	3.3246
14	1878.18	2.4109	3.3722
15	1967.81	2.4048	3.4222
16	2051.83	2.3989	3.4750
17	2130.28	2.3933	3.5309
18	2203.21	2.3878	3.5904
19	2270.71	2.3824	3.6537
20	2332.90	2.3771	3.7214
21	2389.92	2.3718	3.7940
22	2441.94	2.3664	3.8722

Table 5.3 Comparison of Experimental and Calculated Vibrational Term Values (cm^{-1}) and Rotational Constants (cm^{-1}) for D' State of $^{81}Br_2$

v'	G(v')	$E_{v'}$	$G(v')-E_{v'}$	B(v')	B'_{cal}	$B(v')-B'_{cal}$
0	74.22	74.15	0.07	0.041309	0.041299	0.000010
1	222.06	222.03	0.03	0.041137	0.041126	0.000011
2	369.21	369.19	0.02	0.040965	0.040955	0.000010
3	515.66	515.61	0.05	0.040792	0.040783	0.000009
4	661.41	661.33	0.08	0.040620	0.040611	0.000009
5	806.46	806.36	0.10	0.040448	0.040439	0.000009
6	950.80	950.69	0.11	0.040276	0.040266	0.000010
7	1094.43	1094.30	0.13	0.040104	0.040094	0.000010
8	1237.35	1237.22	0.13	0.039931	0.039923	0.000008
9	1379.56	1379.40	0.16	0.039759	0.039749	0.000010
10	1521.04	1520.85	0.19	0.039587	0.039580	0.000007

Table 5.4 Comparison of Experimental and Calculated Vibrational Term Values (cm^{-1}) and Rotational Constants (cm^{-1}) of A' State of $^{81}Br_2$

v''	G(v'')	$E_{v''}$	$G(v'')-E_{v''}$	B(v'')	B''_{cal}	$B(v'')-B''_{cal}$
0	79.38	78.80	0.58	0.057395	0.057379	0.000016
1	236.05	235.84	0.21	0.056932	0.056916	0.000016
2	389.45	389.14	0.31	0.056432	0.056418	0.000014
3	539.25	538.92	0.33	0.055895	0.055881	0.000014
4	685.13	684.81	0.32	0.055320	0.055308	0.000012
5	826.80	826.51	0.29	0.054709	0.054699	0.000010
6	964.01	963.74	0.27	0.054060	0.054050	0.000010
7	1096.51	1096.22	0.29	0.053374	0.053366	0.000008
8	1224.09	1223.77	0.32	0.052651	0.052648	0.000003
9	1346.59	1346.21	0.38	0.051890	0.051890	0.000000
10	1463.83	1463.37	0.46	0.051093	0.051096	-0.000003
11	1575.70	1575.16	0.54	0.050258	0.050270	-0.000012
12	1682.09	1681.48	0.61	0.049386	0.049403	-0.000017
13	1782.94	1782.26	0.68	0.048477	0.048499	-0.000022
14	1878.18	1877.42	0.76	0.047530	0.047555	-0.000025
15	1967.81	1966.98	0.83	0.046547	0.046581	-0.000034
16	2051.83	2050.97	0.86	0.045526	0.045563	-0.000037
17	2130.28	2129.40	0.88	0.044468	0.044500	-0.000032
18	2203.21	2202.33	0.88	0.043373	0.043398	-0.000025
19	2270.71	2269.87	0.84	0.042240	0.042248	-0.000008
20	2332.90	2332.15	0.75	0.041071	0.041056	0.000015
21	2389.92	2389.32	0.60	0.039864	0.039808	0.000056
22	2441.94	2441.55	0.39	0.038620	0.038529	0.000091

Table 5.5 Franck-Condon Factors and R-Centroids (Å) for the D'-A' System of $^{81}Br_2$, J' = J'' = 0

v'' \ v'	0	1	2	3	4	5
0	1.432E-9 2.975	1.656E-8 2.961	1.017E-7 2.949	4.401E-7 2.937	1.503E-6 2.926	4.314E-6 2.916
1	7.217E-8 2.989	7.334E-7 2.975	3.975E-6 2.961	1.522E-5 2.949	4.617E-5 2.937	1.179E-4 2.927
2	1.697E-6 3.004	1.487E-5 2.988	6.983E-5 2.974	2.326E-4 2.961	6.149E-4 2.949	1.372E-3 2.937
3	2.475E-5 3.020	1.826E-4 3.003	7.255E-4 2.987	2.050E-3 2.973	4.607E-3 2.960	8.728E-3 2.948
4	2.480E-4 3.036	1.492E-3 3.018	4.856E-3 3.001	1.125E-2 2.986	2.069E-2 2.972	3.190E-2 2.959
5	1.789E-3 3.054	8.402E-3 3.033	2.139E-2 3.015	3.858E-2 2.999	5.452E-2 2.984	6.331E-2 2.970
6	9.493E-3 3.073	3.263E-2 3.049	6.042E-2 3.029	7.738E-2 3.011	7.409E-2 2.995	5.339E-2 2.979
7	3.706E-2 3.093	8.414E-2 3.066	9.929E-2 3.043	7.343E-2 3.023	3.183E-2 3.003	4.263E-3 2.975
8	1.051E-1 3.116	1.307E-1 3.082	7.135E-2 3.055	1.219E-2 3.023	1.939E-3 3.060	2.344E-2 3.013
9	2.109E-1 3.142	9.200E-2 3.094	3.179E-3 3.025	1.937E-2 3.071	4.962E-2 3.039	3.996E-2 3.017
10	2.847E-1 3.172	3.486E-3 2.992	4.423E-2 3.108	6.464E-2 3.072	2.030E-2 3.038	1.736E-4 3.188
11	2.362E-1 3.210	8.666E-2 3.203	7.624E-2 3.100	4.701E-3 3.048	1.763E-2 3.088	4.176E-2 3.048

Table 5.5 Continued

v'' \ v'	0	1	2	3	4	5
12	1.005E-1 3.267	2.833E-1 3.222	4.828E-4 4.065	4.421E-2 3.097	4.471E-2 3.085	2.625E-3 2.991
13	1.262E-2 3.394	2.291E-1 3.272	2.132E-1 3.250	1.420E-2 2.922	2.592E-3 3.002	4.244E-2 3.102
14	2.442E-4 2.623	3.448E-2 3.404	3.250E-1 3.282	1.407E-1 3.303	1.816E-2 2.870	8.508E-3 3.238
15	1.004E-3 3.280	2.949E-3 2.951	4.941E-2 3.424	3.774E-1 3.296	1.053E-1 3.381	5.174E-3 2.404
16	2.488E-7 3.867	4.704E-3 3.332	1.556E-2 3.111	4.221E-2 3.461	3.847E-1 3.311	9.814E-2 3.458
17	7.749E-5 3.280	1.875E-4 2.743	9.761E-3 3.398	5.026E-2 3.206	1.450E-2 3.569	3.324E-1 3.321
18	1.825E-6 2.450	4.376E-4 3.386	2.845E-3 3.097	8.636E-3 3.522	1.075E-1 3.269	1.094E-3 2.645
19	5.716E-6 3.431	1.164E-4 3.066	6.133E-4 3.594	1.370E-2 3.230	3.046E-4 4.983	1.451E-1 3.313
20	2.402E-6 3.117	8.988E-6 3.929	1.003E-3 3.241	1.572E-5 3.854	2.958E-2 3.320	1.817E-2 3.097
21	1.101E-9 5.592	3.523E-5 3.308	5.644E-5 2.697	2.607E-3 3.380	6.817E-3 3.095	2.287E-2 3.428
22	3.352E-7 3.469	8.788E-6 3.029	7.328E-5 3.580	1.397E-3 3.171	9.536E-4 3.768	3.225E-2 3.263

Table 5.5 Continued

v'' \ v'	6	7	8	9	10
0	1.081E-5 2.906	2.430E-5 2.897	4.988E-5 2.888	9.479E-5 2.879	1.688E-4 2.871
1	2.635E-4 2.916	5.286E-4 2.906	9.696E-4 2.897	1.648E-3 2.888	2.624E-3 2.879
2	2.678E-3 2.926	4.695E-3 2.916	7.523E-3 2.906	1.115E-2 2.897	1.547E-2 2.888
3	1.445E-2 2.937	2.142E-2 2.926	2.888E-2 2.915	3.582E-2 2.905	4.120E-2 2.896
4	4.263E-2 2.947	5.034E-2 2.935	5.311E-2 2.924	5.021E-2 2.914	4.242E-2 2.904
5	6.162E-2 2.956	5.026E-2 2.944	3.344E-2 2.932	1.676E-2 2.920	4.900E-3 2.905
6	2.692E-2 2.964	7.006E-3 2.946	5.977E-6 2.600	4.752E-3 2.944	1.510E-2 2.928
7	1.764E-3 3.007	1.541E-2 2.974	2.917E-2 2.957	3.248E-2 2.944	2.482E-2 2.931
8	3.957E-2 2.994	3.419E-2 2.977	1.628E-2 2.960	2.380E-3 2.934	9.417E-4 2.972
9	1.201E-2 2.992	1.940E-6 3.962	9.078E-3 2.987	2.253E-2 2.967	2.560E-2 2.952
10	1.755E-2 3.026	3.213E-2 3.003	2.417E-2 2.984	7.238E-3 2.962	1.298E-6 3.927
11	2.465E-2 3.022	2.168E-3 2.977	4.200E-3 3.020	1.846E-2 2.990	2.303E-2 2.971
12	9.533E-3 3.059	2.869E-2 3.029	2.233E-2 3.004	4.996E-3 2.976	5.678E-4 3.035

Table 5.5 Continued

v'' \ v'	6	7	8	9	10
13	2.349E-2 3.032	1.253E-3 3.002	7.393E-3 3.043	2.110E-2 3.007	1.860E-2 2.988
14	1.866E-2 3.155	2.620E-2 3.019	1.471E-2 3.040	9.469E-5 2.704	6.698E-3 3.007
15	3.816E-2 3.233	5.089E-3 3.373	1.283E-2 2.952	2.393E-2 3.063	5.506E-3 2.943
16	8.698E-4 5.725	7.434E-2 3.276	1.858E-3 4.003	1.467E-3 2.431	2.541E-2 3.118
17	1.002E-1 3.516	1.896E-2 3.894	1.168E-1 3.332	3.694E-3 4.228	2.477E-3 3.997
18	2.133E-1 3.315	8.469E-2 3.561	4.715E-2 3.720	1.622E-1 3.385	1.328E-2 4.033
19	4.827E-2 3.294	7.299E-2 3.243	3.742E-2 3.627	4.951E-2 3.698	1.827E-1 3.419
20	1.003E-1 3.343	1.273E-1 3.352	2.155E-3 2.210	2.442E-4 4.904	1.364E-2 3.819
21	9.211E-2 3.261	1.268E-2 3.331	1.197E-1 3.352	1.041E-2 4.055	2.996E-2 3.444
22	6.106E-6 1.365	1.299E-1 3.314	1.968E-2 3.452	2.783E-2 3.206	4.675E-3 4.252

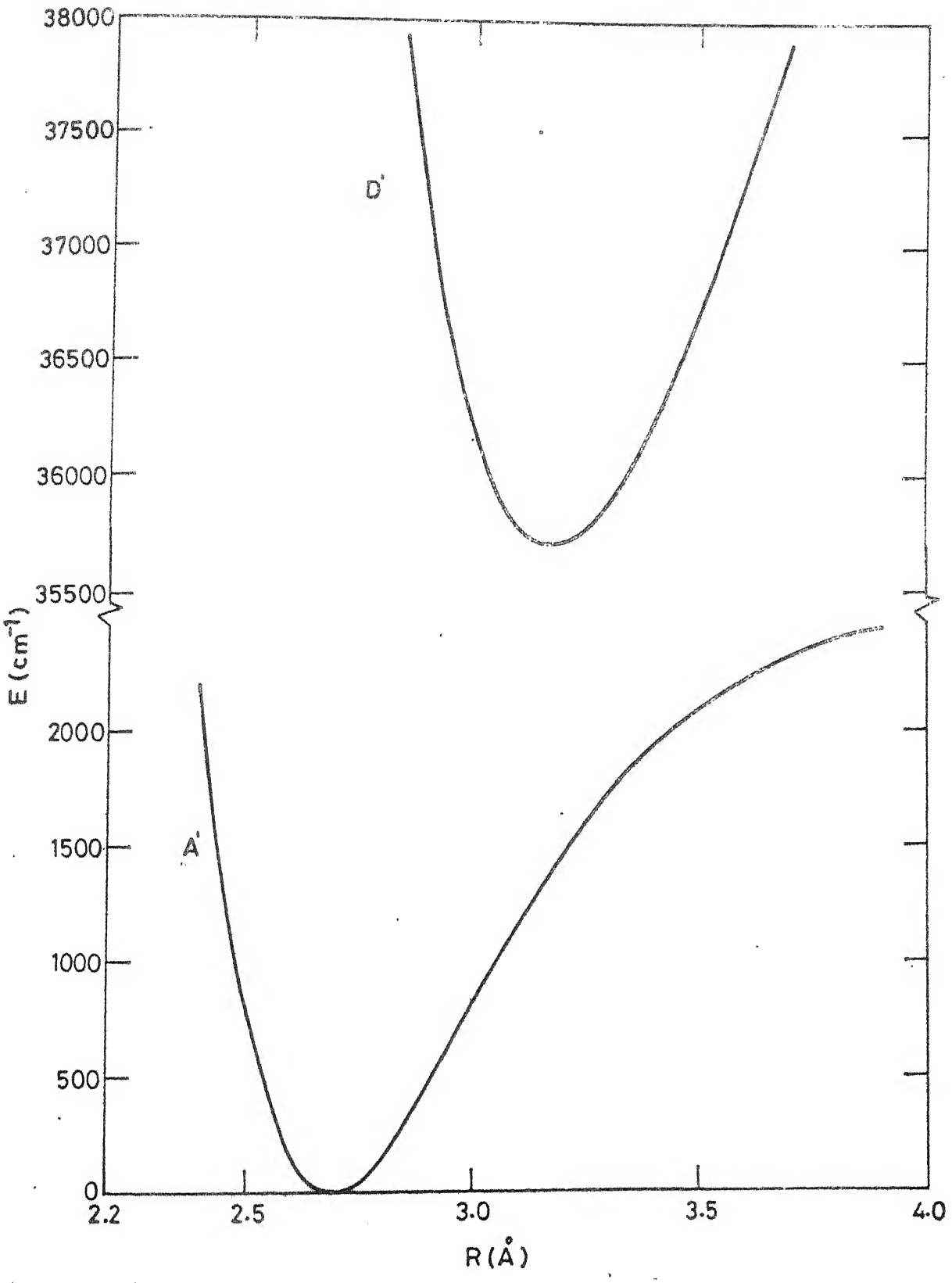

FIG. 5.1 POTENTIAL ENERGY CURVES OF D' AND A' STATES OF $^{81}Br_2$. ENERGIES ARE SHOWN RELATIVE TO THE MINIMUM OF THE A' CURVE

CHAPTER 6

Ar^+ LASER INDUCED FLUORESCENCE OF Br_2

6.1 Introduction

Resonance fluorescence is a technique which started receiving renewed interest with the advent of lasers. The phenomenon of resonance fluorescence involves the excitation of a molecule, initially in the ground state, to a discrete vibrational-rotational level of an excited electronic state, which after a finite time interval undergoes transitions to different vibrational-rotational levels of the ground electronic state. Bromine has a strong diffuse absorption continuum which peaks around 4100 Å and extends beyond 5000 Å. This continuum of Br_2 corresponds to an allowed $^1\Pi_{1u} \leftarrow X\ ^1\Sigma_g^+$ transition with some contribution also from the unbound states in the partially allowed $B\ ^3\Pi_{0_u^+} \leftarrow X\ ^1\Sigma_g^+$ transition. The discrete absorption bands of the $B \leftarrow X$ transition are observed at wavelengths longer than 5000 Å.[66] At wavelength $\lambda > 6500$ Å, absorption bands of weaker $A\ ^3\Pi_{1u} \leftarrow X\ ^1\Sigma_g^+$

transition are also observed.[67] An extensive study of high resolution absorption spectrum of B ← X system of $^{79}Br_2$ and $^{81}Br_2$ has been reported by Barrow et al.[68] An optically pumped quasi-continuous tunable laser over the visible, and infrared regions corresponding to B → X transition has been reported by Wodarczyk and Schlossberg.[101] Recently Venkateswarlu et al[37] have analysed the high resolution resonance fluorescence doublet series of Br_2 in the vacuum ultraviolet and reported the rotational and vibrational constants of the X state. The 5145 Å radiation of argon-ion laser lies in the region covered by the visible absorption system of bromine corresponding to B $^3\Pi_{0_u^+}$ – X $^1\Sigma_g^+$ transition, the energy of the laser radiation being slightly less than the energy of dissociation[102,103] of the excited state of Br_2 as shown in Fig 6.1. So after absorbing this radiation the molecules in the v'' = 0 level of the ground electronic state will give rise to fluorescence whereas those in the levels with v'' > 0 will dissociate. The 4880 Å radiation of the argon-ion laser will lift even the molecules which are in the ground electronic state with v'' = 0 beyond the dissociation limit. Holzer et al[104] used the green line (5145 Å) of argon-ion laser to excite bromine molecules into one of the vibrational-rotational levels (v', J') of the B $^3\Pi_{0_u^+}$ to get resonance fluorescence (RF) spectrum. The higher energy blue exciting line (4880 Å) of the laser may be

used to cause a virtual excitation of the molecules, initially in the ground state, into the continuum of vibrational-rotational levels beyond the convergence limit of the $^3\Pi_{0_u^+}$ state for stimulating the resonance Raman (RR) effect.[105]

In the present work the resonance fluorescence of Br_2 excited by 5145 Å radiation of an argon-ion laser has been investigated. A series of fluorescence doublets resulting from various v' (= 40) $\rightarrow$ v'' transitions has been recorded and analysed. The variation of electronic transition moment $[\mu_e(\bar{R})]$ with R-centroid ($\bar{R}$) has been reported.

6.2 Theory

The v'' values for the doublet series could be identified from the known G''(v) values and the molecular constants. The separation of the resonance fluorescence doublets is related to the lower state rotational constants and the upper state rotational quantum number (J') as given below:

$$\begin{aligned}\Delta\nu_{RP} &= F_v''(J'+1) - F_v''(J'-1) \\ &= [B_v''(J'+1)(J'+2) - D_v''(J'+1)^2(J''+2)^2] \\ &\quad - [B_v''(J'-1)J' - D_v''(J'-1)^2 J'^2] \\ &= (4J'+2)[B_v'' - 2D_v''(J'^2 + J' + 1)]. \qquad (6.1)\end{aligned}$$

Since $D_e'' \sim 10^{-6} B_e''$ for the ground state of Br_2, Eq (6.1)

can approximately be written, for lower vibrational levels, as

$$\Delta\nu_{RP} \simeq (4J' + 2)\, B_v'' \qquad (6.2)$$

So, J' can be obtained by taking it as the integral value nearest to the calculated value of J' using Eq (6.2). Then the positions of the P and R lines of the resonance series for different isotopic species can be calculated using the known spectroscopic parameters of B and X states. On comparing the positions with those obtained from the experiment, the values of v' and J', and the particular isotopic species involved in the fluorescence series can be identified.

Using Eqs. (5.9) and (5.11) the intensity of the fluorescence line corresponding to the transition $(v',J') \rightarrow (v'', J'')$ can be written as

$$I_{v'' J''}^{v'J'} = \left(\frac{64\pi^4 c}{3}\right)\left[\frac{S_{J''}^{J'} N_{v'J'}}{(2J'+1)}\right] \nu^4 |\langle \psi_{v'J'} | \psi_{v''J''} \rangle|^2 |\mu_e(\bar{R})|^2 \qquad (6.3)$$

$$\bar{R} = \frac{\langle \psi_{v'J'} | R | \psi_{v''J''} \rangle}{|\langle \psi_{v'J'} | \psi_{v''J''} \rangle|^2} \qquad (6.4)$$

is the R-centroid, and the square of the overlap integral,

$$|\langle \psi_{v'J'} | \psi_{v''J''} \rangle|^2 ,$$

is the Franck-Condon factor (q).

So, the fluorescence intensity $I_{v'' J''}^{v'J'}$ for $(v', J') \rightarrow (v'', J'')$ transition between two electronic states of a molecule can be written as

$$I_{v'' J''}^{v'J'} \propto q \, \nu^4 \, |\mu_e(\bar{R})|^2 \qquad (6.5)$$

6.3 Experimental Details

The preparation of the quartz sample tube containing pure bromine has been described in Chapter 2 (Section 2.2 and 2.1). The bromine vapor pressure in the sample tube was maintained at about 12 Torr by keeping the side tube containing liquid bromine at the melting point ($-23^{\circ}C$) of carbon-tetrachloride (CCl_4). The gaseous bromine in the cell was excited by 5145 Å radiation of CW argon-ion laser. The laser was operated at constant light mode. The power of the output laser beam was kept fixed at 300 mW. The fluorescence beam was collected at right angles to the direction of the incident laser beam and then dispersed by a Spex double monochromator fitted with holographic gratings. The beam thus dispersed was detected by a thermoelectrically cooled photomultiplier tube and recorded on a linear strip chart-recorder in the photon counting mode. The details of the experimental arrangement have been described in Section 2.4 of Chapter 2. The fluorescence spectra were recorded at reciprocal dispersions of 4 cm^{-1}/mm and 0.4 cm^{-1}/mm. The widths of the input and the output slits of the monochromator were kept fixed at 200μm. The relative intensities of the

recorded lines were corrected for the spectral sensitivity of the photomultiplier tube. The average of the heights of P and R lines corresponding to a particular v'-v" transition was taken as the relative intensity of the corresponding doublet.

6.4 Results and Discussion

The fluorescence doublets recorded in this experiment at a reciprocal dispersion of 4 cm^{-1}/mm are shown in Fig 6.2 together with v' - v" numbering. In the spectrum the doublets corresponding to v" = 5,10 and 17 are missing while those corresponding to v" = 15 and v" = 20 are very weak. In addition to the main fluorescence series other lines having comparatively low intensities can be seen. No systematic pattern could be recognised and hence no attempt has been made to analyse them. However, they may be due to the various vibrational-rotational relaxations or excitations of different isotopic species.

Air wavelengths (Å) and vacuum wavenumbers (cm^{-1}) of the positions of P and R lines of the fluorescence doublets and corresponding relative intensities, corrected for the spectral sensitivity of the photomultiplier tube, are tabulated in Table 6.1. Using the recent vibrational and rotational constants of $X\,{}^1\Sigma_g^+$ state given by Venkateswarlu et al[37] and the spectroscopic parameters of the B state given

by Barrow et al[68] the positions of the peaks of the doublets were found to correspond to the transitions from v' = 40, J' = 14 level of $B\ ^3\Pi_{0_u^+}$ to different v", J" levels of $X\ ^1\Sigma_g^+$ state of $^{81}Br_2$. A typical doublet corresponding to v' = 40 $\rightarrow$ v" = 11 transition recorded at higher dispersion (0.4 cm^{-1}/mm) is shown in Fig 6.3. The energy levels involved in (40-1) fluorescence doublet are shown in Fig 6.4.

A comparison of the average values (normalised to 10) of relative intensities of the doublets with the corresponding $q\lambda^4$ -factors (also normalised to 10) for each of the fluorescence doublets, for the transitions v' = 40 $\rightarrow$ v" = 1 to 10 for which the Franck-condon factors (q's) are known,[106] are shown in Fig 6.6.

The square of electronic transition moment $|\mu_e(\bar{R})|^2$ (in arbitrary units) has been calculated using known values of q and λ in Eq (6.5). The values of R-centroid ($\bar{R}$) and the corresponding $|\mu_e(\bar{R})|^2$ are given in Table 6.2. The variation of $|\mu_e(\bar{R})|^2$ with $\bar{R}$ is shown in Fig 6.7. Since the R-centroids and Franck-condon factors are not known for v" > 10, the curve could not be extended to higher $\bar{R}$ values. This plot is expected to show a peak as discussed in B-X system of I_2.[107-109]

The main source of error is the presence of fluorescence from other isotopic species which could not be accounted for in this study with a multimode laser. Although the contributions to the intensity from fluorescence due to the other isotopic species of Br_2 is comparatively small as known from the resonance fluorescence studies of Br_2 excited by the 5145 Å radiation of argon-ion laser operating in selected longitudinal mode,[110-112] it may not be negligible in the region covered by us. Error due to the possible fluctuation of the output power of the laser beam has been effectively eliminated by operating the laser in the 'light mode'. The side tube containing bromine was kept dipped in pure melting CCl_4 and the vapor pressure of Br_2 in the fluorescence cell remained sensibly constant throughout the experiment. So the change in Br_2 vapor pressure should not be a serious source of error. To prevent radiation trapping of the fluorescence beam the laser beam was passed close to the wall of the cell containing bromine as shown in Fig 6.5.

6.5 Conclusion

The fluorescence spectrum recorded has been identified as that due to transition from $v' = 40$, $J' = 14$ to different v'', J'' levels of $B\ ^3\Pi_{0^+_g} \rightarrow X\ ^1\Sigma^+_g$ system of $^{81}Br_2$. The observed intensities of the doublets agree well with those

expected on the basis of Franck-condon principle. The plot of $|\mu_e(\bar{R})|^2$ versus $\bar{R}$ shows a tendency to peak near 2.4 Å but it is not possible to definitely say anything about the exact location of the peak unless the plot is extended to cover the higher values of R-centroid which becomes possible when Franck-Condon factors and R-centroids for $v'' > 10$ are available.

TABLE 6.1 Positions and Relative Intensities of P and R Lines of the Fluorescence Doublets

	P branch			R branch		
v''	λ (Å)	ν (cm^{-1})	Relative Intensity (arb. units)	λ (Å)	ν (cm^{-1})	Relative Intensity (arb. units)
1	5231.17	19110.9	10.0	5229.91	19115.5	8.6
2	5319.38	18794.0	1.2	5318.05	18798.7	1.5
3	5410.11	18478.8	2.6	5408.65	18483.8	2.0
4	5503.18	18166.3	5.2	5501.73	18171.0	4.8
6	5697.29	17547.3	3.8	5695.70	17552.2	3.7
7	5798.41	17241.3	1.5	5796.87	17245.9	1.4
8	5902.53	16937.2	1.0	5900.85	16942.0	1.1
9	6009.54	16635.6	3.0	6007.85	16640.3	2.9
11	6233.21	16038.7	2.2	6231.34	16043.5	2.7
12	6349.97	15743.7	0.7	6348.12	15748.3	0.5
13	6470.31	15450.9	1.1	6468.31	15455.7	1.0
14	6594.26	15160.5	1.3	6592.26	15165.1	1.3
15	6722.06	14872.3	0.1	6719.93	14877.0	0.2
16	6853.77	14586.5	1.3	6851.61	14591.1	1.2
18	7129.82	14021.7	0.7	7127.48	14026.3	0.6
19	7274.53	13742.8	0.4	7272.09	13747.4	0.3
20	7423.85	13466.4	0.1	7421.37	13470.9	0.1

TABLE 6.2 Electronic Transition Moments for Various Values of R-Centroid

v''	R-centroid (Å)	Franck-Condon factor(q)	Intensity(I) (arb units)	$q_{12})^4$-factor (arb.units)	$\|\mu_e(\bar{R})\|^2$ (arb.units
1	2.339	0.00592	3.43	3.94	1.00
2	2.348	0.00096	0.50	0.60	0.96
3	2.360	0.00152	0.85	0.88	1.09
4	2.369	0.00309	1.83	1.68	1.25
5	2.340	3.0E-06			
6	2.390	0.00258	1.39	1.22	1.31
7	2.399	0.00103	0.53	0.45	1.34
8	2.413	0.00088	0.38	0.36	1.21
9	2.421	0.00228	1.09	0.87	1.44
10	2.465	5.0E-06			

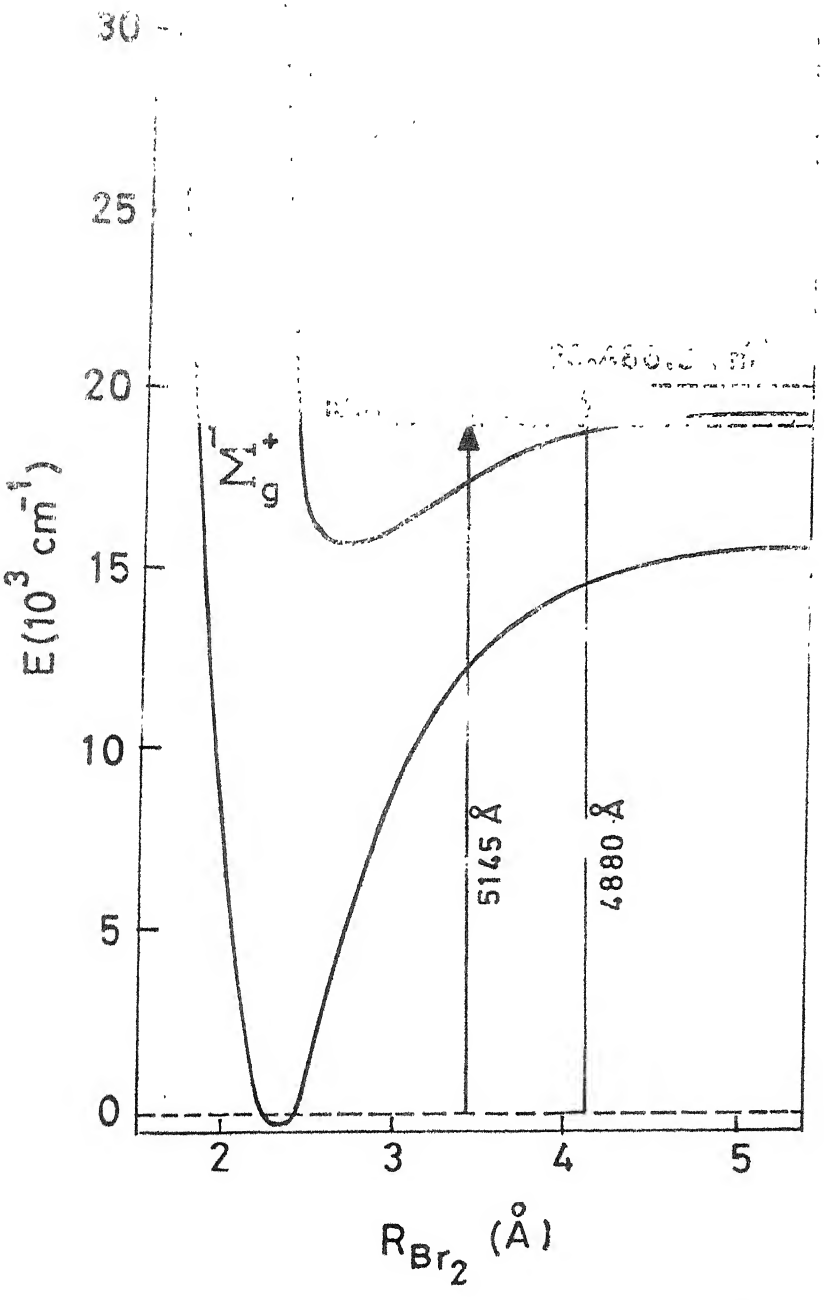

FIG. 6.1 POTENTIAL CURVES FOR $^1\Sigma_g^+$ AND $^3\Pi_{ou}^+$ STATES OF Br_2. THE RELATIONSHIPS OF 5145 Å AND 4880 Å EXCITING RADIATIONS OF Ar^+ LASER TO THE CONVERGENCE LIMIT OF EXCITED STATE HAVE BEEN SHOWN BY VERTICAL ARROWS [103]

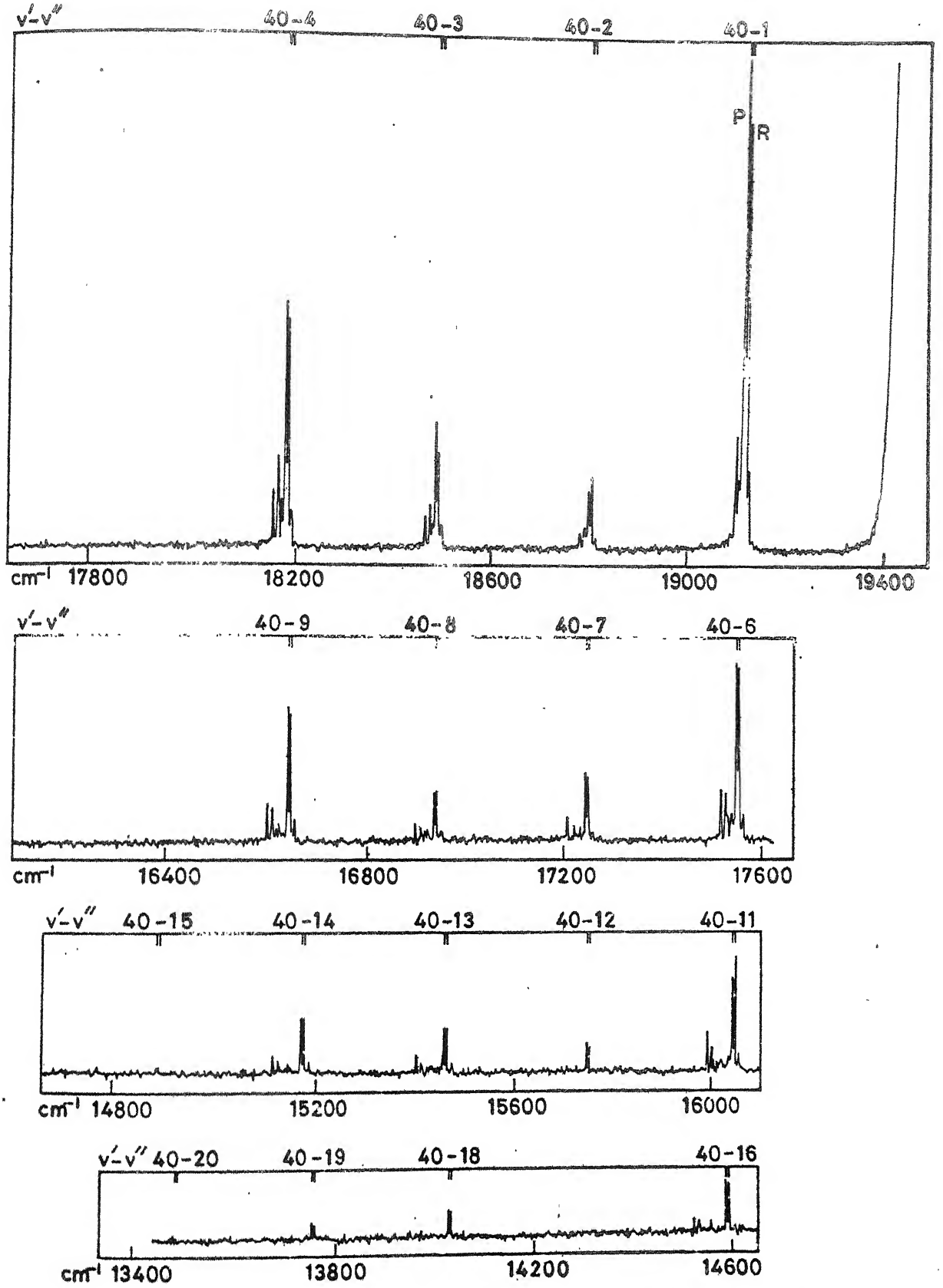

FIG. 6.2 FLUORESCENCE DOUBLETS RECORDED AT A RECIPROCAL DISPERSION OF 4 cm^{-1}/mm

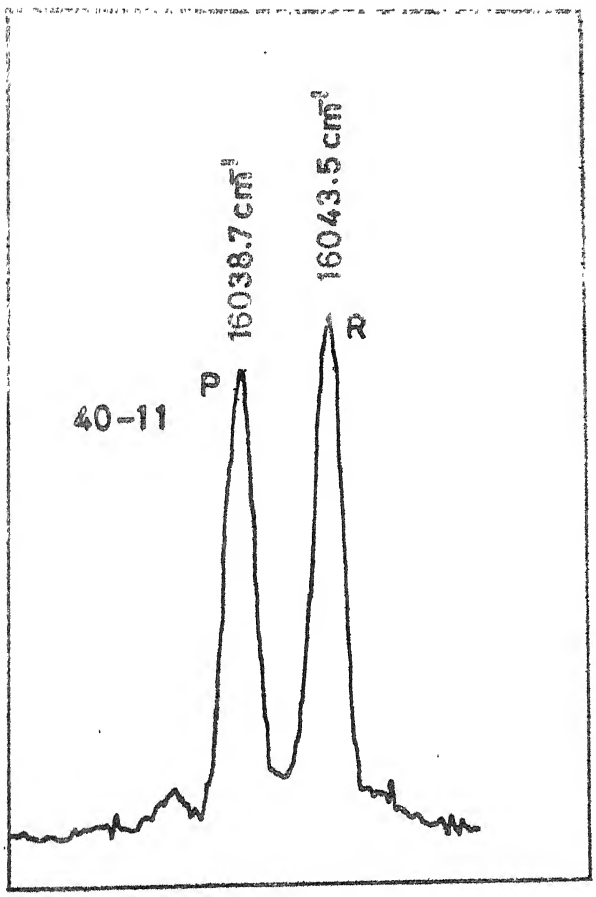

FIG.6.3 A TYPICAL v' = 40 → v'' = 11 DOUBLET RECORDED AT A RECIPROCAL DISPERSION OF 0.4 Å /mm.

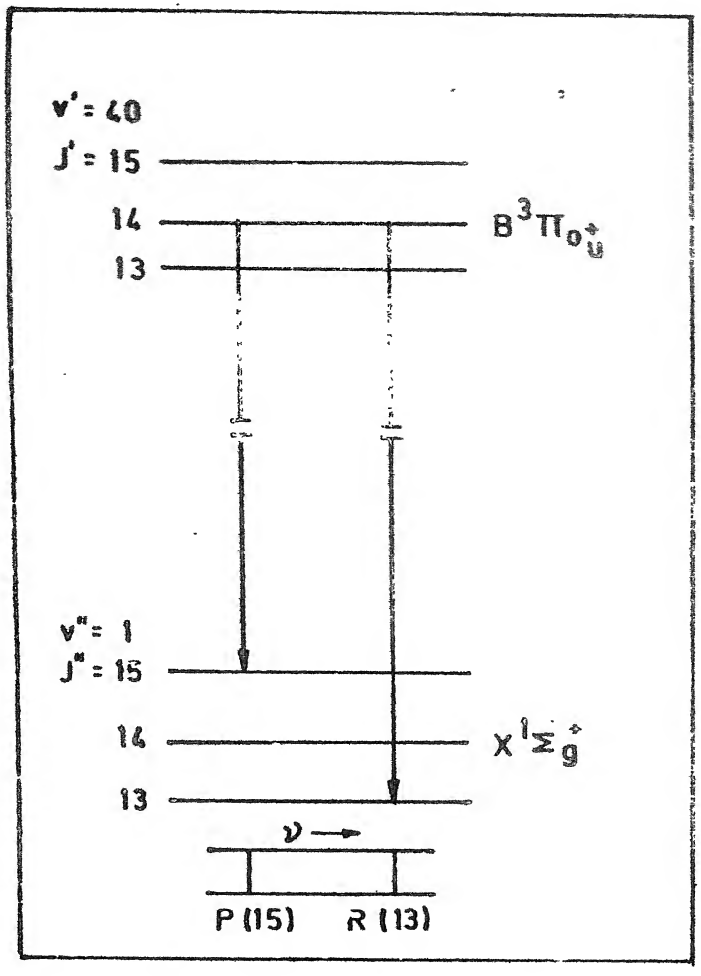

FIG.6.4 ENERGY LEVELS INVOLVED IN (40-1) FLUORESCENCE DOUBLET (not to scale)

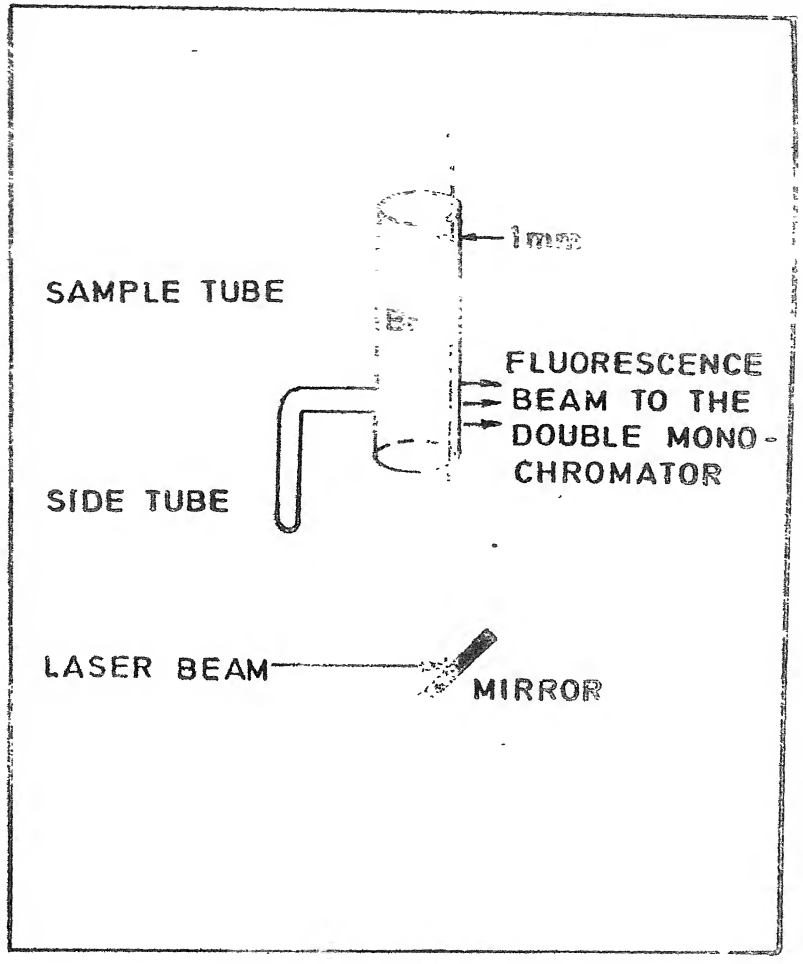

FIG.6.5 LASER EXCITATION OF Br_2 IN THE SAMPLE TUBE

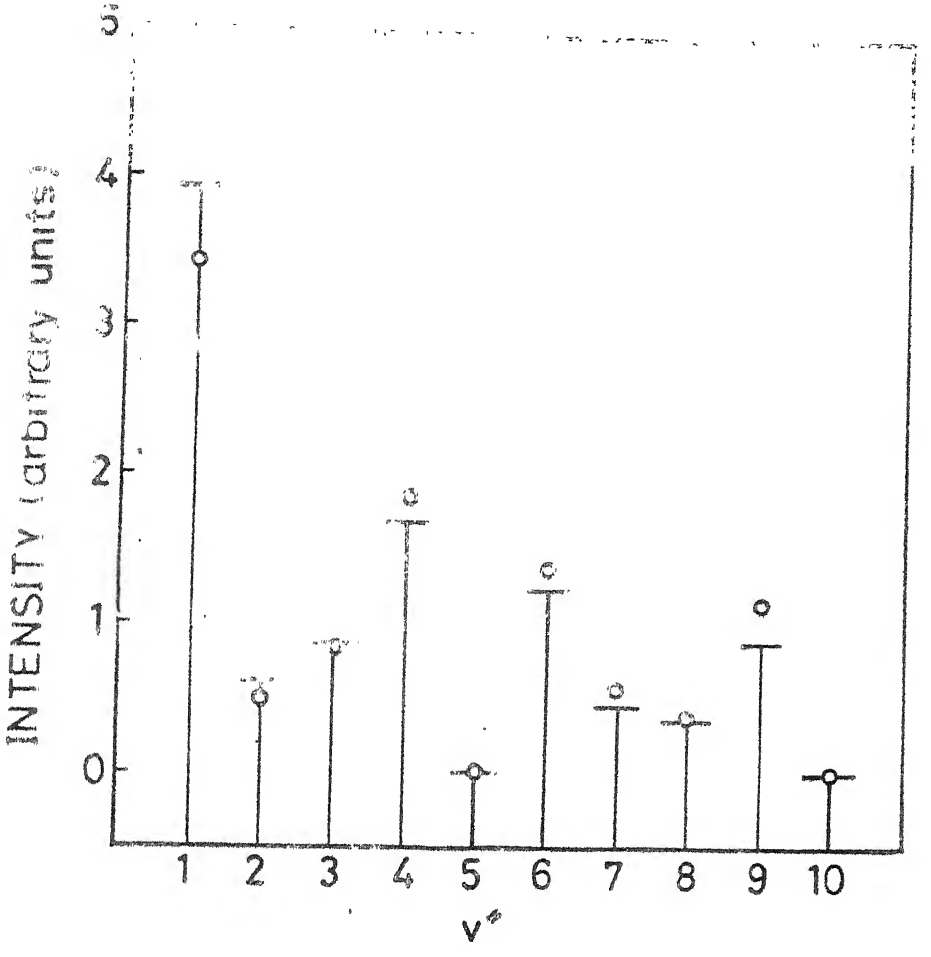

FIG 6.6 A COMPARISON OF THE AVERAGE VALUES (NORMALISED TO 10) OF RELATIVE INTENSITIES WITH THE CORRESPONDING $q\bar{\nu}^4$ -FACTORS (ALSO NORMALISED TO 10) FOR THE TRANSITIONS $v' = 40 \longrightarrow v'' = 0$ to 10. THE CIRCLES REPRESENT THE EXPERIMENTAL VALUES OF RELATIVE INTENSITIES. THE HORIZONTAL BARS REPRESENT THE CALCULATED VALUES OF $q\bar{\nu}^4$ -FACTORS.

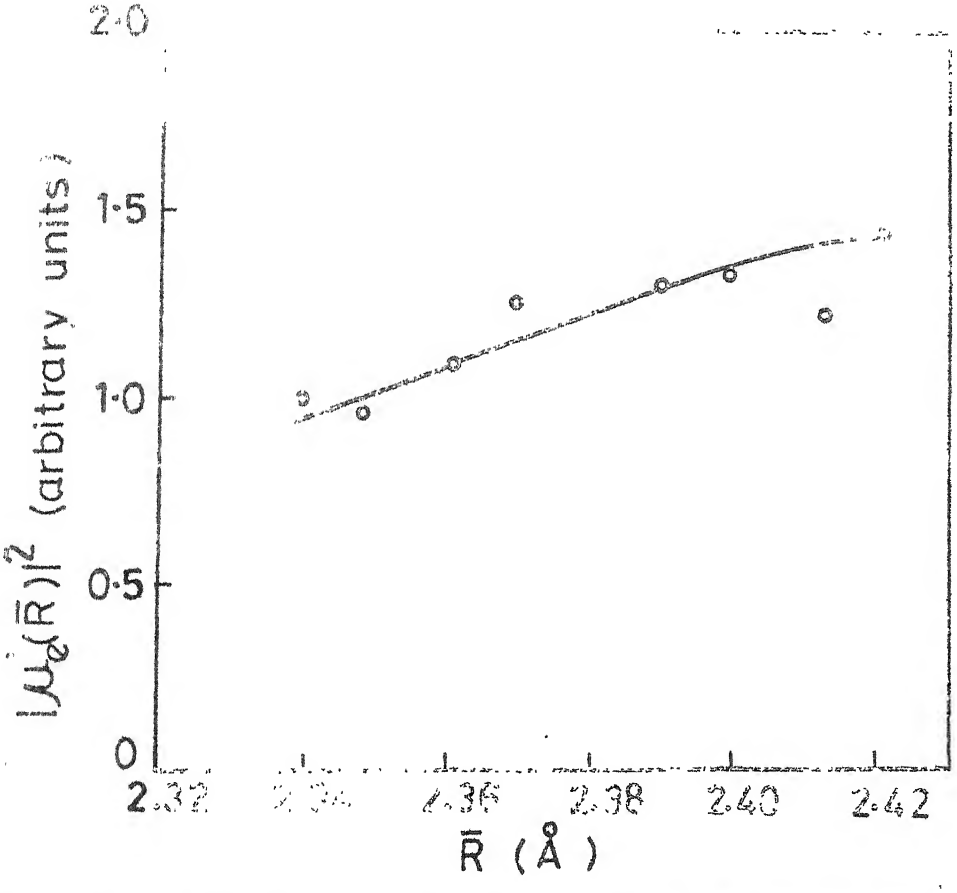

FIG. 6.7 VARIATION OF ELECTRONIC TRANSITION MOMENT WITH R-CENTROID

CHAPTER 7

SELF-QUENCHING OF B STATE OF Br_2 EXCITED BY Ar^+ LASER

7.1 Introduction

Self-quenching cross-sections for different vibrational levels (v') of the upper state of bromine corresponding to $B\ ^3\Pi_{0_u^+} \rightarrow X\ ^1\Sigma_g^+$ fluorescence was first reported by Capelle et al[113] on the basis of lifetime studies of bromine fluorescence after exciting selected vibrational levels of the B state of bromine using a nitrogen laser pumped tunable dye laser. Afterwards, McAfee, Jr and Hozack[114] reported the quenching cross-sections for five vibrational-rotational levels near the dissociation limit of the B state of bromine molecules after measuring the lifetimes by selective excitation of these levels using different single longitudinal modes in an argon-ion laser with pulse durations of 1-5 μs. Clyne et al[115,116] studied the kinetics of B state of Br_2 using a pressure-tuned narrow-band pulsed dye laser. In the present

work the self-quenching cross-section corresponding to (40-1) transition in $^{81}Br_2$ excited by 5145 Å radiation of a cw Ar^+ laser is calculated by studying the variation of the fluorescence intensity with the vapor pressure of Br_2 molecules.

7.2 Theory

After absorbing laser photons of frequency $h\nu$ the bromine molecules, initially in the ground electronic state, will be excited to a vibrational-rotational level (v',J') of a higher electronic state. These excited molecules can either reradiate this energy as fluorescence or redistribute the energy in collisions with unexcited bromine molecules. The process can be expressed symbolically as[117]

$$Br_2^* \longrightarrow Br_2 + h\nu \qquad (7.1)$$

$$Br_2^* + Br_2 \longrightarrow 2Br \text{ (or } Br_2) + Br_2 \qquad (7.2)$$

where Eq. (7.1) represents the fluorescence process and Eq. (7.2) the self-quenching phenomenon. The self-quenching process may cause the excited molecule to be non-radiatively de-excited to the ground state or to dissociate into two unbound bromine atoms. In the case of collision-induced predissociation to nearby repulsive electronic states whose potential curves cross that of the B state, the dominent quenching products can be expected to be free bromine atoms.

The self-quenching process is proportional to the concentration of the excited bromine molecules and that of the bromine molecules in the ground state which are denoted, respectively, by $[Br_2^*]$ and $[Br_2]$. In the steady state the number of excitation transitions per second must be equal to the number of decay transitions per second. So, in that case, we may write

$$\sigma_a I_o [Br_2] = \tau^{-1} [Br_2^*] + \sigma_s \bar{v} [Br_2] [Br_2^*] \qquad (7.3)$$

where σ_a is the absorption cross-section (cm^2) for photons of frequency ν, I_o is the irradiance ($cm^{-2} s^{-1}$) by incident photons, τ is the effective life-time of the excited state, σ_s is the self-quenching cross-section (cm^2) for bromine molecule in the vibrational-rotational level of B state and $\bar{v}$ is the mean relative collision speed ($cm\ s^{-1}$).

In the case of spontaneous predissociation τ may contain a non-radiative component (τ_{nr}) in addition to the radiative component (τ_{rad}), so that

$$\tau = \tau_{rad} + \tau_{nr} . \qquad (7.4)$$

Now, for a transition from a particular excited state, the intensity of fluorescence is given by

$$I_f = A [Br_2^*] \qquad (7.5)$$

where A is the transition probability per unit time.

Combining (7.3) and (7.5) we get

$$I_f^{-1} = (\tau A \sigma_a I_o)^{-1}[Br_2]^{-1} + \sigma_s \bar{v}(A \sigma_a I_o)^{-1}. \qquad (7.6)$$

Converting concentration of bromine to pressure (Torr) of bromine P_{Br_2} and remembering that $\bar{v} = (8kT \pi^{-1} \mu^{-1})^{\frac{1}{2}}$ where k is the Boltzmann constant (1.380662×10^{-14} erg k^{-1}), T is the absolute temperature (^oK), and μ is the reduced mass(g) of Br_2^* and Br_2 collision partners, we get

$$I_f^{-1} = (\tau A \sigma_a I_o)^{-1}[P_{Br_2}/(7.501 \times 10^{-4} kT)]^{-1}$$
$$+ \sigma_s(8kT \pi^{-1} \mu^{-1})^{\frac{1}{2}}(A \sigma_a I_o)^{-1}. \qquad (7.6)$$

So, a plot of the reciprocal of bromine fluorescence intensity as a function of the reciprocal of the bromine vapor pressure will be a straight line from which the self-quenching cross-section σ_s can be obtained as

$$\sigma_s = 7.501 \times 10^{-4} (\pi/8)^{\frac{1}{2}} (kT\mu)^{\frac{1}{2}} \tau^{-1} (\text{Intercept/Slope}) \quad (7.7)$$

7.3 Experimental Details

The bromine molecules in the sample tube were excited by 5145 Å radiation of Ar^+ laser operating in constant light mode. The output power of the laser beam was kept fixed at 300 mW. The first Stokes doublet of the fluorescence spectrum was recorded at different vapor pressures of Br_2. The vapor pressure of Br_2 in the sample tube was controlled by maintaining the temperature of the side arm by means of a

cold bath kept in a Dewar flask. The temperature of the cold bath was continuously monitored by a calibrated copper-constantan thermocouple thermometer. The temperature of the cold bath was varied between $-50^{\circ}C$ to $-70^{\circ}C$. The vapor pressure of Br_2 was calculated using the vapor pressure data given in Ref.(118). The experimental set-up has been described in detail in Section 2.4 of Chapter 2.

7.4 Results and Discussion

The resonance fluorescence doublets, containing R(13) and P(15) lines of (40-1) band of $B \rightarrow X$ fluorescence in $^{81}Br_2$ excited by 5145 Å radiation of Ar^+ laser, at two different vapor pressures of bromine are shown in Fig 7.1. The variation of the fluorescence intensity with the vapor pressure of bromine is tabulated in Table 7.1. The straight line obtained by plotting the reciprocal of fluorescence intensity against the reciprocal of bromine vapor pressure is shown in Fig 7.2. The values of I_f^{-1} for different $P_{Br_2}^{-1}$ were fitted to a linear least-squares program to calculate the value of (Intercept/Slope). Taking $\tau = 3.57$ μs,[114] the self-quenching cross-section (σ_s) is calculated to be 14 $Å^2$. The main source of error in this experiment seems to be the inaccuracy involved in the calculation of bromine vapor pressure from the known temperature of the cold bath. The laser was operated in the 'light mode' to avoid the error due to possible fluctuation of its output power. To minimize the

error due to radiation trapping of the fluorescence beam the laser beam was passed close to the wall of the sample tube containing Br_2 as discussed in Chapter 6.

7.5 Conclusion

The self-quenching cross-section (σ_s) of v' = 40, J' = 14 level in B state of $^{81}Br_2$ is calculated as 14 $Å^2$ by studying the variation of fluorescence intensity of the doublet of (40-1) band with the vapor pressure of bromine. By selectively exciting various vibrational levels (v') of the B-state using a tunable laser this method can be used to study the variation of σ_s with v' so that the region where the repulsive state $^1\Pi_{1u}$ crosses the B state giving rise to predissociation can be located precisely. This work could not be carried out here due to nonavailability of a proper tunable laser.

Table 7.1 Intensity of the Fluorescence Doublet at Various Vapor Pressures of Bromine

Br_2 Vapor Pressure (Torr)	Fluorescence Intensity (arb.units)	Reciprocal of Br_2 Vapor Pressure $(Torr)^{-1}$	Reciprocal of Fluorescence Intensity (arb units)
1.09	10.0	0.92	0.100
0.93	9.8	1.08	0.102
0.79	9.6	1.27	0.104
0.67	9.4	1.49	0.106
0.56	8.7	1.79	0.115
0.48	8.2	2.08	0.122
0.40	8.1	2.50	0.123
0.34	7.5	2.94	0.133
0.20	5.3	5.00	0.189
0.15	5.1	6.67	0.196
0.13	4.6	7.69	0.217
0.12	4.3	8.33	0.233
0.11	4.2	9.09	0.238
0.10	3.7	10.00	0.270

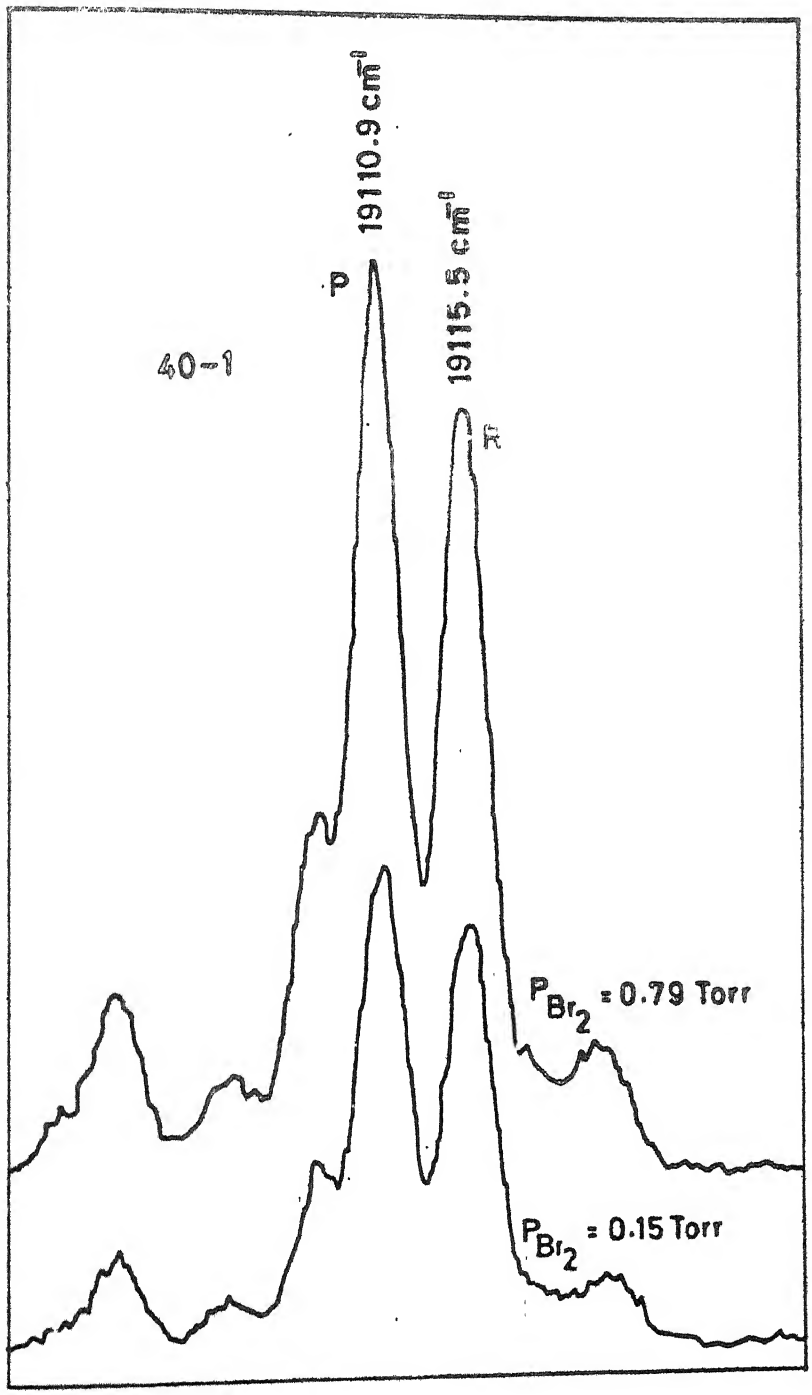

FIG. 7.1 LASER INDUCED RESONANCE FLUORESCENCE DOUBLETS CORRESPONDING TO THE (40-1) BAND OF $B^3\Pi_{o_u^+} \rightarrow X^1\Sigma_g^+$ TRANSITION IN BROMINE AT TWO DIFFERENT VAPOR PRESSURES AS INDICATED.

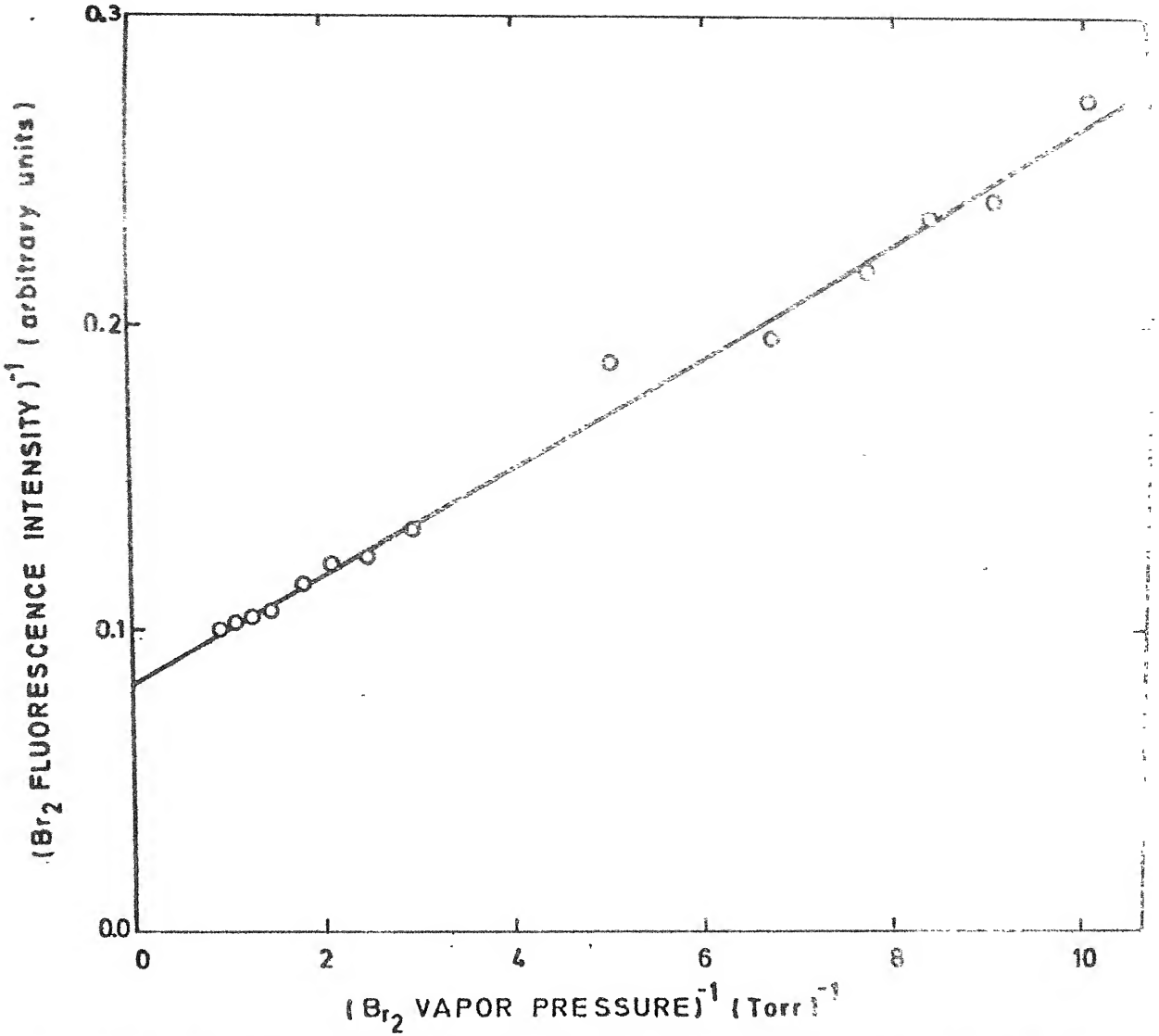

FIG. 7.2. STERN-VOLMER PLOT OF THE RECIPROCAL OF Br_2 FLUORESCENCE INTENSITY AS A FUNCTION OF THE RECIPROCAL OF Br_2 VAPOR PRESSURE.

CHAPTER 8

SUMMARY AND CONCLUSIONS

The overall accomplishments in this work may be summarised in the following paragraphs.

The 2900 Å emission system of $^{81}Br_2$ and natural bromine and the transient absorption system of the photoflashed Br_2 in the region 2870-2410 Å have been used for vibrational analysis. Most of the bands in the emission as well as the transient absorption system are red degraded. The emission spectrum overlaps the trasient absorption spectrum over a large region (2870-2600 Å) and the positions of the band heads for a large number of emission and transient absorption bands were found to coincide within our experimental accuracy. The bands were found to fit well into a single vibrational scheme. It has been inferred that the emission and the transient absorption bands correspond to the same system (D' - A' system) having the lower state as $^3\Pi_{2u}$ arising out of the configuration $(\sigma_g)^2(\pi_u)^4(\pi_g)^3(\sigma_u)^1$ which in Mulliken's notation is abbreviated as 2431. The upper state of the system seems to be one of the low lying

ion-pair states which tends to dissociate into Br^- and Br^+. These ion-pair states are characterised by low vibrational frequencies and large internuclear distances. This designation of the lower state as $^3\Pi_{2u}$ is consistent with the observation of transient absorption spectrum with a time delay of about 50μs between the photolysis flash and the source of continuum. The intensities of the band heads estimated in the visual scale 0-10 and vacuum wavenumbers of the band heads analysed have been given in Chapter 3. The analysis was checked by using the observed isotope shifts of the three isotopic species of bromine ($^{81}Br_2$, $^{79}Br^{81}Br$ and $^{79}Br_2$). The positions of the band heads of all the three isotopic species of bromine have simultaneously been fitted to the polynomial in $\rho(v'+\frac{1}{2})$ and $\rho(v''+\frac{1}{2})$ representing the band system. The σ of the fit was about 1.3 cm^{-1}. This simultaneous fit of the band heads distributes the errors in the measurement of the band heads among the two electronic states so that the errors in the values of the individual constants of both the states get minimized. The precision of the estimates of the vibrational constants of all of the three isotopic species of bromine have been reported. The use of transient absorption data of photoflashed Br_2 has helped to extend the vibrational analysis to include the transitions involving the lower state vibrational levels down to $v'' = 0$ and the upper state vibrational levels up to $v' = 46$.

Rotational analysis of 0-8, 0-9, 0-10, 0-11, 1-8, 1-12, 3-5 and 4-5 bands of $^{81}Br_2$ is done using high resolution ($\sim$0.1 Å/mm) D' $\rightarrow$ A' emission spectrum of $^{81}Br_2$ photographed in the 20th and 21st order. The P and R lines are resolved down to fairly low values of J in most of the bands and the rotational structure extends to high J values. The absence of a systematic intensity alternation in the rotational structure of the bands containing unresolved Λ /Ω -doublets is in conformity with the assignment of D' - A' as the transition giving rise to the band system. The rotational constants B_v'', D_v'', B_v', D_v' of the bands were obtained by band-by-band unweighted and uncorrelated least squares solution under the assumption that the experimental errors of the lines in the bands are randomly scattered. The results for the bands having either upper or lower vibrational level as common were merged to obtain the best, i.e., minimum variance, linear and unbiased (MVLU) single value for each of the rotational constants. The rotational analysis of 0-10, 0-11, 1-12, 3-5 and 4-5 bands of $^{81}Br_2$ are presented for the first time. The final rotational constants of upper and lower states were obtained from the least squares fits of B_v', D_v', B_v'' and D_v'' to their standard polynomial representations as discussed in Chapter 4. The rotational constants obtained in this work are expected to be fairly reliable. Further work with still higher dispersion and greater resolution to determine the lowest value of J in the rotational structure and

to check the presence of Q branch will be helpful to confirm the value of Ω of the states involved in the system.

The vibrational and rotational constants obtained for $^{81}Br_2$ have been used to calculate the RKR potentials of the D' and A' states of $^{81}Br_2$. These RKR potentials were then used to get the exact vibrational wavefunctions by direct numerical solution of radial Schrödinger equation. The Franck-Condon factors (FCFs) and R-centroids ($\bar{R}s$) for D' - A' system of $^{81}Br_2$ for $0 \leq v'' \leq 22$ and $0 \leq v' \leq 10$, and $J' = J'' = 0$ have been reported in Chapter 5. To demonstrate the reliability of the values of FCFs and R-centroids comparisons of experimental values of G(v) and B(v) with the calculated eigenvalues E_v and the values of rotational constants calculated from the expectation values of $(1/R^2)$ have been made. The FCFs qualitatively agree with the observed intensity distribution of D' - A' emission band system of Br_2. The FCFs are expected to be reliable to one or two digits in the fourth significant figure for their larger values.

The resonance fluorescence doublets corresponding to $v' = 40 \longrightarrow v''$ transitions in B $^3\Pi_{0_u^+} \rightarrow X\ ^1\Sigma_g^+$ system of Br_2 excited by 5145 Å radiation of a cw Ar^+ laser have been recorded and analysed in Chapter 6. The upper level of the doublets were found to be $v' = 40$ and $J' = 14$ of B state of $^{81}Br_2$. The observed relative intensities of the doublets were compared with those expected on the basis of the known FCFs.

The variation of electronic transition moment with R-centroid ($\bar{R}$) has been plotted. The plot can further be extended if the values of FCFs and $\bar{R}$s for v">0 are available. The self-quenching cross-section (σ_s) of the level in B state of $^{81}Br_2$ excited by 5145 Å radiation of Ar^+ laser has been calculated by studying the variation of fluorescence intensity with Br_2 vapor pressure. This gives a straightforward method to find the values of σ_s. Using a proper tunable laser the variation of σ_s for various vibrational levels (v') of B state can be obtained to locate the region where the repulsive state $^1\Pi_{1u}$ crosses the B state giving rise to predissociation.

REFERENCES

1. R S Mulliken, Rev Mod Phys 2, 60 (1930), 506 (1930).
2. R S Mulliken, Rev Mod Phys 3, 89 (1931).
3. R S Mulliken, Rev Mod Phys 4, 1 (1932).
4. L Pauling and E B Wilson, Jr, "Introduction to Quantum Mechanics", Chaps X and XII, McGraw-Hill, New York, 1935.
5. G Herzberg, "Molecular Spectra and Molecular Structure", Vol I, Spectra of Diatomic Molecules, 2nd ed, Van Nostrand Reinhold Co, New York, 1950.
6. L D Landau and E M Lifshitz, "Course of Theoretical Physics", Vol 3, Quantum Mechanics, Chap XI, Pergamon Press, Oxford, 1965.
7. L I Schiff, "Quantum Mechanics", Chap 12, 3rd ed, McGraw-Hill, New York, 1968.
8. B P Straughan and S Walker, Eds, "Spectroscopy", Vol 3, Chapman and Hall, London, 1976.
9. M Born and R Oppenheimer, Ann Physik 84, 457 (1927).
10. F Hund, Z Physik 36, 657 (1926).
11. R S Mulliken, Phys Rev 36, 699 (1930).
12. R S Mulliken, Phys Rev 37, 1412 (1931).
13. R S Mulliken, Phys Rev 46, 549 (1934).
14. R S Mulliken, Phys Rev 57, 500 (1940).
15. R S Mulliken, J Chem Phys 55, 288 (1971).
16. H Hemmati and G J Collins, Chem Phys Lett 75, 488 (1980).
17. P Venkateswarlu, Proc Ind Acad Sci 24A, 473 (1946).
18. P Venkateswarlu, Proc Ind Acad Sci 24A, 480 (1946).
19. P Venkateswarlu, Proc Ind Acad Sci 25A, 119 (1947).
20. P Venkateswarlu, Proc Ind Acad Sci 25A, 133 (1947).

21. P Venkateswarlu, Proc Ind Acad Sci 25A, 138 (1947).

22. P Venkateswarlu, Proc Ind Acad Sci 26A, 22 (1947).

23. P Venkateswarlu, Ind J Physics 21, 43 (1947).

24. R K Asundi and P Venkateswarlu, Ind J Phys 21, 101 (1947).

25. P Venkateswarlu, Phys Rev 81, 821 (1951).

26. P Venkateswarlu and R D Verma, Proc Ind Acad Sci 46A, 251 (1957).

27. P Venkateswarlu and R D Verma, Proc Ind Acad Sci 46A, 416 (1957).

28. R D Verma, Proc Ind Acad Sci 48A, 197 (1958).

29. P Venkateswarlu and B N Khanna, Proc Ind Acad Sci 49A, 117 (1959).

30. B N Khanna, Proc Ind Acad Sci 49A, 293 (1959).

31. Y V Rao and P Venkateswarlu, J Mol Spectrosc 9,173(1962).

32. Y V Rao and P Venkateswarlu, J Mol Spectrosc 13, 288(1964).

33. P Venkateswarlu and D R Rao, Proc Ind Acad Sci 64A,9(1966).

34. P Venkateswarlu, Can J Phys 47, 2525 (1969).

35. P Venkateswarlu, Can J Phys 48, 1055 (1970).

36. P Venkateswarlu, Ind J Phys Comm Vol Pt II, 273 (1977).

37. P Venkateswarlu, V N Sarma and Y V Rao, J Mol Spectrosc 96, 247 (1982).

38. R K Asundi and P Venkateswarlu, Ind J Phys 21, 76 (1947).

39. P Venkateswarlu and R D Verma, Proc Ind Acad Sci 47A, 150 (1958).

40. P Venkateswarlu and R D Verma, Proc Ind Acad Sci 47A, 161 (1958).

41. P Venkateswarlu, Can J Physics 53, 812 (1975).

42. J K Rice, A K Hays and J R Woodworth, Appl Phys Lett 31, 31 (1977).

43. J R Woodworth and J K Rice, J Chem Phys 69, 2500 (1978).

44. C H Chen and M G Payne, Appl Phvs Lett 28, 219 (1976).

45. A K Hays, Opt Comm 28 209 (1979).

46. J R Murray, J C Swingle and C E Turner, Jr, Appl Phys Lett 28, 530 (1976).

47. J J Ewing, J H Jacob, J A Mangano and H A Brown, Appl Phvs Lett 28, 656 (1976).

48. R S Bradford, Jr, E R Ault and M L Bhaumik, Appl Phvs Lett 27, 546 (1975).

49. JJ Ewing and C A Brau, Appl Phys Lett 27, 557 (1975).

50. A K Hays, J M Hoffman and G C Tisone, Chem Phys Lett 39, 353 (1976)

51. Y Uchida and Y Ota, Jap J Phys 5, 59 (1928).

52. P B V Haranath and P T Rao, Ind J Phys 29, 205 (1955).

53. W H B Cameron and A Elliott, Proc Roy Soc London 169A, 463 (1938-39).

54. A G Briggs and R G W Norrish, Proc Roy Soc London A276, 51 (1963).

55. Y V Rao, Private Communication.

56. K Wieland, J B Tellinghuisen and A Nobs, J Mol Spectrosc 41, 69 (1972).

57. J Tellinghuisen, Chem Phys Lett 49, 485 (1977).

58. A Sur and J Tellinghuisen, J Mol Spectrosc 88, 323 (1981)

59. H M Crosswhite, Johns Hopkins Spectroscopic Report No.13 (1958).

60. H M Crosswhite, J Res Nat Bur Stand Sect A 79, 17 (1975).

61. B Eldén, J Opt Soc Am 43, 339 (1953).

62. F S Tomkins and M Fred, J Opt Soc Am 41, 641 (1951).

63. D L Albritton, W J Harrop, A L Schmeltekopf, R N Zare and E L Crow, J Mol Spectrosc 46, 67 (1973).

64. D L Albrittōn, A L Schmeltekopf and R N Zare "Molecular Spectroscopy: Modern Research, Vol II", edited by K N Rao, Academic Press, New York, pp 1-67 (1976).

65. D L Albritton, A L Schmeltekopf and R N Zare, J Mol Spectrosc 67, 132 (1977).

66. J A Coxon, J Mol Spectrosc 37, 39 (1971)

67. J A Coxon, J Mol Spectrosc 41, 548 (1972).

68. R F Barrow, T C Clark, J A Coxon and K K Yee, J Mol Spectrosc 51, 428 (1974).

69. Y P Varshini, Rev Mod Phys 29, 664 (1957).

70. D Steele, E R Lippincot and J T Vanderslice, Rev Mod Phys 34, 239 (1962).

71. R Rydberg, Z Physik 73, 376 (1931); 80, 514 (1933).

72. O Klein, Z Physik 76, 226 (1932).

73. A L G Rees, Proc Phys Soc (London) 59, 998 (1947).

74. J T Vanderslice, E A Mason, W G Maisch and E R Lippincott, J Mol Spectrosc 3, 17 (1959); 5, 83 (1960).

75. R H Davis and J T Vanderslice, J Chem Phys 45, 95 (1966).

76. J N Huffaker, J Mol Spectrosc 65, 1 (1977).

77. J Franck, Trans Faraday Soc 21, 536 (1925).

78. E U Condon, Phys Rev 32, 858 (1928).

79. E U Condon, Am J Phys 15, 365 (1947).

80. R N Zare, J Chem Phys 40, 1934 (1964).

81. W G Richards and R F Barrow, Proc Phys Soc 83, 1045 (1964).

82. S Weissman, J T Vanderslice and R J Battino, J Chem Phys 39, 2226 (1965).

83. R J Spindler, J Quant Spectrosc Radiat Transfer 5, 165 (1965).

84. F L Zeleznik, J Chem Phys 42, 2836 (1965).

85. F R Gilmore, J Quant. Spectrosc Radiat Transfer 5, 369 (1965).

86. N I Zhirnov and A S Vasilevskii, Opt Spectrosc 25, 13 (1968).

87. W R Jarmain, J Quant Spectrosc Radiat Transfer 11, 421 (1971).

88. J A Coxon, J Quant Spectrosc Radiat Transfer 11, 443 (1971)

89. A W Mantz, J K G Watson, K Narahari Rao, D L Albritton, A L Schmeltekopf and R N Zare, J Mol Spectrosc 39, 180 (1971).

90. A S Dickinson, J Mol Spectrosc 44, 183 (1972).

91. H E Fleming and K Narahari Rao, J Mol Spectrosc 44, 189 (1972).

92. J Tellinghuisen, J Mol Spectrosc 44, 194 (1972).

93. J L Dunham, Phys Rev 41, 721 (1932).

94. R T Pack, J Chem Phys 57, 4612 (1972).

95. J Tellinghuisen, Computer Phys Comm 6, 221 (1974).

96. Z Kopal, Numerical Analysis, Chap VII, Chapman and Hall, London, 1961.

97. J Tellinghuisen, J Quant Spectrosc Radiat Transfer 19, 149 (1978).

98. R De L Kronig and I I Rabi, Phys Rev 29, 262 (1927).

99. J W Coolev, Math Comp 15, 363 (1961).

100. R N Zare and J K Cashion, University of California Radiation Laboratory Report, UCRL-10881 (1963).

101. F J Wodarczyk and H R Schlossberg, J Chem Phys 67, 4476 (1977).

102. J Behringer, "Molecular Spectroscopy (Specialist Periodical Reports)," Vol 2, The Chemical Society, London, 1974, p 100.

103. C F Shaw, III, J Chem Education 58, 343 (1981).

104. W Holzer, W F Murphy and H J Bernstein, J Chem Phys 52, 469 (1970).

105. W Holzer, W F Murphy and H J Bernstein, J Chem Phys 52, 399 (1970).

106. Appendix I of Ref (68). A xerox copy of Appendix I containing the Franck-condon factors and R-centroids of $B\ ^3\Pi_{0_u^+} - X\ ^1\Sigma_g^+$ system of Br_2 was generously supplied by Professor K Narahari Rao.

107. L Brewer and J Tellinghuisen, J Chem Physics 56, 3929 (1972).

108. J B Koffend, R Bacis and R W Field, J Chem Physics 70, 2366 (1979).

109. T K Balasubramanian, G L Bhale, M N Dixit and N A Narasimham, J Mol Spectrosc 88, 259 (1981).

110. S H Dworetsky and R S Hozack, J Chem Phys 59, 3856 (1973).

111. R M Lum and R S Hozack, J Mol Spectrosc 58, 325 (1975).

112. H Chang and D M Hwang, J Mol Spectrosc 65, 430 (1977).

113. G Capelle, K Sakurai and H P Broida, J Chem Phys 54, 1728 (1971).

114. K B McAfee, Jr and R S Hozack, J Chem Phys 64, 2491 (1976).

115. M A A Clyne and M C Heaven, J Chem Soc Faraday II 74, 1992 (1978).

116. M A A Clyne, M C Heaven and E Martinez, J Chem Soc Faraday II 76, 405 (1980).

117. M H Ornstein and V E Derr, J Opt Soc Am 66, 233 (1976).

118. C D Hodgman, Ed, Hand Book of Chemistry and Physics 31st edn, p 1862, Chemical Rubber Publishing Co, Ohio (1949).